

## Recent progress on advanced solid adsorbents for CO<sub>2</sub> capture: From mechanism to machine learning



Mobin Safarzadeh Khosrowshahi <sup>a,\*</sup>, Amirhossein Afshari Aghajari <sup>b</sup>, Mohammad Rahimi <sup>c, \*\*</sup>, Farid Maleki <sup>d</sup>, Elahe Ghiyabi <sup>e</sup>, Armin Rezanezhad <sup>f</sup>, Ali Bakhshi <sup>a</sup>, Ehsan Salari <sup>g</sup>, Hadi Shayesteh <sup>h</sup>, Hadi Mohammadi <sup>i</sup>

<sup>a</sup> Nanotechnology Department, School of Advanced Technologies, Iran University of Science and Technology (IUST), Narmak, 16846, Tehran, Iran

<sup>b</sup> Zachry Department of Civil and Environmental Engineering, Texas A&M University, Dwight Look Engineering Building, College Station, TX, 77840, United States

<sup>c</sup> Department of Mechanical Engineering, McMaster University, Hamilton, Ontario, Canada

<sup>d</sup> Department of Polymer Engineering & Color Technology, Amirkabir University of Technology, No. 424, Hafez St, Tehran, Iran

<sup>e</sup> Department of Biomedical Engineering, Faculty of Electrical and Computer Engineering, University of Tabriz, Tabriz, Iran

<sup>f</sup> Faculty of Mechanical Engineering, Department of Materials Science and Engineering, University of Tabriz, 51666-16471, Tabriz, Iran

<sup>g</sup> Institute of Polymeric Materials, Sahand University of Technology, P.O.Box 51335-1996, Sahand New Town, Tabriz, Iran

<sup>h</sup> Faculty of Chemical Engineering, Iran University of Science and Technology (IUST), Narmak, Tehran, 16846, Iran

<sup>i</sup> School of Civil Engineering, College of Engineering, University of Tehran, Tehran, Iran

### ARTICLE INFO

#### Keywords:

CO<sub>2</sub> capture

Adsorption

Solid adsorbents

Machine learning

Physisorption

Porous materials

### ABSTRACT

Environmental pollution has become a serious issue due to the rapid development of urbanization, industrialization, and vehicle traffic. Notably, fossil fuel combustion significantly contributes to rising atmospheric CO<sub>2</sub> levels. To address this problem, various carbon capture and storage (CCS) technologies have been developed, aiming to reduce CO<sub>2</sub> emissions and mitigate their impact on climate change. Absorption using aqueous amines has long been recognized as a method for removing diluted CO<sub>2</sub> from gas streams, but it comes with drawbacks such as high energy intensity and corrosion issues. The use of solid adsorbents, however, is now being seriously considered as a potential alternative, offering a possibly less energy-intensive separation method. The primary focus of this study is to outline the recent development of advanced solid adsorbents, including zeolites, carbon-based materials, MOFs, COFs, boron nitride, magnetic nanoparticles, and mesoporous silica, along with their CO<sub>2</sub> uptake behavior. In CO<sub>2</sub> capture procedures, selecting the appropriate adsorbent is crucial, yet it's not a straightforward task to determine the most promising sorbent beforehand due to various factors affecting performance and economy. In recent years, machine learning (ML) algorithms, particularly artificial neural networks (ANN) and convolutional neural networks (CNN) have emerged as valuable tools for predicting physical properties, expediting the selection of optimal adsorbents for CO<sub>2</sub> capture, optimizing synthesis conditions of adsorbents, and understanding advantageous variables for gas-solid interaction. The secondary objective of this review is to establish a correlation between recent advancements and potential future breakthroughs in the domain of machine learning-assisted CO<sub>2</sub> adsorbents. In summary, this review aims to provide a comprehensive guideline for selecting tailored solid adsorbent materials according to recently reported research to achieve high-performance CO<sub>2</sub> capture. By exploring various materials, their properties, and the mechanisms that influence their effectiveness, this review intends to facilitate informed decisions and innovative solutions for CO<sub>2</sub> adsorbents.

### Abbreviations

AC

Activated carbon

(continued on next column)

(continued)

Ar

Argon

(continued on next page)

\* Corresponding author.

\*\* Corresponding author.

E-mail addresses: [m\\_safarzadeh@nt.iust.ac.ir](mailto:m_safarzadeh@nt.iust.ac.ir) (M. Safarzadeh Khosrowshahi), [rahimm19@mcmaster.ca](mailto:rahimm19@mcmaster.ca) (M. Rahimi).

(continued)

BET	Brunauer-Emmett-Teller
BJH	Barrett-Joyner-Halenda
CCS	Carbon capture and storage
CNT	Carbon nanotube
BTC	Benzene-1,3,5-tricarboxylate
DFT	Density Functional Theory
DTA	Differential Thermal Analysis
FDZA	freeze-drying
FESEM	Field Emission Scanning Electron Microscopy
FTIR	Fourier transform infrared
GCMC	Grand Canonical Monte Carlo
HOMO	Highest occupied molecular orbital
HRTEM	High-resolution transmission electron microscopy
IAST	Ideal Adsorbed Solution Theory
IUPAC	International Union of Pure and Applied Chemistry
LUMO	Least unoccupied molecular orbital
MIL	Materials Institute Lavoisier
MLP	Multilayer perceptron
MMMs	Mixed-matrix membranes
MWCNT	Multi-walled carbon nanotube
N <sub>2</sub>	Nitrogen
NH <sub>3</sub>	Ammonia
NMR	Nuclear Magnetic Resonance
OMC	Ordered mesoporous carbons
PC	Porous carbon
PEG	Polyethylene glycol
PEO	Polyethylene oxide
PSD	Pore size distribution
RBF	Radial basis function
rGO	Reduced graphene oxide
S <sub>BET</sub>	Specific surface area
SBA-15	Santa Barbara Amorphous-15
SiO <sub>2</sub>	Silicon dioxide
TEM	Transmission electron microscopy
TGA	Thermogravimetric analysis
V <sub>total</sub>	Total pore volume
wt	Weight
XANES	X-ray absorption near-edge structure
XLPEO	Cross-linked amorphous poly(ethylene oxide)
XPS	X-ray photoelectron spectroscopy
XRD	X-ray diffraction
ZIF	Zeolitic imidazolate framework
ZnCl <sub>2</sub>	Zinc chloride

chemical absorption using aqueous amines is believed to be the most efficient technique. However, this method needs steam that is around 125 °C [10]. Additionally, it has several disadvantages, including a high energy intensity that is primarily related to solvent regeneration, corrosion problems, the need for large volumes of adsorbents since corrosive solvent must be diluted, amine losses, and operational costs. As a result, solid-state adsorbents used in the physical sorption of CO<sub>2</sub> from the air or flue gas are preferable [11]. As shown in Fig. 1, to uptake CO<sub>2</sub>, a variety of solid-phase adsorbents have been studied, including C-based material (porous carbon, CNT, graphene, and fullerene C60), mesoporous silicas, zeolites, metal-organic frameworks (MOFs), covalent organic frameworks (COFs), polymers, and magnetic nanoparticles [12–14].

High selectivity (CO<sub>2</sub>/N<sub>2</sub>), CO<sub>2</sub> adsorptive capability, reasonably priced, thermal and chemical stability, moderate heat adsorption (Q<sub>st</sub>), as well as rapid kinetics, would all be characteristics of the ideal sorbent [15]. Even though some of these materials have exceptional CO<sub>2</sub> capture performance, they have significant disadvantages that restrict their potential as commercial-scale CO<sub>2</sub> capture sorbents, such as the need for costly and dangerous precursors, complex multi-step synthesis processes, and challenging waste disposal procedures [16]. Therefore, to create the ideal adsorbent, some physical features such as the pore size (ultra-micropores), appropriate heteroatoms (N, O, B, and P), suitable ligands, and the surface chemistry (polar groups) must be tuned [17,18]. Thus, the most crucial step in the CO<sub>2</sub> physisorption process is selecting the best adsorbent and surface modification technique while taking into account the presence of previously mentioned variables and the cost of synthesis [19]. Machine learning (ML) models of the characteristics of solid adsorbents can be used to speed up the design, discovery, and optimization of sorbents. ML models can be trained using data from experiments and intensive simulations (i.e., MD, GCMC, or DFT). The adoption of ML techniques can allow the virtual screening of intractably enormous search spaces since the prescreening of a candidate structure would take a fraction of a second rather than minutes or hours [20–23]. To determine operational CO<sub>2</sub> uptake variables (like those related to pore topology and surface chemistry) without human bias, multivariate analyses, such as random forest (RF), support vector machine (SVM), decision tree (DT), back propagation neural network (BPNN), and Bayesian methods, were thoroughly examined [24,25]. So far, various

## 1. Introduction

Nowadays, the steadily rising of anthropogenic carbon dioxide (CO<sub>2</sub>) is one of the most significant challenges. To avoid global warming and climate change, reducing these emissions has proven to be quite difficult [1]. The Paris Climate Agreement seeks continued attempts to keep global warming to 1.5 °C and to keep it far below 2 °C [2]. By reducing CO<sub>2</sub> emissions into the environment and switching to a zero-emission power production alternative, future catastrophic repercussions can be averted [3]. Consequences of this harmful gas's continued release into the atmosphere include an upsurge in the average global temperature, desertification, the melting of the polar ice caps, severe floods, and drought [4,5]. The burning of fossil fuels, which appear to be the most prevalent and pollution-free source of power globally and hence play a crucial part in a pleasant and sustainable living, is thought to be the primary source of CO<sub>2</sub> emissions. Thus, utilization of alternative fuels like biofuels and H<sub>2</sub> in the long term, and carbon capture and storage (CCS) are the only currently viable options to cover energy demands while minimizing CO<sub>2</sub> emissions [6,7]. CCS methods propose to remove and transport CO<sub>2</sub> from major industrial sources and either store it underground or utilize it by converting it into useable nanomaterials or hydrocarbons [8]. Post-combustion, pre-combustion, and oxyfuel are the three primary ways that CCS allows for the continued use of fossil fuels during the transition to a low-carbon energy system. The process of post-combustion includes eliminating CO<sub>2</sub> from the flue gases produced after combustion [9]. When it comes to post-combustion CO<sub>2</sub> uptake,

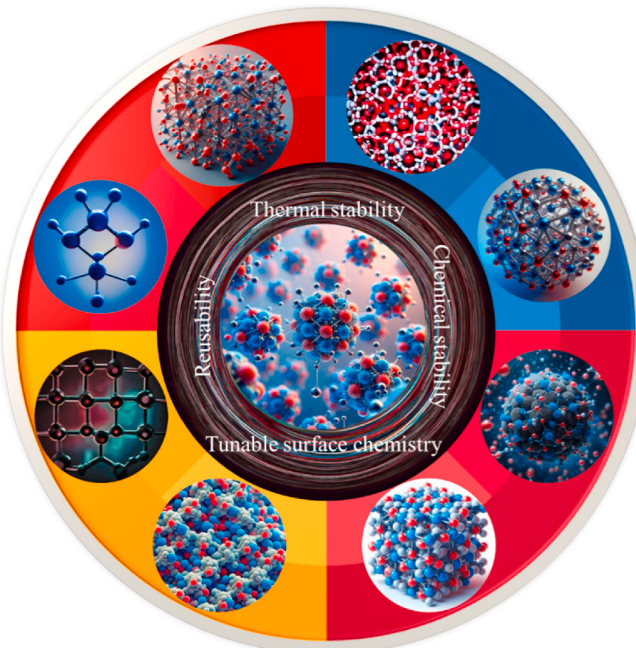


Fig. 1. Schematic of various solid adsorbents with their pros for CO<sub>2</sub> uptake.

reviews have been published about solid adsorbents, most of which have focused on routine adsorbents such as zeolites, MOFs, and porous carbon. In this study, for the first time, in addition to routine adsorbents, we investigate less commonly discussed solid adsorbents such as magnetite nanoparticles, mesoporous silica, COFs, fullerene, and boron nitride.

This review discusses some of the recent developments in the study of advanced solid adsorbents for CO<sub>2</sub> capture. The chemical and physical adsorption mechanism of CO<sub>2</sub> will be covered in the first section of the review. In the following part, different kinds of physical adsorbents that have been developed over the recent years to adsorb CO<sub>2</sub> will be examined. The history of these adsorbents is limited to the past two years to better evaluate their progress. This focus aims to address previous challenges and enhance the adsorption rate, providing a clearer understanding of recent advancements and their potential for high-performance CO<sub>2</sub> capture. Additionally, the pros and cons of these adsorbents are thoroughly examined, and the parameters influencing the rise in gas sorption are assessed. Additionally, a comparison is made regarding the economics of these adsorbents, covering aspects from synthesis to adsorption. This comparison aims to provide insights into the cost-effectiveness of each material, guiding the selection of the most viable options for large-scale CO<sub>2</sub> capture applications. As of right moment, no study has thoroughly compiled and examined every

publication of machine learning for CO<sub>2</sub> capture by solid adsorbents. To fill this gap, the last section of this paper offers a thorough introduction to the ML techniques employed in the creation, discovery, and improvement of these CO<sub>2</sub> capture sorbents.

## 2. CO<sub>2</sub> capture

“Global warming” describes a rise in the earth’s average surface temperature driven by excessive greenhouse gas (CO<sub>2</sub>, N<sub>2</sub>O, CH<sub>4</sub>, and chlorofluorocarbons) emissions [26]. Since rising atmospheric CO<sub>2</sub> concentrations are known to be the principal cause of unfavorable changes in climate patterns, this gas accumulation must be limited to halt global warming [27]. Worldwide energy-related CO<sub>2</sub> emissions are now at 40 Gt, and the Paris Agreement necessitates around 10 Gt CO<sub>2</sub> must be adsorbed each year, with up to 160 Gt CO<sub>2</sub> stored by 2050 [28]. “CO<sub>2</sub> capture” term is the separation of this gas from effluent gas produced during the burning of fossil fuels in power plants. Researchers have developed various CO<sub>2</sub> capture and sequestration systems, in which carbon capture reduces emissions by up to 8 Gt. Nonetheless, there is still a considerable gap between the aims of removing this gas and their realization [29,30]. The cost of CO<sub>2</sub> capture in CCS constitutes around 80% of the entire cost, thus there is a need for appropriate

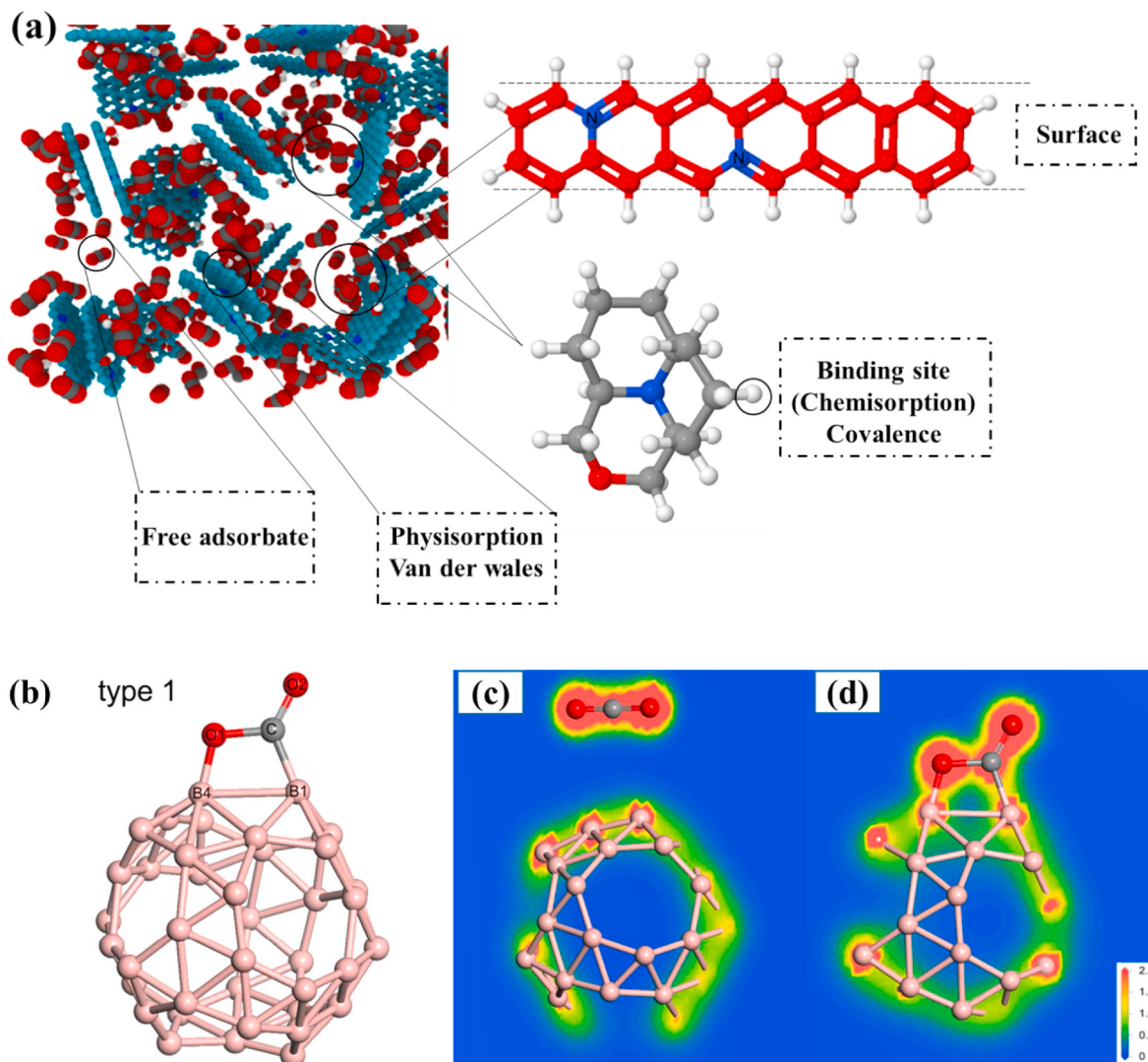


**Fig. 2.** (a) Schematic of physisorption, and chemisorption on the surface. Physisorption is done with the participation of van der Waals bonds on the surface, while in chemisorption, adsorption occurs on binding sites. (b) Optimized structure of B<sub>40</sub>, (c) electron density distribution of physisorption, and (d) chemisorption. Reprinted with permission from Ref. [39]. Copyright (2015) Elsevier.

technology that significantly reduces operational costs [31]. Pre-combustion carbon capture, post-combustion carbon capture, chemical looping combustion, and the oxy-combustion carbon capture method are the techniques for capturing CO<sub>2</sub>. While oxy-combustion and post-combustion can be used in typical coal- or gas-fired power plants, pre-combustion capture is suited to integrated gasification combined cycle (IGCC) facilities [32]. Of them, post-combustion capture is one of the most promising methods for carbon capture in terms of energy efficiency, low cost, and equipment portability [33]. Utilizing chemical absorption, physical adsorption, and membrane separation, post-combustion CO<sub>2</sub> capture from flue gas is accomplished after the combustion stage [34]. Regardless of membrane separation, each of the solid sorbents under consideration uses either one of the three sorption mechanisms according to Fig. 2 a; physical adsorption, chemical absorption, or a combination of both. Physisorption is also known as van der Waals adsorption since there is no chemical connection between the sorbent and the sorbate in this form of sorption. Target CO<sub>2</sub> molecules and the solid adsorbent surface only generate weak van der Waals interactions (Ion-quadrupole interaction) and have a low heat of adsorption. CO<sub>2</sub> molecules can be swiftly freed from the forces keeping them to the surface by raising the temperature or lowering the pressure. As a result, the adsorbent can work across multiple cycles, and regeneration of the sorbent is effortless ( $\approx$ 40–50% less than chemisorption) [35]. In contrast, the target gas provides a covalent chemical reaction in chemisorption to adhere to specific locations on the adsorbent with a substantially higher heat of adsorption, about the same as the heat of the reaction [36,37]. Contrary to physisorption, the strong binding energy between the adsorbent and the adsorbate in this process is believed to render chemisorption challenging to regeneration [38]. Regarding this, Dong et al.'s calculations using density functional calculations (as simulated and optimized in Fig. 2b) demonstrated that there was no chemical connection (Fig. 2c) between CO<sub>2</sub> and B<sub>40</sub> fullerene since as CO<sub>2</sub> adsorbed to B<sub>40</sub>, the electrons localized at the two molecules separately. On the other hand, the electrons exhibited considerable accumulation in the B–O and B–C area when CO<sub>2</sub> was chemisorbed (Fig. 2d) to B<sub>40</sub>. Since the carbon atoms in CO<sub>2</sub> possessed a positive charge, they chemisorbed strongly to the basic sites on B<sub>40</sub> [39].

Absorption is the most widely utilized technique for CO<sub>2</sub> sorption at industrial scale and is regarded as the most advanced CO<sub>2</sub> capture technology [40]. However, this method has several limitations, the most significant of which are the requiring high energy for the regeneration of sorbent and device corrosion [41,42]. Adsorption is a method for cost-effective carbon capture and storage that uses solid adsorbents comprising zeolites, carbon-based materials, and MOF [43]. It has been determined that the CO<sub>2</sub> absorption capability of the aforementioned solid adsorbents equal to or above 2 mmol g<sup>-1</sup> is comparable with commercial amines (30% monoethanolamine) employed in industrial processes. Due to the lower activation energy of CO<sub>2</sub> (15 kJ mol<sup>-1</sup>) than N<sub>2</sub> (18 kJ mol<sup>-1</sup>), which also roughly relates to the effective kinetic diameter ((CO<sub>2</sub> (3.3 Å) versus N<sub>2</sub> (3.64 Å)), solid sorbent-based adsorption is selective towards CO<sub>2</sub> [44,45]. Additionally, high critical CO<sub>2</sub> volumes and significant quadrupole moments lead to decreased diffusional resistance and increased sorption capacity of these sorbents [46]. Different solid adsorbents uptake CO<sub>2</sub> on their surfaces or skeletons using a variety of mechanisms, including cation exchange, layered adsorption, diffusion through micro- and mesoporosity, acid-base interaction, electrostatic charges, and bonding with surface groups [47]. For instance, Gao et al. reported that the synthetic mesoporous MgO contained a range of basic sites that made acid-base interaction with acidic-CO<sub>2</sub>. Low acid-base interaction evolved to medium and high acid-base interaction as a result of the surface species switching from bicarbonate to bidentate and unidentate carbonates as the sorption temperature increased [48]. The MOFs' ability to adsorb CO<sub>2</sub> is significantly influenced by the linkers (type and size). Density functional theory (DFT) was used by Liu et al. to demonstrate that the most preferred sorption location on IRMOF-1 is the side position with CO<sub>2</sub>

parallel attack at the hydrogen side of the linker edge (PS). The van der Waals force is the primary contact force between CO<sub>2</sub> and the linker of IRMOF-1 [49]. The simulation by Song et al. showed a substantial relationship between the quantity of oxygen-containing functional groups, particularly carboxyl and hydroxyl, and the saturation sorption capacity of CO<sub>2</sub>. Furthermore, the adsorption generated by oxygen-containing functional groups was exothermic and belonged to the category of physisorption based on the values of enthalpy (-12.2 to -20 kJ mol<sup>-1</sup>) [50]. The CO<sub>2</sub> sorption mechanism on S-doped nanoporous carbon/rGO was described by Kwiatkowski et al. using the class models. They found that surface chemistry was crucial for the energetics of adsorption and the clustering patterns of the CO<sub>2</sub> molecules, even if the volume of tiny pores is a key factor determining the magnitude of the adsorption process. Their findings implied that particular surface chemistry, rather than the total amount of polar groups, was what significantly influenced the adsorption processes. CO<sub>2</sub> probably oxidized sulfoxides and sulfones after being adsorbed, changing the surface's characteristics [51]. Another explanation supported the idea that the increased CO<sub>2</sub> capture capability results from acid-base interactions between basic functional groups containing nitrogen as heteroatom, and acidic CO<sub>2</sub> [52]. Despite several ideas and various simulation methods, it appears that the precise process of adsorption on various adsorbents is still complicated and requires more investigation.

### 3. Development of CO<sub>2</sub> solid sorbents

As compared to traditional separation approaches for CO<sub>2</sub> capture, adsorption procedures utilizing innovative solid sorbents that can reversibly adsorb CO<sub>2</sub> from flue gas offer numerous potential benefits, such as lower energy for regeneration, more capacity, high N<sub>2</sub>/CO<sub>2</sub> selectivity, and ease of handling. It is crucial to keep in mind that an average flue gas from a fossil fuel-fired power plant contains 8–10% H<sub>2</sub>O. The presence of water vapor is capable of reducing the CO<sub>2</sub> adsorptive capacity owing to competing electrostatic interactions and dispersion-repulsion interactions with the surface [53,54]. As a result, the most crucial variable in the solid adsorbent process is the selection of the best sorbent for specific conditions. High separation, fast adsorption kinetics, gentle regeneration conditions, thermal stability, chemical stability, and mechanical stability in the long-term adsorption-desorption cycle are all requirements for an effective sorbent [55]. Every adsorbent has flaws that prevent its usage in the separation process. For instance, due to its microporous nature, zeolite has some downsides such as low diffusion and pore blockage. Additionally, the calcination procedure occasionally has problems including high costs and the inclusion of impurities including feldspar, and quartz [56]. Because of its high capacity for gas uptake and customizable porosities that can enable highly selective binding of CO<sub>2</sub>, MOFs have gained significant interest in CO<sub>2</sub> capture [57–59]. However, the MOF preparation process is more time-consuming, and expensive, making industrialization challenging. The MOF's moisture sensitivity throughout the CO<sub>2</sub> sorption process puts its framework at risk of failure [60–62]. Additionally, it is still problematic to customize MOFs for employment in the adsorption process by changing their S<sub>BET</sub> and pore volume, as well as their surface chemistry (acid-base characteristics and functional groups) [63].

Due to their high specific surface areas (up to 3400 m<sup>2</sup> g<sup>-1</sup>), customizable surface characteristics, strong chemical-thermal stabilities, and low prices, porous carbons (commonly referred to as activated carbon) have drawn a lot of interest as the cheapest carbon-based materials [64]. However, this adsorbent cannot be used for large-scale applications due to the low selectivity and sorption capacity of CO<sub>2</sub> and N<sub>2</sub>, which can be improved using modification techniques such as impregnation, grafting, functionalizing with amine/acid/alkalis/salt groups and doping with heteroatoms. It is worth mentioning that the expensive and cumbersome production technique for these sorbents modified with the aforementioned methods has limited their use. Additionally, their complicated development process and reduced

durability provide new challenges for CO<sub>2</sub> uptake [65]. Also, total pore volumes can be restricted by the existence of tiny micropores, which is detrimental to the material requirements for pre-combustion CO<sub>2</sub> capture, which typically takes place under high (>20 bar) pressure [66].

Mesoporous silica is suitable for CO<sub>2</sub> uptake due to its high S<sub>BET</sub> and large pore volume. However, it has certain downsides, including difficult functionalizing, and a sporadic particle size distribution [67,68]. For instance, there are two key barriers to commercialization for mesoporous silica created through surfactant templates in synthetic approaches. I) Owing to their lengthy hydrophobic organic groups, ionic and neutral surfactants are costly and have confined biodegradability. II) The economic viability of the synthetic procedures is reduced by the necessity of solvent removal or recovery operations as well as the customary surplus solvent requirement (water or alcohol). Additionally, due to the high vapor pressure of the surplus solvent, high-pressure reactors are required for hydrothermal treatment (tuning pore size) [69].

Another adsorbent is crystalline-structured COFs, which are categorized as porous organic polymers (POPs) and made from blocked monomers with strong covalent bonds. Due to their unique characteristics, such as their large S<sub>BET</sub>, remarkable chemical-physical stability, and crystallinity, COFs are a fascinating sorbent [70,71]. Despite their numerous benefits, the creation of these structures (i.e., solvothermal, ionothermal, and sonochemical) needs costly linkers, specialized monomers, high temperatures, significant amounts of hazardous solvents, and time [72,73].

Considering all of the positive characteristics of solid adsorbents, there are also significant drawbacks to using these sorbents, which should be considered while selecting an optimal adsorbent. The novel adsorbents that have solved the aforementioned issues are explained in depth in the sections that follow, and the variables influencing an upsurge in adsorption are thoroughly examined.

### 3.1. Magnetic nanoparticles

Magnetic nanoparticles (MNP) are capable of responding to an external magnetic field and potentially allowing simple placement/recovery, so the separation energy is less, and raw material input requirements. Owing to low cost and high biocompatibility (i.e. relatively low toxicity), based magnetite has been widely applied in biotechnology, catalysis, and environmental engineering [74–79]. Additionally, magnetic-based nanocomposites have been developed and utilized for their ability to adsorb CO<sub>2</sub>. Decorating MNP like Fe<sub>3</sub>O<sub>4</sub> with graphene oxide, polyaniline [80], chitosan [81], and ZIF-8 [82] results in to access cost-effective synthesis methods of high-performance CO<sub>2</sub> magnetic absorbents with good regenerative properties. Under high pressure, each magnet nanocomposite has demonstrated excellent CO<sub>2</sub> enhancement adsorptive capability, resulting from both adsorption functional groups (from the mesoporous reagent with a high specific area) and Fe<sub>3</sub>O<sub>4</sub> nanoparticles. The easy separation capability of this type of material causes that, in composition with other conventional CO<sub>2</sub> capture like Cu<sub>2</sub>O [83], Ru and CeO<sub>x</sub> [84], etc., it increases the life and reversibility of catalysts in alternating cycles of CO<sub>2</sub> sorption and ensures the economic justification of the use of MNP. In one of the first works regarding the usage of MNP in CO<sub>2</sub> adsorption, reported by Mishra et al. [85], under 12 bar and ambient temperature, the Fe<sub>3</sub>O<sub>4</sub>-MWNT (multi-walled carbon nanotubes) nanocomposite had an adsorption capacity of 0.0594 mol g<sup>-1</sup> while the functionalized-MWNTs (f-MWNTs) had an adsorption capacity of 0.0143 mol g<sup>-1</sup>. The highest adsorption capacity of the nanocomposite and f-MWNTs at 12 bar and 50 °C was 0.0379 and 0.0101 mol g<sup>-1</sup>, respectively. The highest adsorption capacity of the nanocomposite and f-MWNTs at 12 bar and 100 °C was 0.0248 and 0.0097 mol g<sup>-1</sup>, respectively (Fig. 3a). The adsorption capabilities of the f-MWNTs and nanocomposite increase with equilibrium pressure at each temperature, which can be due to the condensation of CO<sub>2</sub> molecules in

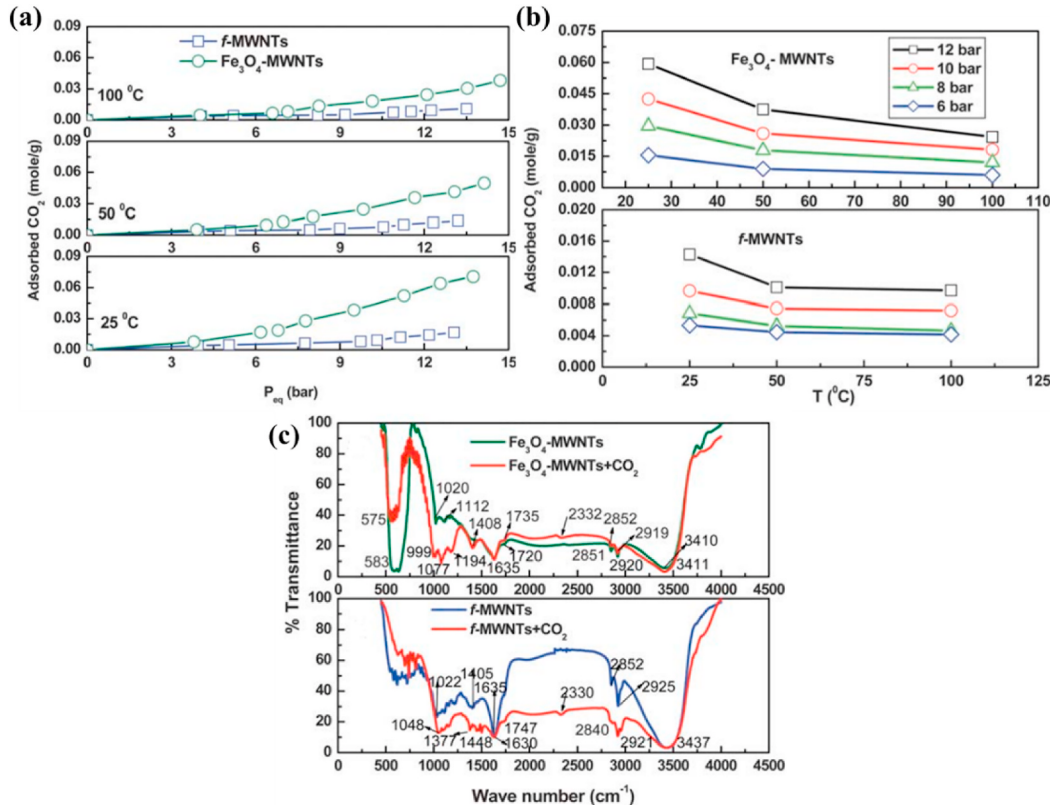


**Fig. 3.** (a) Adsorption isotherms for f-MWNTs and the magnetite-MWNT nanocomposite at different temperatures, (b) Adsorptive capability of f-MWNTs and the magnetite-MWNT nanocomposite at various temperatures, and (c) FTIR spectra of (up) f-MWNTs and adsorbed CO<sub>2</sub> on it, (down) the magnetite-MWNT nanocomposite and adsorbed CO<sub>2</sub> on it. Reproduced with permission from Ref. [85]. Copyright (2011) Royal Society of Chemistry.

mesopores under high pressures (Fig. 3b). The  $\text{Fe}_3\text{O}_4$ -MWNT nanocomposite's ability to adsorb  $\text{CO}_2$  was found to be significantly increased when compared to the f-MWNTs. The increased chemical interaction of  $\text{CO}_2$  molecules with magnetite nanoparticles in the case of the nanocomposite could be responsible for the improvement in  $\text{CO}_2$  uptake capability.  $\text{CO}_2$  molecules might connect to the functional groups in the case of f-MWNTs and then physically adsorb in the pores. In the case of the  $\text{Fe}_3\text{O}_4$ -MWNT nanocomposite,  $\text{CO}_2$  molecules chemically interact with the  $\text{Fe}_3\text{O}_4$  nanoparticles in addition to physical adsorption in pores and attachment with functional groups (chemisorption-physisorption). According to the FTIR spectra (Fig. 3c), this chemical reaction between  $\text{CO}_2$  molecules and  $\text{Fe}_3\text{O}_4$  nanoparticles could result in the creation of iron bicarbonate and iron carbonate, which would boost the nanocomposite's ability to uptake  $\text{CO}_2$  in comparison to f-MWNTs.

According to the FTIR study by Hakim et al. [86] on the  $\text{CO}_2$  adsorption mechanism of  $\text{FeO}$ ,  $\text{Fe}_2\text{O}_3$ , and  $\text{Fe}_3\text{O}_4$ -based magnetic iron oxide, carbonate production on iron oxides was found as a result of the development of bicarbonate, monodentate carbonate, linear and bending  $\text{CO}_2$ , and bidentate carbonate on the surface.  $\text{Fe}_2\text{O}_3$  exhibits all basic sites in the weak, medium, strong, and very strong phases, according to its basicity distribution. Despite having the potential for  $\text{CO}_2$  adsorption,  $\text{Fe}_3\text{O}_4$  is constrained by its stability when adsorbed at higher  $\text{CO}_2$  concentrations, which causes it to oxidize and transform into  $\text{Fe}_2\text{O}_3$ . Additionally, Li et al. [77] developed functionalized amine polymer-modified magnetite nanoparticles. The data obtained showed that polyethyleneimine (PEI) coating enhanced  $\text{CO}_2$  sorption and that PEI had a higher capacity for  $\text{CO}_2$  molecules than any other polymer. In another study, Oddo et al. [87] created magnetic nanoparticles covered with various amino functional groups for  $\text{CO}_2$  capture. All functionalized particles maintained their magnetic characteristics and showed good stability up to 100 °C. Given that MNP showed the highest sorption capability and stability, this is especially pertinent for amino acids. When  $\text{CO}_2$  sorption and particle regeneration were repeated several

times at high temperatures, MNP demonstrated excellent recyclability and stability, losing only 11% of its sorption capacity after four cycles, in contrast to diethylenetriamine functionalized MNP, which saw a drop of more than 30% after just one cycle, indicating that the functional groups were irreversibly degraded during regeneration. The assessment of the relationship between temperature and sorption capacity in the range of 25–45 °C showed that the  $\text{CO}_2$  sorption declined with rising temperature. This outcome supports the theory that amino groups and  $\text{CO}_2$  undergo an exothermic reaction that results in the creation of carbamates or bicarbonates.

In addition to the surface functionalizing of MNP, core-shell structures with MNP core and stable mesoporous shells like  $\text{SiO}_2$  also improve the efficiency of this type of nanoparticles in  $\text{CO}_2$  capture. Guha et al. [88] reported functionalized nitrogen-rich melamine in the pores of mesoporous silica supported on a magnetite core. According to their results, the  $\text{CO}_2$  adsorption reveals that functionalized core-shell nanoparticles rendered a moderately good  $\text{CO}_2$  adsorption capacity (0.48 mmol g<sup>-1</sup>), up to 1 bar pressure, with high selectivity over  $\text{N}_2$  (33 folds). Temperature-dependent  $\text{CO}_2$  adsorption isotherm study suggests a low heat of adsorption ( $\approx 25$ –35 kJ mol<sup>-1</sup>), indicating the physisorption nature of sorption. In addition to the aforementioned magnetite sorbents, other types of magnetic materials have been reported for these applications, including  $\text{CaFe}_2\text{O}_4$ ,  $\text{CaFe}_2\text{O}_5$ ,  $\text{AFeO}_2$  (A = Li, Na), M-doped  $\beta\text{-NaFeO}_2$  (M = Ni or Cu),  $\text{NiO}$ ,  $\text{MgAl}_2\text{O}_4$ , and  $\text{Co}_3\text{O}_4$  [89–94]. Alkaline ferrites have been the subject of several investigations among the MNP used in  $\text{CO}_2$  capture because of their high adsorption capacity and lengthy regeneration cycles.  $\text{NaFeO}_2$  and  $\text{LiFeO}_2$  as two important members of this type of material have been the main focus of studies. Yanase et al. [95] studied on effect of temperature on the adsorption properties of  $\beta\text{-NaFeO}_2$  in the presence of water vapor. According to their results, XRD patterns (Fig. 4a) revealed that  $\beta\text{-NaFeO}_2$  reacted with  $\text{CO}_2$  and  $\text{H}_2\text{O}$  molecules to generate  $\alpha\text{-Fe}_2\text{O}_3$  and  $\text{Na}_2\text{CO}_3\cdot\text{H}_2\text{O}$  (these phases cannot be seen at 75 and 100°). Thus, it was obvious that less  $\text{CO}_2$

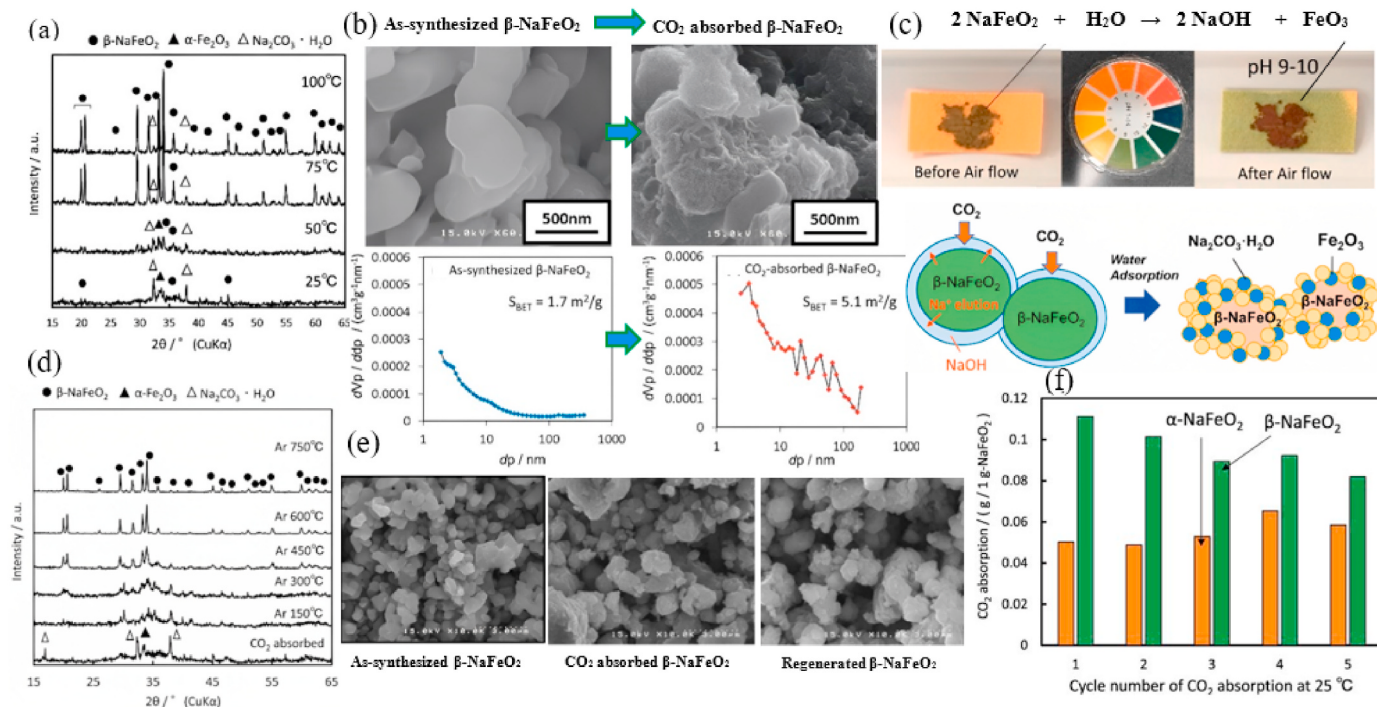


**Fig. 4.** (a) XRD patterns of  $\beta\text{-NaFeO}_2$  adsorbed  $\text{CO}_2$  for 5 h at temperatures of 25, 50, 75, and 100 °C under a  $\text{CO}_2$  in the presence of 80% RH flow, (b) SEM micrographs and Pore size distributions of the  $\beta\text{-NaFeO}_2$  powders before (left) and after  $\text{CO}_2$  adsorption (right) at 25 °C under 80%RH, (c) The  $\text{CO}_2$  adsorption process of  $\beta\text{-NaFeO}_2$  in the presence of water vapor, along with the pH testing of the powder under an air flow with water vapor at 25 °C, (d) XRD patterns of  $\beta\text{-NaFeO}_2$  adsorbent (heated at 150–700 °C for 5 h under an Ar gas flow), (e) SEM micrographs of as-synthesized, adsorbed  $\text{CO}_2$ , and regenerated  $\beta\text{-NaFeO}_2$ , respectively, left to right in the presence of water vapor at 25 °C, and (f) Effects of cycling  $\text{CO}_2$  adsorption/desorption on the ability of  $\beta\text{-NaFeO}_2$  (green) and  $\alpha\text{-NaFeO}_2$  (orange) to adsorb  $\text{CO}_2$  in the presence of water vapor (80%RH) in the air at 25 °C. Reproduced with permission from Ref. [95]. Copyright (2019) Elsevier.

was sorbed because of  $\beta\text{-NaFeO}_2$  decomposition to iron oxide and sodium carbonate. Changing the morphology of  $\beta\text{-NaFeO}_2$  powder (Fig. 4b) after  $\text{CO}_2$  uptake at 25 °C and 80%RH resulted in increasing the specific surface area (from 1.7  $\text{m}^2 \text{ g}^{-1}$  to 5.1  $\text{m}^2 \text{ g}^{-1}$ ) and the pore volume. The pH tests (Fig. 4c) revealed that the  $\beta\text{-NaFeO}_2$  powder was dark green before exposure to water vapor and  $\text{CO}_2$ , but became dark red after adsorbing  $\text{CO}_2$ , showing that  $\alpha\text{-Fe}_2\text{O}_3$  was generated after  $\text{CO}_2$  capture. In addition, the pH paper's color changed to yellowish green, showing that the pH increased to 9–10 because of  $\text{CO}_2$  adsorption in the presence of water vapor. The pH shift was probably brought on by the surface of the  $\beta\text{-NaFeO}_2$  particles forming a basic solution. The presence of single phase  $\beta\text{-NaFeO}_2$  after heating the adsorbent powder under argon flow at 600–750 °C for 5 h (Fig. 4d) indicated regeneration of  $\beta\text{-NaFeO}_2$  at this situation, that this reversibility is not observed at lower temperatures. By adsorbing  $\text{CO}_2$  on the surface of powder and even after regeneration of adsorbent, particles grew (according to SEM micrographs) owing to water vapor and adsorption/desorption cycles in regeneration processes (Fig. 4e). For the first adsorption cycle,  $\text{CO}_2$  adsorption of  $\beta\text{-NaFeO}_2$  at 25 °C for 5 h in the presence of water vapor (80%RH) was around 0.11 g (Fig. 4f). As the cycle number was increased to 5, the capacity of  $\beta\text{-NaFeO}_2$  gradually reduced to approximately 0.08 g.

### 3.2. Carbon-based nanostructures

C-based materials are a significant class of adsorbent for  $\text{CO}_2$  uptake because they offer several advantages, including superb moisture resistance because of their hydrophobic surfaces, high thermodynamic/mechanical stability, tunable porous structures, relatively low energy efficiency for recycling use, and, foremost, an inexpensive supply of precursors [96]. A carbon monolayer packed into a honeycomb lattice, known as graphene, has shown to be an interesting material with a variety of prospects for new technology advancements and scientific discovery [97–99]. The sorption/desorption isotherms displayed

significant hysteresis, indicating powerful electrostatic interactions among the polar  $\text{CO}_2$  molecules and unsaturated  $\text{sp}^2$  bonds close to the edge of the graphene plane [100]. The usage of pristine graphene can be in the form of oxidized, integrated with amine groups, or composite since it typically exhibits moderate adsorption [101]. A 3D porous graphene aerogel (GA) was recently created by Wu et al. using a one-pot hydrothermal method and freeze-drying which possessed 2.27  $\text{mmol g}^{-1}$  at 25 °C under 0.1 bar (Fig. 5a). The organic amine reagents (TEPA), which have a lot of amino groups, functioned as both a cross-linker for linking the graphene oxide (GO) sheets and as adsorption sites to more effectively adsorb  $\text{CO}_2$ . As can be seen in the SEM micrographs (Fig. 5b–c), the aerogels had three-dimensional porous morphology whereas the GO exhibited severe agglomeration. Their findings indicated that the presence of water could boost the amount of  $\text{CO}_2$  sorption because water directly contributed to the interaction between  $\text{CO}_2$  and amine which produced bicarbonates. Under dry conditions, according to former literature, it appears that 2 mol of amino groups are needed to sorb 1 mol of  $\text{CO}_2$  ( $\text{CO}_2 + \text{RNH}_2 = \text{NH}_4^+ \text{R}_2\text{NCOO}^-$ ), but only 1 mol of amino groups is required under wet conditions ( $\text{CO}_2 + \text{R}_1\text{R}_2\text{NH} + \text{H}_2\text{O} = \text{R}_1\text{R}_2\text{NH}_2^+ + \text{HCO}_3^-$ ) [102,103]. The fabrication of CuBTC@GO,  $\text{TiO}_2$ @GO, and MOF@GO composites provides an effective adsorbent to improve  $\text{CO}_2$  adsorptive capability. According to simulation and DFT studies, due to the additive GO's high atomic density and the population of oxygen-functionalities on its graphitic skeleton, these composites exhibit enhanced porosity and dispersion forces. Fig. 5 d illustrates the great distribution of  $\text{TiO}_2$  on GO nanosheets, for instance. In the composite with the greatest GO concentration (Fig. 5e), the  $\text{TiO}_2$  particles formed larger, stiffer agglomerates on top of the GO nanosheets [104, 105]. Additionally, GO is an appealing option to be utilized as a nano-filler in mixed-matrix membranes that diminish polymer chain mobility and lengthen the complicated path of gas diffusion in the polymer matrix. Enhancing gas diffusivity selectivity has been proven in this way smaller molecules with less resistance will diffuse more readily, and larger ones will be constrained [106]. As shown in Fig. 5 f, Luan et al.

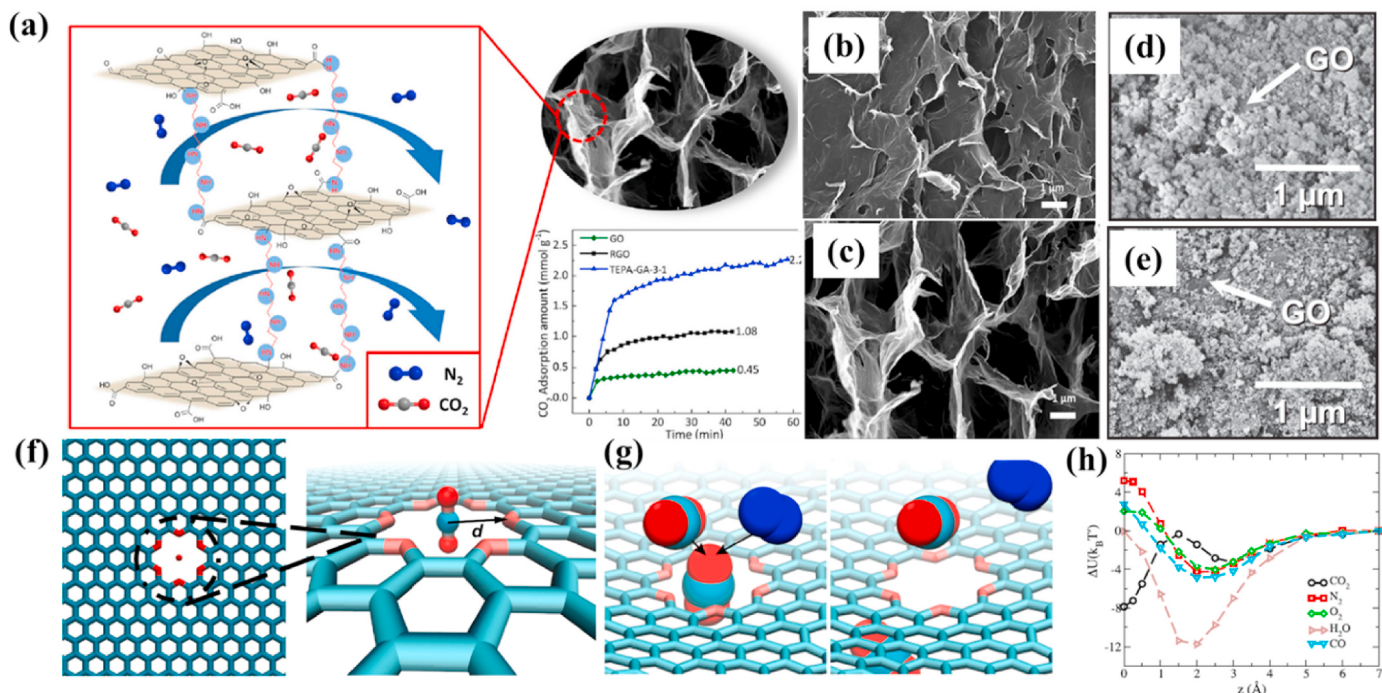


**Fig. 5.** (a) Schematic of 3D porous graphene aerogel for  $\text{CO}_2/\text{N}_2$  selectivity, (b–c) FESEM micrographs of three-dimensional porous morphology of graphene aerogel. Reproduced with permission from Ref. [102]. Copyright (2022) Springer Nature. (d–e) Distribution of  $\text{TiO}_2$  on GO nanosheets Reproduced with permission from Ref. [105]. Copyright (2015) Elsevier. (f–g) (f–g) crown-nanopore embedded in graphene with a sorbed  $\text{CO}_2$  (red-cyan) molecule and repulsed  $\text{N}_2$  (blue) from top and side view, and (h)  $E_{\text{ad}}$  energies for  $\text{CO}$ ,  $\text{N}_2$ ,  $\text{O}_2$ ,  $\text{CO}_2$ , and  $\text{H}_2\text{O}$  molecules versus distances to the crown pore. Reproduced with permission from Ref. [107]. Copyright (2022) American Chemical Society.

simulated O-crown nanopores (like crown ethers) incorporated into graphene that could effectively permit CO<sub>2</sub> to flow and block other flue gases (CO, N<sub>2</sub> (Fig. 5g), O<sub>2</sub>, and H<sub>2</sub>O). According to Fig. 5 h, analysis of the potential energy as a function of distance, CO<sub>2</sub> was the only gas to reach a potential minimum when its center of mass was on the graphene plane ( $z = 0$ ). All other gas molecules that were taken into consideration faced a barrier. Thus, CO<sub>2</sub> is efficiently sorbed to the center of the O-crown pores whereas other molecular species are repelled by them. The electrostatic attraction between the crown pore and the C-atom in the center of the CO<sub>2</sub> molecule overcomes the electrostatic repulsion between the O-crown pore and two oxygen atoms in the CO<sub>2</sub> [107].

The simulations indicate that fullerene (C<sub>60</sub>) adsorbents, like graphene, have a low capacity for adsorption in their unmodified state. On this subject, the interactions of CO<sub>2</sub> with pure, Li-, Na-, and Ca-doped C<sub>60</sub> systems were modeled by Gao et al. The findings demonstrated that CO<sub>2</sub> sorption on pure C<sub>60</sub> was extremely low. Among the aforementioned substances, the sorption of CO<sub>2</sub> on C<sub>60</sub> was greatly improved when C<sub>60</sub> was doped by a Ca atom because this raised the dipole moment of C<sub>60</sub> and the electrostatic interaction between adsorbate and adsorbent. The energy difference between the Ca–C<sub>60</sub>–CO<sub>2</sub> cluster and the CaC<sub>60</sub> and CO<sub>2</sub> was determined to be  $-0.637$  eV, which was significantly higher than on the pristine C<sub>60</sub> ( $E_{ads} = -0.037$  eV), as can be shown in Fig. 6 a (the stable simulated structure) [108].

With heptazine units joined by amino groups in the plane and a weak van der Waals force between layers, the novel form of adsorbent g-C<sub>3</sub>N<sub>4</sub> has a layered structure resembling graphite. G-C<sub>3</sub>N<sub>4</sub> nanosheets have built-in nanopores in the plane and are very amine-rich, which promotes the selective transport of CO<sub>2</sub> molecules [111,112]. Additionally, the atomic thickness of this adsorbent in membranes can reduce transport resistance, and interlayer channels or intrinsic porosities ( $\leq 1$  nm) can offer quick and precise paths for tiny molecules [113,114]. Cheng et al. recently added g-C<sub>3</sub>N<sub>4</sub> to a Pebax membrane for CO<sub>2</sub> separation. This

compound was synthesized from dicyclodiamide under 2, 4, and 6 h thermal etching. Unlike porous g-C<sub>3</sub>N<sub>4</sub> nanosheets (DCN-6), as shown in Fig. 6 b, multi (DCN-2) or few-layer g-C<sub>3</sub>N<sub>4</sub> (DCN-4) could improve the CO<sub>2</sub>/N<sub>2</sub> selectivity, whereas g-C<sub>3</sub>N<sub>4</sub> with fewer/thinner layers had lower transport barriers, which resulted in higher CO<sub>2</sub> diffusion. Due to the overly large nanopores that appeared on the nanosheet, the gas routes were shortened, but subsequently, the separation of CO<sub>2</sub> over N<sub>2</sub> was reduced [109].

The development of a new class of materials would appear to be preferable given the difficult synthesis of g-C<sub>3</sub>N<sub>4</sub>. One of the intriguing materials with distinctive adsorption characteristics is porous boron carbon nitride (BCN), owing to the presence of B–C bonds. However, it is difficult to synthesize low-cost porous BCN with customizable porosity because the B–C bond can only form at extremely high temperatures [115]. Bahadur et al. [110] developed BCN-conjugated nanoporous carbons that possessed S<sub>BET</sub> as high as  $2991\text{ m}^2\text{ g}^{-1}$  and an adsorption capacity of  $23.25\text{ mmol g}^{-1}$  ( $0^\circ\text{C}$  under 30 bar). Fig. 6 c shows that in this process, aminoguanidine, a precursor with a high N-content, was incorporated at  $900^\circ\text{C}$  with boric acid, casein, and potassium acetate. SEM/TEM micrographs of the optimum sample (Fig. 6d-g) revealed a non-uniform sponge-like porous skeleton with internal porous structures. This type of morphology confirmed that under high pressures, mesopores are crucial to boosting the adsorptive capability. Conversely, at low pressures, basic groups and micropores are more beneficial in the adsorption process.

Due to the intricacy of their synthesis, the high cost of hazardous activators, and the high cost of pricey precursors, the primary issue with newly developed carbon-based adsorbents is that they cannot be employed in industry. It appears that carbon nanotubes (single and multi-walled) and biomass-derived porous carbon can solve this issue. Mixing MWCNTs with different materials, such as SiO<sub>2</sub> particles, causes the development of special physical and chemical features, such as

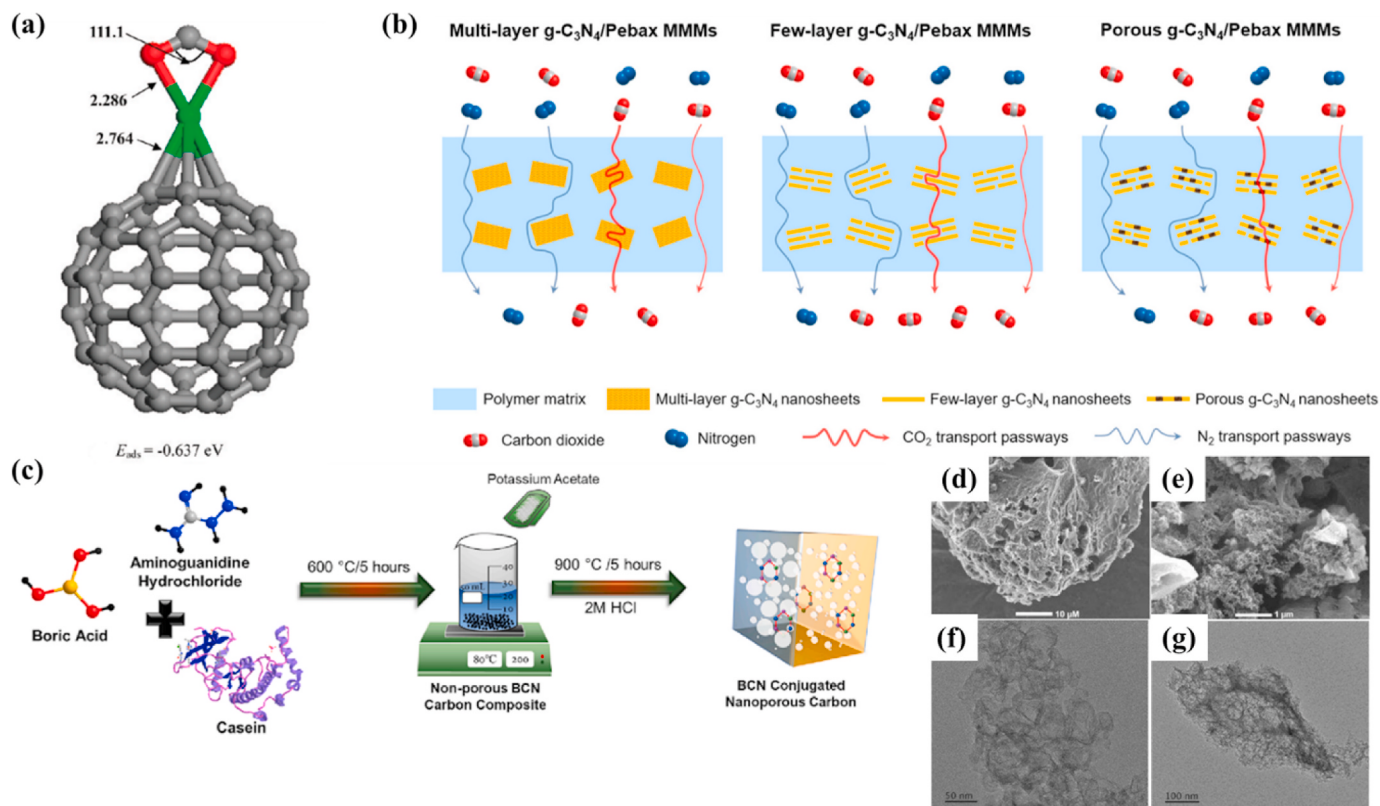


**Fig. 6.** (a) Stable simulated structure of C<sub>60</sub> for CO<sub>2</sub> capture. Reprinted with permission from Ref. [108]. Copyright (2011) American Chemical Society. (b) Schematic of multi-layer, few-layer, and porous g-C<sub>3</sub>N<sub>4</sub>/Pebax membrane for CO<sub>2</sub> separation. Reprinted with permission from Ref. [109]. Copyright (2020) Elsevier. (c) Process of BCN synthesis at  $900^\circ\text{C}$ , and (d–g) SEM/TEM micrographs of porous BCN. Reproduced with permission from Ref. [110]. Copyright (2023) Elsevier.

excellent dispersibility and high pore volume, which are related to an increase in the rate of sorption [116]. For instance, in research done by Lee and Park [117], MWCNTs were coated with  $\text{SiO}_2$  and Polyethylenimine (PEI). The prepared sorbent under specific conditions (15 vol%  $\text{CO}_2$ ,  $\text{N}_2$  balance,  $T_{\text{ads}} = 60^\circ\text{C}$ ) demonstrated an outstanding  $\text{CO}_2$  uptake of around 2.85 wt% when the PEI loading was 50 wt%, in contrast to the unmodified structure with poor adsorption capacity. The heightened affinity between  $\text{CO}_2$  and the amine groups (acid-base interaction) caused by a greater abundance of sites for  $\text{CO}_2$  sorption was the cause of this high adsorption capacity [118]. Fig. 7a illustrates the process of  $\text{CO}_2$  sorption on modified MWCNT based on acid-base interaction. The temperature is slightly raised by heat release from sorption in an exothermic mechanism. Consequently, it is anticipated that the transition of amine groups (carbamate) will cause a decrease in

regeneration ability [119]. The primary drawback of amine-functionalized CNTs is that their practical application in the field is now constrained by their rather expensive cost. It is therefore necessary to regenerate the amine-functionalized CNTs via a series of regeneration cycles before their actual application is realistic [120].

Using liquefied larch sawdust as the carbon precursor, Zhang et al. [121] recently developed hierarchically porous MWCNTs/carbon foams (MCF) nanocomposites by in-situ polymerization, foaming, and pyrolyzation, featuring a lot of ultra-micropores and mesopores. MWCNTs integrated into the foam greatly boosted the compressive strength (Fig. 7b) of the CF as high as 0.07 MPa (113%), as well as the degree of graphitization ( $I_D/I_G = 0.88$ , Fig. 7c). Due to the existence of ultra-micropores, the optimal sample (MCF-2 wt%) demonstrated significant  $\text{CO}_2$  sorption capacities of 4.58 and 3.19 mmol g<sup>-1</sup> at 0 and

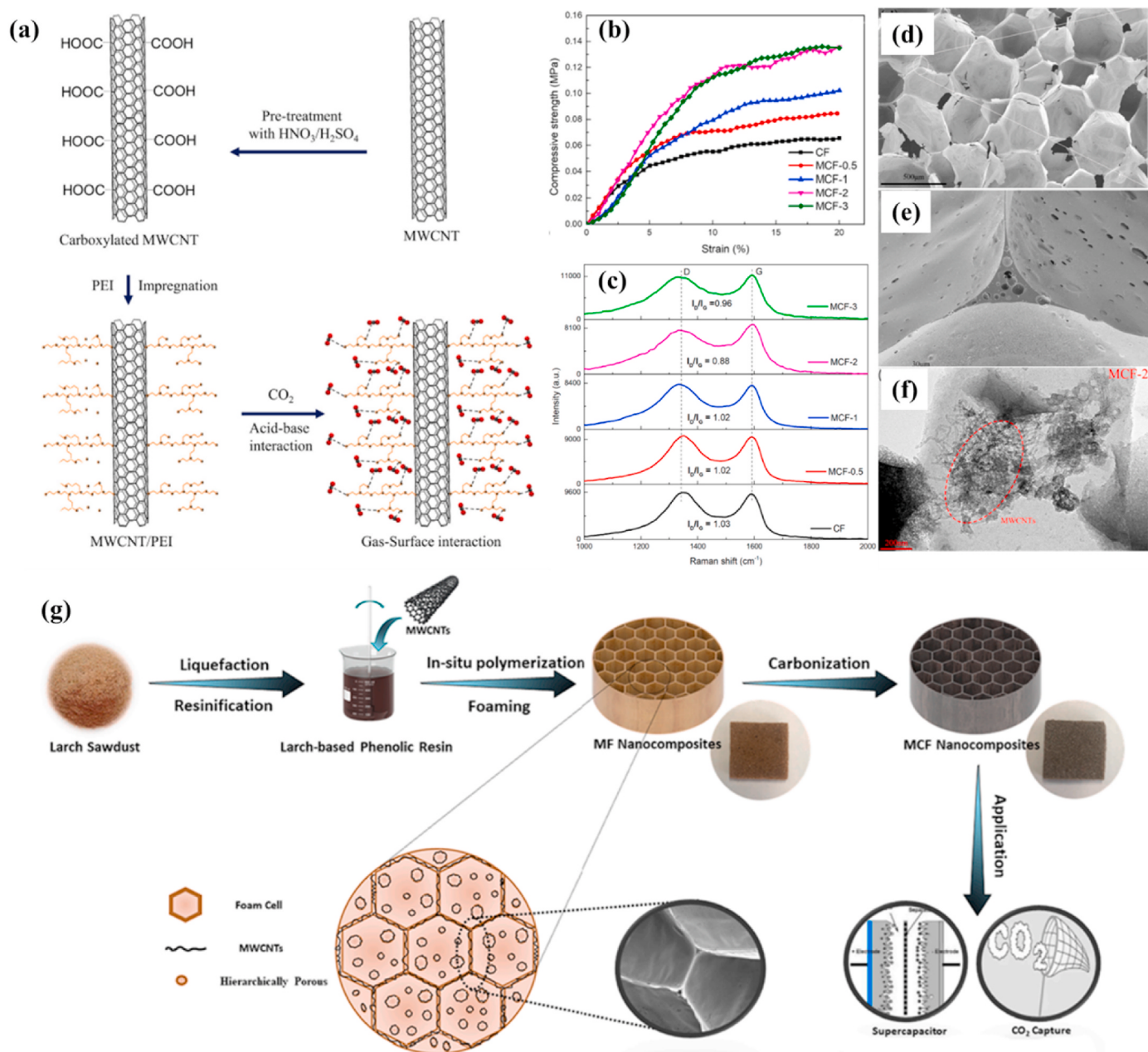
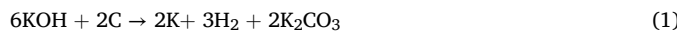


**Fig. 7.** (a) Mechanism of  $\text{CO}_2$  uptake on amine-riched MWCNT based on acid-base interaction. Reprinted with permission from Ref. [119]. Copyright (2015) Elsevier. (b) Compressive strength of prepared MWCNTs/carbon foams (MCF). (c) Raman Spectroscopy of various MCF. (d–e) SEM micrographs of cell-like MCF-2 wt %. (f) TEM images of MCF-2 wt %. (g) synthetic procedure of porous MWCNTs/carbon foams. Reproduced with permission from Ref. [121]. Copyright (2021) Elsevier.

25 °C, respectively. The cell frameworks of the MCFs were roughened in certain particles, as evidenced by SEM micrographs (Fig. 7d-e), and MWCNTs were observed to be embedded/dispersed in the CF matrix by TEM analysis (Fig. 7f). However, as can be seen in Fig. 7 g, the time-consuming and expensive synthetic procedure employed to create these MCF nanocomposites limited their commercial use.

Because of their inexpensive price, tailororable pore arrangement, plentiful surface functional groups, and abundance of C-based precursors in nature, porous carbons (derived from biomass or synthetic precursor) are the most common carbon-based sorbents nowadays. Conventional ways of producing porous carbon need some form of activation, either physical or chemical. CO<sub>2</sub>, steam, NH<sub>3</sub>, and N<sub>2</sub>/Ar are employed as activating agents in physical activation, whereas alkaline and acid solutions (KOH, ZnCl<sub>2</sub>) are utilized in chemical activation at high temperatures [122,123]. Furthermore, novel methods of porous carbon carbonization/activation, such as self-activation, soft and hard templates, hybrid dual-template, plasma, and microwave, have been able to replace traditional approaches [45,124]. The prevalence of porous carbon among other adsorbents can be attributed to the range of production methodologies [125,126]. The most used chemical reagent for creating porous carbons is KOH. Numerous studies have shown that KOH, a strong base, increases the creation of pores and provides high S<sub>BET</sub>, which are the two key factors in determining an adsorbent's effectiveness. During the pyrolytic process, it engages in a series of chemical reactions with the lignocellulosic biomass (cellulose, hemicellulose, and lignin), including decomposition, dehydration, polymerization, and aromatization [40]. A considerable quantity of micropores is introduced into the carbon skeleton during the chemical reaction that is responsible for this activation/carbonization process, as indicated by Eq. (1) [127]:



Recently, Yu et al. [128] synthesized N-riched porous carbon by chemically activating (KOH as reagent) commercial melamine formaldehyde resin (MF), which had a high N content of 16.07 wt% and an S<sub>BET</sub> as high as 1658 m<sup>2</sup> g<sup>-1</sup>. The best sample demonstrated a CO<sub>2</sub> uptake up to 4.95 and 3.30 mmol g<sup>-1</sup> at 0 and 25 °C under 1 bar, respectively. This uptake was directly related to S<sub>BET</sub> and N content. ZnCl<sub>2</sub> is a metal salt

that works as a potent dehydration reagent to prevent tar from forming, which typically does during the heat treatment process and then builds up in the newly produced pores [129]. Zhang et al. [130] used ZnCl<sub>2</sub> as a reagent to synthesize highly efficient hollow polyhedral cellular cork-based porous carbon with uniform micron-sized honeycomb cells and numerous meso and micropores. Findings indicated that the ideal sample had an adsorption capacity of 4.64 mmol g<sup>-1</sup> at 0 °C, with some physico-chemical properties such as high carbon yield (>80 wt%), high S<sub>BET</sub> (up to 1853 m<sup>2</sup> g<sup>-1</sup>), and high pore volume (up to 0.839 cm<sup>3</sup> g<sup>-1</sup>). The resultant porous carbon retained the pretreatment cork's honeycomb microstructure, as seen in Fig. 8a-b. Additionally, HRTEM analyses of cell walls revealed an abundance of micropores, as seen in Fig. 8 c. These micropores in porous carbon skeletons have a major impact on adsorption [131]. The results showed that surface functional groups, as a complementary of microporous/ultra-microporous, contributed around 40% to the CO<sub>2</sub> sorption process. It has been noted that the addition of heteroatoms (B, N, S, and O) enhanced surface alkalinity and possessed stronger electronegativity, which in turn increased the CO<sub>2</sub> uptake [132]. The most prevalent heteroatom, nitrogen, can be incorporated into the structure of carbon using one of two methods: (i) impregnating with nitrogen-containing activators (like pectin, melamine, urea, and paraphenylenediamine); or (ii) creating porous carbon from polymers that contain nitrogen and heating it with gaseous NH<sub>3</sub>. Nitrogen (especially N-pyridinic, because it has a lone pair of electrons, therefore demonstrates stronger basicity) can elevate basicity and surface polarity to increase adsorptive capability; nonetheless, in some cases, it can block the pores and reduce the capacity of porous carbon [133–136]. By KOH activator, Ma et al. [137] developed N-doped porous carbon from cylindrical rod-like polyacrylonitrile fiber (Fig. 8d), and this sorbent had the maximum CO<sub>2</sub> uptake of 3.95 mmol g<sup>-1</sup> at 25 °C under 1 bar pressure. Fig. 8e-h illustrated that when the KOH/PC mass ratio was 1, the obtained samples maintained fiber skeleton, but the fiber length decreased as the activation temperature rose (from 550 to 700 °C). Due to KOH activation, the fibrous morphologies were destroyed when the KOH/PC mass ratio rose from 1 to 2, and the as-obtained sorbents displayed irregular particles, as illustrated in Fig. 8 i. The carbon lattices can expand and produce more porosity as a result of the potassium penetration. Furthermore, there doesn't appear to be a connection between nitrogen concentration and adsorption rate. For

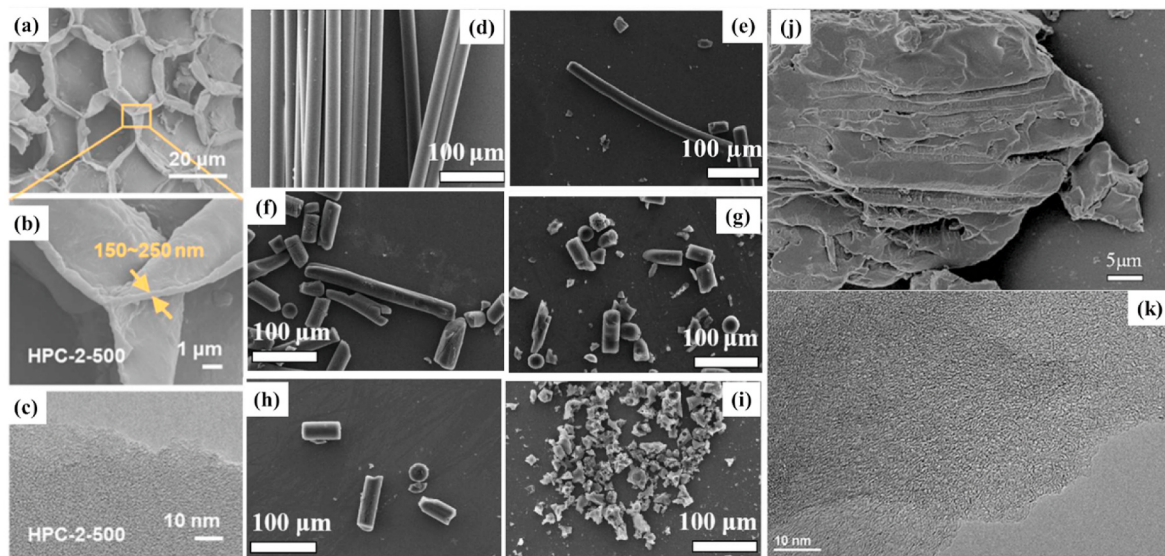


**Fig. 8.** (a–c) FESEM and HRTEM micrographs of pretreatment cork's honeycomb microstructure and obtained porous carbon utilizing ZnCl<sub>2</sub>. Reproduced with permission from Ref. [130]. Copyright (2022) Elsevier. (d) FESEM of cylindrical rod-like polyacrylonitrile fiber, (e–i) developed N-doped porous carbon resulted from polyacrylonitrile fiber in various temperatures (from 550 to 700 °C) and mass ratios. Reproduced with permission from Ref. [137]. Copyright (2023) Elsevier. (j–k) SEM and TEM micrographs of self-sulfur-doped porous carbon obtained from high-sulfur content petroleum coke. Reproduced with permission from Ref. [139]. Copyright (2023) Elsevier.

instance, the sample with 2.83% nitrogen, has the same potential to adsorb (5.72 mmol g<sup>-1</sup> at 0 °C) as the sample with 9.84% nitrogen (5.61 mmol g<sup>-1</sup> at 0 °C). As a result, finding the optimal KOH/PC mass ratio and achieving the optimum amount of nitrogen appear to be functioning in conjunction to improve the adsorption capacity [138].

Recently, Bai et al. [139] developed self-sulfur-doped porous carbon from high-sulfur content petroleum coke using KOH as a reagent at 650 °C with a mass ratio of 3. As a result of the synergistic impact of the narrow micropore volume and S-functionality, this material showed the maximum CO<sub>2</sub> adsorption of 5.57 mmol g<sup>-1</sup> at 0 °C under 1 bar pressure. According to SEM micrographs (Fig. 8j), this sorbent with uneven blocks had a macroporous structure, and a large amount of disorganized micropore structure, as seen in Fig. 8 k (a TEM image). The fast transmission and penetration of CO<sub>2</sub> inside the carbon scaffolding is greatly facilitated by this macropore morphology. Furthermore, S-doping dramatically enhances the surface basicity and surface polarity of the carbon structure due to the stronger electronegativity of sulfur atoms rather than carbon, which improves the CO<sub>2</sub>-sorbent interaction [51, 140]. However, it seems that co-doping can be more successful than single-element doping, at least according to the findings of the DFT. Results show that E<sub>ad</sub> value of sorbed CO<sub>2</sub> on the edge of the pyrrolic-nitrogen (N-5) and O-containing functional groups (C=O, -C-O-C, -OH, and COOH) co-doped carbon surface rises [141].

Another approach for boosting adsorptive capability is metal impregnation (such as iron, magnesium, or cobalt), which involves immersing biomass or carbon-based materials in metal salts or metal oxides. More adsorption sites can become available as a result of the metal ions being bonded to the surface or interior of porous carbons after the impregnation. One of the best metals used to generate metal-carbon composites for CO<sub>2</sub> uptake is magnesium (Mg). At low temperatures, MgO is advantageous for CO<sub>2</sub> sorption. The following equation describes the reaction [142,143]:



The findings of Zhu et al. [144] indicated that metal-dopants existing in the form of metal cations could improve the binding of CO<sub>2</sub> to carbon bonds through electrostatic interactions and Lewis basicity.

The order of porosity also improves CO<sub>2</sub> uptake in addition to the factors previously mentioned (pore volume, size of porosity, heteroatoms, metal-doping, and activator/PC mass ratio) to enhance the sorption. OMCS (ordered mesoporous carbons), which are often synthesized using either soft templates (Pluronic F127, P123) or hard templates (SBA-15 and SBA-16), have found several uses in a variety of sectors, including adsorption and separation. The textural characteristics of these porous carbons were tuned using the different weight ratios of the precursor and block copolymer, which resulted in the creation of ultramicropores [145]. Order-meso structures not only have the maximum sorption but also the highest separation of CO<sub>2</sub>/N<sub>2</sub>. This separation interaction is due to the larger quadrupole moment and polarizability of CO<sub>2</sub> compared to N<sub>2</sub>, which are 2.85 and 1.5 times higher, respectively [146].

### 3.3. Zeolites

Zeolites are crystalline minerals composed of aluminum (Al) and silicon (Si) compounds, known for their porous framework and versatility in commercial applications as ion-exchange matrices, adsorbents, and catalysts [147]. Altering the chemical structure of these frameworks by substituting a portion of the Si atoms with Al or other tetrahedral atoms results in a discernible modification of zeolites' characteristics. This modification influences how the framework interacts with various materials, providing an opportunity to tailor their ion-exchange properties and create distinct adsorbent surfaces. Due to the unique three-dimensional arrangement of these tetrahedral atoms, this substitution generates a variety of structures, including rings, cages, channels,

and pores, leading to the formation of diverse zeolite frameworks [148]. Zeolites can be customized to possess attributes such as a significant surface area, the ability to selectively capture gases, the capacity for regeneration, thermal stability, environmental compatibility, and sustained performance for extended periods in gas adsorption applications [149]. The presence of negatively charged aluminosilicates frameworks and aluminum's strong affinity to oxygen can result in the entrapment of CO<sub>2</sub> within the structure [149,150]. As the substitution's oxidation state decreases (e.g. Al (+3) Vs. Si (+4)), it results in an increase in negative charges, ultimately giving rise to cationic active sites [150]. The kinetic diameter of CO<sub>2</sub> (0.33 nm) requires small and fine-tuned pore structures with at least 8 members of Si/Al in the rings where the diffusion and pore distribution will play important roles. As the size of the pore or wall expands, a combination of gases is more likely to infiltrate the structure and become capable of being adsorbed through the mechanism of electrostatic interaction. Thus, it is crucial to consider the topology and interconnection of pores and channels, as these elements vary significantly across different frameworks [151]. The flexibility of structure under low pressure leads to a critical point in the adsorption isotherm where the size and interconnection of pores increase. The dimensions of the zeolite's pores, as well as its overall internal space, are influenced by the radius of the inserted cations [152]. In practical cases like flue gases, the amount of water content is crucial for better CO<sub>2</sub> capturing as the water will be entrapped by electrostatic interaction and Al atoms. Wang et al. demonstrated a synergic effect of low water vapor content on 5 Å zeolite [153]. The conducted Monte Carlo simulations in low CO<sub>2</sub> concentration showed 0.7–53.4% increased CO<sub>2</sub> adsorption with water concentration below 0.1 ppm whereas the 0.3–5 ppm water vapor resulted from adverse outcomes as the water occupied the space. They indicated the role of electrostatic interaction where the water vapor decreases the selectivity of CO<sub>2</sub> in the CO<sub>2</sub>/(N<sub>2</sub> + O<sub>2</sub>) system.

Further improvements of zeolite properties are contributed to the modified zeolite structures by utilizing zeolite templated carbons (ZTC) [154], metal-organic frameworks (MOFs)/Zeolite composites [155], amine functionalization [156], ion-exchange [156], acid/base-based modifications [154] and thermal treatment [154]. Lestari et al. synthesized Indonesian activated natural zeolite (ANZ)/MOF-type Materials of Institute Lavoisier (MIL-100(Fe)) composite by ultrasonic-based ex-situ method [155]. The CO<sub>2</sub> adsorption capacity of MIL-100(Fe), ANZ, and ANZ/MIL-100(Fe) 20 wt% composites were 1.413, 2.756, and 7.009 mmol g<sup>-1</sup> under 2 bar pressure and temperature of 25 °C, respectively. Liang et al. utilized amine-functionalized HY zeolite for hot flue gas adsorption [156]. The 20% monoethanolamine (MEA) and 20% ethylenediamine (ED) immobilization on zeolite demonstrated actual amine loading of 16.79% and 14.98%, respectively. The CO<sub>2</sub> adsorption capacity was measured at 0.98 and 1.76 mmol g<sup>-1</sup> for 20% MEA@HY and 20% ED@HY zeolites under a temperature of 90 °C and a CO<sub>2</sub> flow rate of 30 mL min<sup>-1</sup>, respectively. The N<sub>2</sub> adsorption capacity was measured at 0.027 mmol g<sup>-1</sup> for both 20% MEA@HY and 20% ED@HY zeolites under a temperature of 60 °C. The results indicated CO<sub>2</sub>/N<sub>2</sub> selectivity and thermal stability of the amine-modified zeolites. Furthermore, cyclic adsorption/desorption at the temperature of 90 °C showed immobilized amine. The amine immobilization decreased S<sub>BET</sub> as the amine groups blocked the micropores of zeolite. In comparison, the enhanced immobilization of the ED was due to its possession of dual amino groups, which formed strong ionic bonds with the Brønsted acid sites present in the XY zeolite. Wahono et al. utilized a simple radio frequency (RF) plasma polymerization and anchoring of allylamine polymer on mordenite-clinoptilolite zeolite [157]. The sorption capacity of zeolite and amine@zeolite were 0.32 and 0.31 mmol g<sup>-1</sup>, respectively. The normalized adsorption based on specific surface area indicates the affinity of the amine@zeolite for CO<sub>2</sub> uptake. Wang et al. synthesized zeolite-doped amine-modified aerogels by utilizing SiO<sub>2</sub>-Al<sub>2</sub>O<sub>3</sub>-ZrO<sub>2</sub> aerogel [158]. The composite demonstrated an adsorption capacity of 5.33 mmol g<sup>-1</sup>. Utilizing light-responsive materials for photocatalytic adsorption of CO<sub>2</sub> demonstrated promising results under

sunlight irradiation. During exposure to solar radiation, the  $\text{CO}_2$  adsorption rates for the  $\text{TiO}_2/\text{synthetic zeolite}$  and  $\text{TiO}_2/\text{natural clinoptyllite zeolite}$  composites significantly escalated from initial values of 21.1% and 28.4% to remarkably elevated levels of 61.8% and 78.9%, respectively [159].

Indira et al. synthesized hierarchical zeolite A by utilizing eco-friendly hydrothermal and freeze-drying methods (Fig. 9a) [160]. They compared freeze-dried (FDZA) and conventional oven-dried (ODZA) samples in which FDZA had increased surface area (IV-type adsorption-desorption isotherm with H4 hysteresis loop), and pore volume (Fig. 9e) and decreased particle size (Fig. 9c). As shown in Fig. 9b, the crystalline zeolite A possessed crystallite size of 52.71 nm and 57.07 nm for FDZA and ODZA, respectively. The hierarchical structure of FDZA has more spherical morphology (Fig. 9c1-4) as the freeze-drying was applied by the ice-templating method. FDZA method inhibited the solvent-zeolite contact where the sublimation of ice content generates a layered structure (Fig. 9c1-4) and decreased the crystallite size and particle size. Resulted sample from FDZA had better  $\text{CO}_2$  adsorption ( $1.3 \text{ mmol g}^{-1}$ ) at higher pressures, faster adsorption rate at  $25^\circ\text{C}$ , and stronger interaction with  $\text{CO}_2$  ( $Q_{st} = 29.29 \text{ kJ mol}^{-1}$ ) (Fig. 9d). As depicted in Fig. 9f, the mechanism of intra-crystalline mesopores in freeze-drying is illustrated which generates the hierarchical structure of the zeolite. In TGA analysis, the FDZA demonstrated an initial weight loss of 12.5% up to  $250^\circ\text{C}$  and 2% in the range of  $250\text{--}500^\circ\text{C}$  which corresponded to the water removal from pores (Fig. 9g). Thus, the FDZA was a hydrophilic (favorable for  $\text{CO}_2$  uptake) zeolite with lower weight loss as the majority of dehydration happened in freeze-drying steps.

#### 3.4. Boron nitride

Hexagonal boron nitride (h-BN), an instance of the two-dimensional material, has a bulk crystal structure that is comparable to that of graphite, and its isolated layer resembles graphene in many ways attributable to its 2D honeycomb structure. In contrast to graphite, the boron and nitrogen atoms' differing on-site energies cause a significant

bandgap (5.97 eV) and a small (1.7%) lattice difference. With its intrinsic high  $S_{\text{BET}}$  and polarity, boron nitride emerges as a strong contender for  $\text{CO}_2$  sorption [161–164]. This importance of high  $S_{\text{BET}}$  arises from the fact that it furnishes a substantial contact region for  $\text{CO}_2$  molecules to engage with the BN material. Consequently, the greater the extent of available surface area, the higher the  $\text{CO}_2$  sorption potential on the material [165,166]. Moreover, Due to its robust chemical stability across various conditions, BN proves ideal for adsorption purposes. It exhibits a minimal reactivity with  $\text{CO}_2$  and other gases, guaranteeing the subsequent desorption of captured  $\text{CO}_2$  and facilitating the reusability of the BN sorbent [167,168]. BN's impressive thermal stability grants it the ability to withstand the high temperatures typically employed in desorption processes for releasing captured  $\text{CO}_2$  [169,170]. BN's inherent polarity, which involves the presence of positively and negatively charged regions, plays a pivotal role in its capability to attract and interact with polar molecules like  $\text{CO}_2$ . This polarity is instrumental in enhancing its adsorption capacity, as it simplifies the process of  $\text{CO}_2$  molecules binding to the BN surface. According to the results, the ability to control the  $\text{CO}_2$  capture and release process can be achieved by a straightforward manipulation of the charges borne by BN nanomaterials, either activating or deactivating them [171]. BN is commonly regarded as safe and non-toxic, a crucial factor in material selection for carbon capture to mitigate environmental and health risks [163,172]. Recently, Choi et al. [173] investigated the potential of boron-rich BN nanotubes (BNNTs) for  $\text{CO}_2$  sorption at room temperature by manipulation of charges utilizing ab initio calculations. They discovered that linear  $\text{CO}_2$  molecule adsorption would commence with a barrier-less physical adsorption process owing to the electron donation from  $\text{CO}_2$  to the double-acceptor defect site, and then transition to the chemical absorption state by breaking one  $\text{C}=\text{O}$  double bond.

The incorporation of carbon significantly improved the materials'  $\text{CO}_2$  adsorption capacity with values ranging from 3.74 to 3.91  $\text{mmol g}^{-1}$  at 298 K and ambient pressure, compared to pure BN materials, which had much lower  $\text{CO}_2$  adsorption [164]. Mighri et al. [174] directed their research towards the development of nanostructured

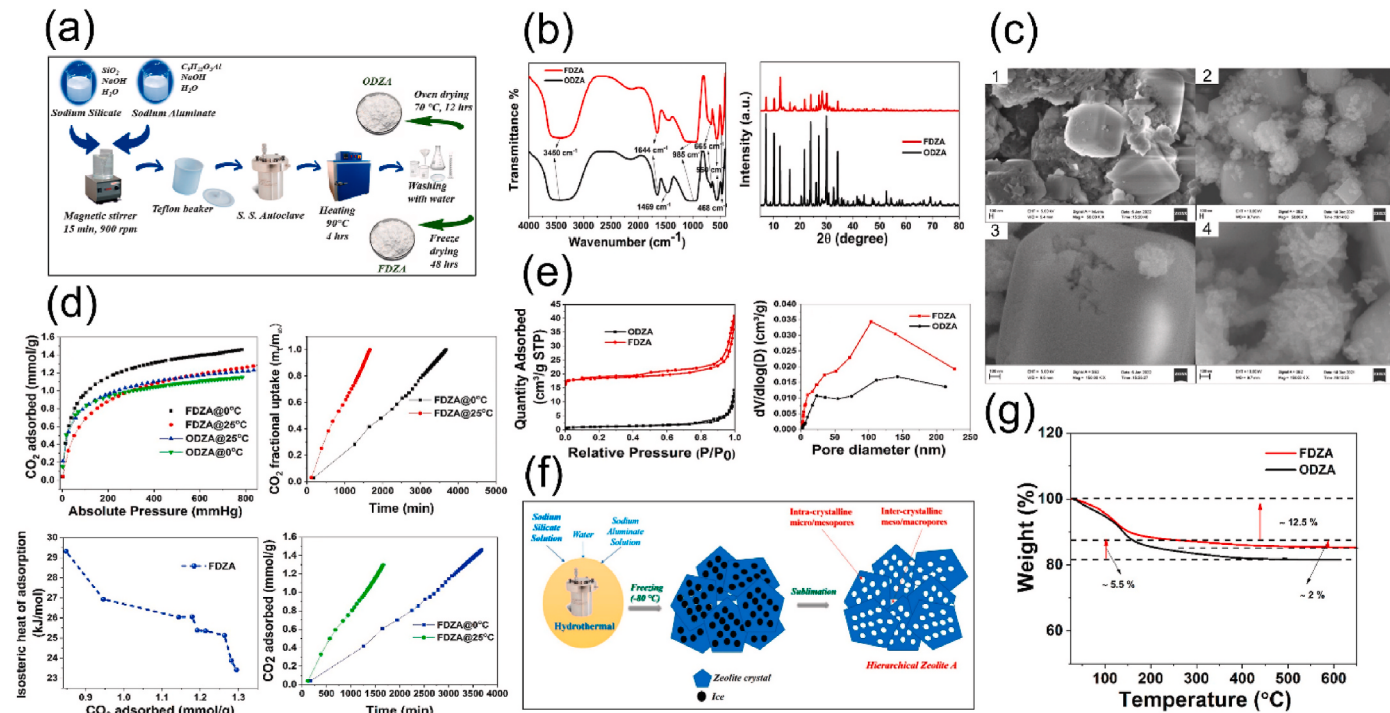


**Fig. 9.** (a) Illustration of zeolite A synthesis route, (b) FTIR and XRD analysis of FDZA and ODZA, (c) FESEM micrographs of ODZA and FDZA, (d)  $\text{CO}_2$  adsorption of FDZA and ODZA, Fractional uptake of  $\text{CO}_2$ , Isosteric heat of adsorption and  $\text{CO}_2$  sorption over time, (e)  $\text{N}_2$  adsorption-desorption isotherm and BJH plot, (f) mechanism of hierarchical structure FDZA and (g) TGA results of FDZA and ODZA. Reprinted with permission from Ref. [160]. Copyright (2023) Elsevier.

carbon-doped BN for  $\text{CO}_2$  capture. They synthesized nanosphere carbon-doped BN by subjecting a nanostructured blend of alkyl amine borane (soft template) adduct and ammonia borane to pyrolysis at 1100 °C. The resulting sorbent exhibited an interconnected microporous structure, boasting an impressive specific surface area of up to 767  $\text{m}^2 \text{ g}^{-1}$  and a pore volume of 0.32  $\text{cm}^3 \text{ g}^{-1}$ , which possessed remarkable  $\text{CO}_2$  uptake of 3.43 mmol  $\text{g}^{-1}$  at 0 °C and high  $\text{CO}_2/\text{N}_2$  selectivity of 21.

In addition to carbon doping, Huang et al. [172] synthesized boron nitride nanosheets functionalized with aminopolymers (PEI) to enhance  $\text{CO}_2$  uptake from 0.29 mmol  $\text{g}^{-1}$  (pristine BN) to 3.12 mmol  $\text{g}^{-1}$  at 75 °C. Shankar et al. [162] investigated the versatile role of porous boron nitride in both capturing  $\text{CO}_2$  and enabling its simultaneous photoreduction. The results demonstrated that porous BN could effectively capture  $\text{CO}_2$  from gas mixtures, with a maximum adsorption capacity of 2.34 mmol  $\text{g}^{-1}$  at 25 °C. Furthermore, when coupled with a photoreduction catalyst, the captured  $\text{CO}_2$  could be converted into valuable chemicals under UV irradiation. Zeng et al. [175] employed an innovative “intermediate template” method to synthesize 2D porous boron nitride sheets doped with transition metals such as Fe, Ni, and Co (Fig. 10a) for  $\text{CO}_2$  sorption. Among synthesized samples, Fe-doped h-BN exhibited relatively high porosity, boasting  $S_{\text{BET}}$  of 260.67  $\text{m}^2 \text{ g}^{-1}$ , and displayed  $\text{CO}_2$  sorption of 7.69  $\text{cm}^3 \text{ g}^{-1}$  at 25 °C under atmospheric pressure. Fig. 10 b shows that the morphologies (FESEM) and microstructures (TEM/HRTEM) of prepared Fe, Ni, and Co-BN had lamellar stacked, honeycomb, and white fungus-like structures, respectively. The slightly bent lattice fringes observed in the TEM images suggest that the introduction of Fe, Ni, and Co can influence the crystalline structure of BN. Fig. 10 c shows the comparison of the  $\text{CO}_2$  adsorption capacities of different boron nitride materials and the impact of transition metal doping on their adsorption performance. Interestingly, the undoped boron nitride material, had the highest adsorption capacity among them, even though it had the highest specific surface area. Based on their DFT calculations, the adsorption capability of sorbent could be attributed to both the porous structure of the sheets and the presence of transition metals, which significantly reduce the adsorption energy of

$\text{CO}_2$  on h-BN.

### 3.5. Metal-organic frameworks

Porous organic frameworks, comprising metal-organic-frameworks (MOFs) and covalent-organic-frameworks (COFs), represent a novel class of solid adsorbents. These frameworks, characterized by their high surface area, significant  $\text{CO}_2$  adsorption capacity, and notable chemical and structural diversity, are ideal candidates for  $\text{CO}_2$  capture and storage [176,177]. MOFs are considered an extensive class of crystalline materials with immense internal surface area and ultrahigh porosity. These, along with the high degree of flexibility for both inorganic and organic components of their structures, make MOFs of significant interest for upcoming applications in the clean energy industry [178]. MOFs represent a recently developed category of materials, characterized by their exceptional porosity and remarkable chemical and structural variability. The remarkable versatility in combining different metal and ligand components has yielded an extensive collection of over 100,000 unique MOF structures cataloged in the Cambridge Structural Database [179]. Many of these structures exhibit extraordinary attributes, including ultralow densities, with the lowest recorded value documented at 0.13  $\text{g cm}^{-3}$  [180]. Moreover, their pore volumes account for approximately 90% of the total free space [181], while their surface areas can reach exceedingly high values of up to 10,000  $\text{m}^2 \text{ g}^{-1}$  [182,183]. Fundamentally, MOFs epitomize the chemical structure's beauty as well as the power of combining inorganic and organic chemistry, disciplines usually regarded as disparate. One of the specifications of the MOFs is their congenial structures and diverse topology, many of which are derived from nature [184]. MOFs consist of metal-based nodes interconnected by organic linkers via coordination bonds, forming one-, two-, or three-dimensional coordination networks [185]. The structure of MOFs can be systematically tailored by modifying the organic linkers or connectivity of the metal ions [185,186]. This synthetic approach enables the optimization of the pore size and surface properties, offering advantages over zeolite materials. However,

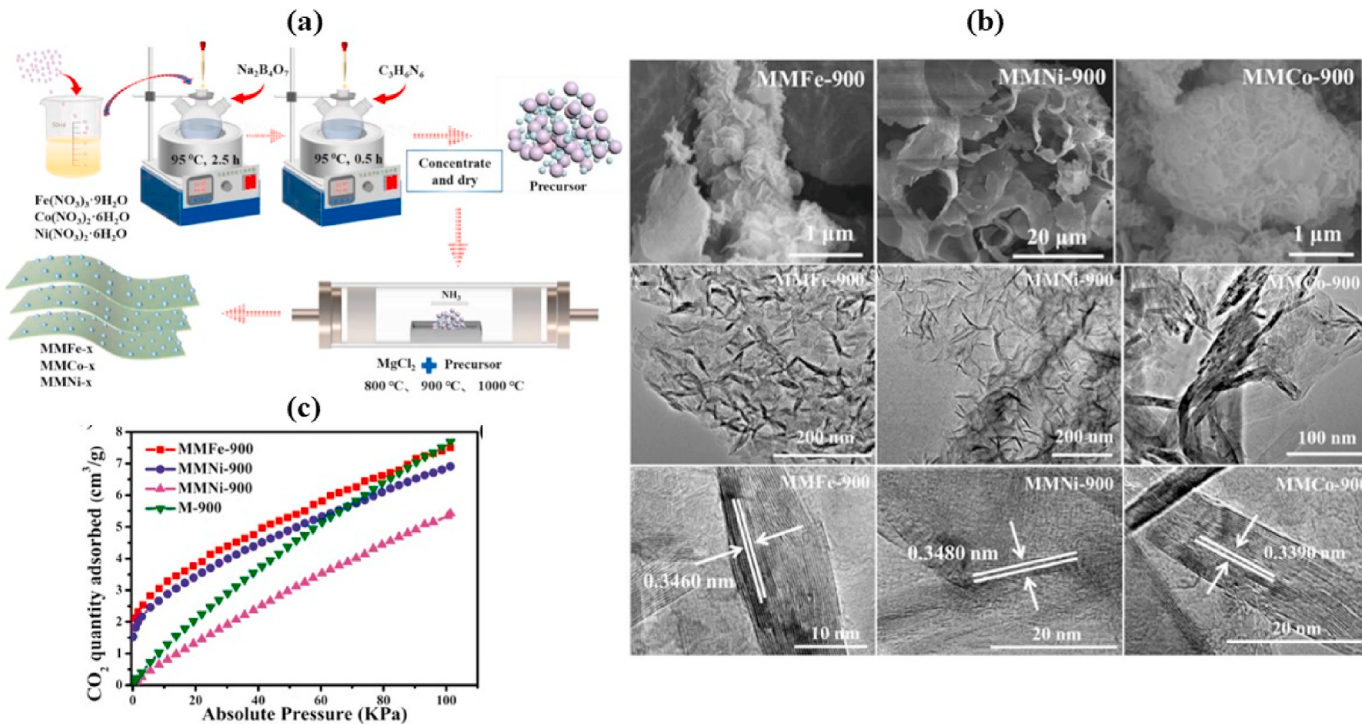


**Fig. 10.** (a) Schematic preparation of transition metal doped 2D porous h-BN resulted from mixing sodium tetra-borate, melamine, and transition metal nitrates by thermal treatment under an ammonia atmosphere, (b) SEM images of prepared samples; TEM images and HRTEM images of obtained results, (c)  $\text{CO}_2$  adsorption curves. Reproduced with permission from Ref. [175]. Copyright (2022) Elsevier.

achieving high crystallinity in MOF synthesis remains a challenge, requiring careful optimization of the reaction conditions such as reactant concentration, metal-to-ligand ratio, co-solvent concentration, solution pH, reaction temperature, and reaction time. MOFs can be categorized into four distinct subsets based on their structural characteristics: rigid, dynamic/flexible, surface-functionalized, and frameworks with open metal sites [187]. Rigid MOFs possess a stable porous structure characterized by fixed porosity. On the other hand, the configuration of dynamic frameworks can be manipulated by varying the guest molecules, and their properties are influenced by external stimuli such as pressure and temperature. Flexible MOFs exhibit advantageous features for the capture and release of gaseous molecules [188,189]. In rigid MOFs, the selective adsorption of gases relies on the interactions between the adsorbent and adsorbate. However, in the case of flexible MOFs, selective adsorption arises from the inherent flexibility and breathing behavior of these frameworks. Consequently, the investigation of gas adsorption in flexible MOFs is significantly more complex, often displaying stepwise adsorption or hysteretic desorption isotherms for CO<sub>2</sub> and other gases [190,191]. The modification of MOFs for CO<sub>2</sub> adsorption is typically carried out through two methods: functionalization of metal nodes and functionalization of linkers [192]. According to the literature, synthesis method, pre-synthetic and post-synthetic modifications could also be done to increase their CO<sub>2</sub> uptake. For instance, modification with metals such as Fe, Cu, Zn, Mg, etc., or quantum dots such as Cs<sub>3</sub>Bi<sub>2</sub>Br<sub>9</sub> can improve advanced MOF structure in terms of along with enhancing the gas adsorption specifications and stability [193]. In the study done by Gaikwad et al., the microwave method in developing Bimetallic USTA-16 MOF was implemented resulting in an improvement in CO<sub>2</sub> sorption. Adding Mg, Mn, and Cu a new bimetallic USTA-16 MOF was synthesized using a microwave reaction. The addition of the metals did not alter the ideal functionality and crystallinity of the pristine UTSA-16. In addition, the optimum ratio of the metal composition stood for 7:2 which resulted in the highest CO<sub>2</sub> adsorption capacity of 5.56 mmol g<sup>-1</sup> [194]. Another instance is MOF-Aluminum formate Al(HCOO)<sub>3</sub>, which can be cheaply derived from commodity chemicals, and demonstrate brilliant CO<sub>2</sub> adsorption capacity as well as excellent CO<sub>2</sub>/N<sub>2</sub> selectivity [195]. Hua et al. developed a peculiar porous metal ([Co(L)].DMF.2H<sub>2</sub>O)<sub>n</sub> (1, DMF = N,N-dimethylformamide) constructed via using a heterofunctional 4, 6-bis(4'-carboxyphenyl) pyrimidine (H<sub>2</sub>L) linker. The solvothermal approach was used to generate the porous cobalt-based MOF, which exhibited an exquisite structural characteristic. It was shown that the sorbent had great selective CO<sub>2</sub> capture as well as catalytic conversion under mild conditions because of the synergy of open metal sites. Meanwhile, it was demonstrated that this sorbent possessed 345.28 and 676.25 mg g<sup>-1</sup> in the solution and vapor phase, respectively [196]. Shang et al. [197] measured the CO<sub>2</sub> separation and adsorption of a water-stable aluminum-based porphyrin metal-organic framework (AL-PMOF) by inserting transition metals as sorption sites. The results demonstrated that among the pristine Al-PMOF and the transition metals, the Co-inserted Al-PMOF had the highest CO<sub>2</sub> adsorption capacity (3.32 mmol g<sup>-1</sup>). In addition, it showed the highest CO<sub>2</sub>/N<sub>2</sub> and CO<sub>2</sub>/CH<sub>4</sub> selectivity as high as 87 and 20, respectively, under 1.0 bar and 0 °C. Moreover, synthesis time and temperature are effective parameters for decorating optimal metal-integrated MOF. A simple condensation reflux approach for CO<sub>2</sub> capture was used to create MOF-74(Ni), a highly effective nickel-based metal-organic framework. It was found that the structure and the isosteric heat of CO<sub>2</sub> adsorption in this sorbent could both be altered by varying the synthesis period and temperature. The improved version, MOF-74(Ni)-24 (time, h)-140 (temperature), had outstanding CO<sub>2</sub> adsorption capabilities of 8.29/6.61 mmol g<sup>-1</sup> at 273/298 K under 1 bar. This capacity is a lot greater than what has been reported for other materials such as MOF-74-Ni (2.0/2.1 times), UTSA-16 (1.5/1.6 times), and DA-CMP-1 (3.6/4.9 times) under comparable circumstances [198].

In addition to metal incorporation, functionalizing the MOF-808

with amino acids increased CO<sub>2</sub> uptake, because robust bound amine moieties to the MOF backbone make the environment and chemistry within the pores, resulting in the release and binding of CO<sub>2</sub> under mild situations without heat application [178]. Humid conditions are one the most challenging ones in terms of CO<sub>2</sub> capture due to competitive adsorption of CO<sub>2</sub> and H<sub>2</sub>O on the active sites. For instance, Glycine at the Cu site in Cu-BTS-MOFs provides steric and thermodynamic protection against H<sub>2</sub>O assault, which is the cause of the material's increased stability against moisture. Simultaneously, Gly@Cu-BTC can effectively boost CO<sub>2</sub> uptake thanks to its carboxyl or amino groups [199]. Park et al. synthesized amine and fluorine co-functionalized MIL-101 (Cr) and examined for CO<sub>2</sub> uptake to deal with the aforementioned challenge. The results demonstrated that the fluorine and amine groups contributed to adsorptive sites in this structure [200]. The design technique presented by Yiwen et al. [201] involved the development of a core-shell-MOF system. In this system, the core MOF was specifically designed to selectively adsorb CO<sub>2</sub>, while the shell MOF acted as a barrier to hinder the diffusion of H<sub>2</sub>O into the core region. The decision was made to utilize the zirconium (Zr)-based UiO MOF platform as a result of its inherent structural rigidity and chemical stability. Fig. 11 a illustrates the design of an optimal core-shell MOF for CO<sub>2</sub> capture. Fig. 11 b illustrates the potential core ligand and shell ligand configurations of the optimized core-shell MOF [201]. The core component was selected as the UiO-67 derivative comprising 2,2'-dicyclohexylamino-[1,1'-biphenyl]-4,4'-dicarboxylate, denoted as (CyNH)<sub>2</sub>-BPDC, due to its notable CO<sub>2</sub>/N<sub>2</sub> selectivity (31) and high CO<sub>2</sub> capacity of 0.0104 cm<sup>3</sup> g<sup>-1</sup>. Furthermore, the shell was constructed using a UiO-67 derivative incorporating 2-amino-[1,1'-biphenyl]-4,4'-dicarboxylate (Fig. 11 c), known as NH<sub>2</sub>-BPDC, owing to the high CO<sub>2</sub>/H<sub>2</sub>O diffusion selectivity of 307. Fig. 2C presents FESEM images of (CyNH)<sub>2</sub>-UiO-67 and cs-MOF-1 along with their respective size distributions. The PSD boosted from 174 ± 36 nm for the seeds to 249 ± 37 nm for cs-MOF-1 according to Fig. 11 c. This increase in size was aligned with the growth of NH<sub>2</sub>-UiO-67 shells on the (CyNH)<sub>2</sub>-UiO-67 seeds.

The adsorption of CO<sub>2</sub> by MOFs is closely associated with the presence of polar groups on the linker. Introducing functional groups containing polar entities, such as -Cl, -OH, and -COOH, onto MOFs with Lewis basic sites can greatly enhance the adsorption capacity of CO<sub>2</sub> [202,203]. These polar groups interact with CO<sub>2</sub>, resulting in a higher capacity for CO<sub>2</sub> adsorption and/or a preference for CO<sub>2</sub> uptake over other guest molecules, including C<sub>2</sub>H<sub>2</sub>, N<sub>2</sub>, CH<sub>4</sub>, and H<sub>2</sub>O. Functional groups like amine, amide, halide, and hydroxyl have been found to increase the capacity for CO<sub>2</sub> adsorption and selectivity in MOFs [192, 204]. Moreover, new MOFs have one-dimensional, zigzag-patterned microporous channels. For instance, CuMOF-Bipy's capacity to exclude nitrogen while adsorbing CO<sub>2</sub> is mostly related to the narrow and zigzag design of its channels [205]. A modified MOF for CO<sub>2</sub> uptake using a novel unsaturated amine grafting method was employed in the work by Liu et al. [206]. This was accomplished by using N-(2-aminoethyl) ethanamine (AEEA) to alter metal sites in the MIL-100(Fe), UiO-66 (Zr), and MIL-100(Cr) materials that had low coordination levels. The results showed that the interaction between open spaces in the metallic framework and secondary amines from AEEA is necessary for the bonding process. The CO<sub>2</sub> adsorption active site is the major amine that has been exposed. Due to its significant S<sub>BET</sub>, P<sub>V</sub><sub>t</sub>, and pH properties, MIL-100(Cr), which had a high concentration of coordinatively unsaturated chromium ions, allowed amine grafting while maintaining the active site. The ideal preparation conditions for MF-Cr-AEEA were found to be M = 1 and t = 12 h, which produced a material that outperformed other MOFs in terms of high CO<sub>2</sub> adsorption capacity (2.05 mmol g<sup>-1</sup>) at 400 ppm of CO<sub>2</sub>. MF-Cr-AEEA, with an average pore size of 25.82 nm, preserved the original MIL-100(Cr) crystal structure after alteration. 80 °C and 40 min were shown to be the ideal desorption conditions, showing the lowest energy requirement for regeneration.

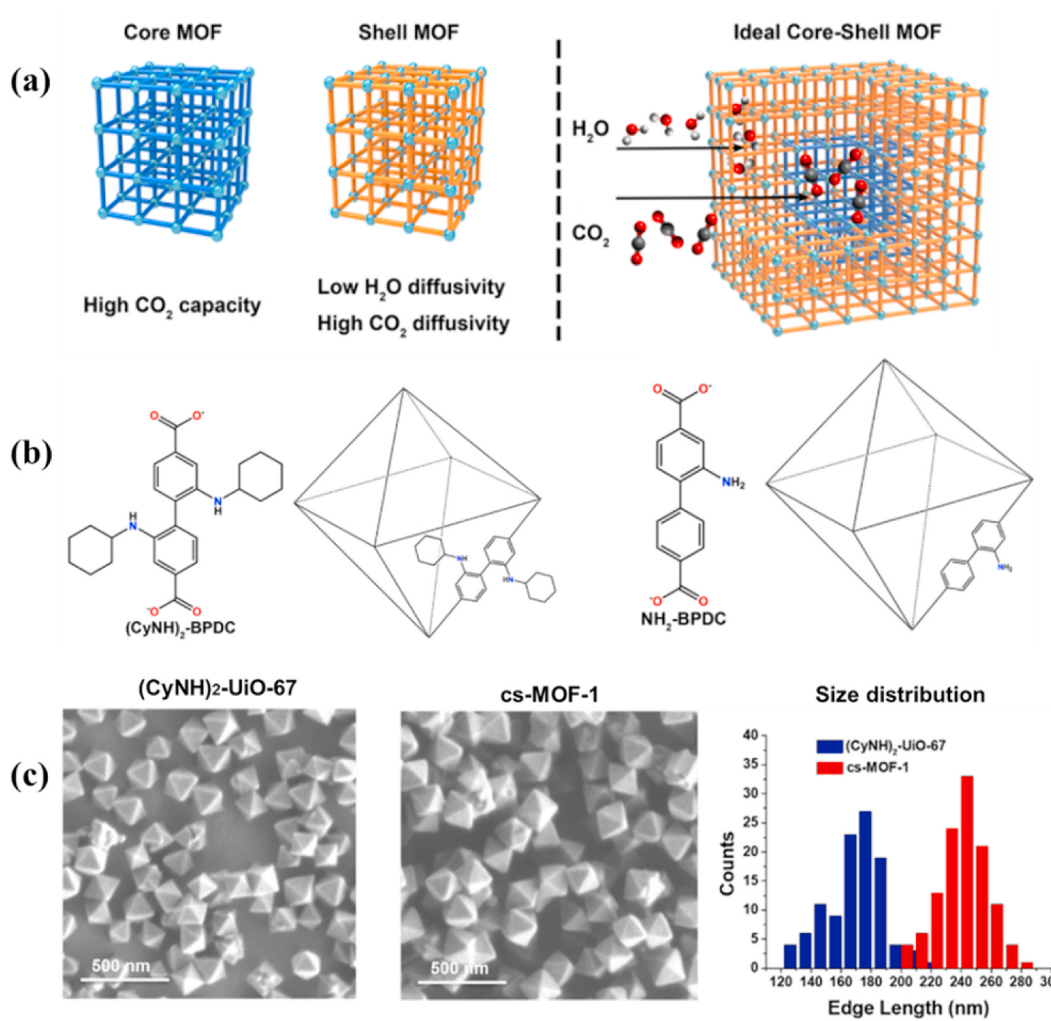


**Fig. 11.** (a) Optimization of a core-shell MOF for CO<sub>2</sub> capture, (b) Core and shell ligands for a possible core-shell MOF, and (c) SEM image of (CyNH)<sub>2</sub>-UiO-67 and cs-MOF-1 as well as their size distribution (based on 100 counts). Adapted from Ref. [201]. Copyright CC BY 4.0 (2023) <https://creativecommons.org/licenses/by/4.0/>.

### 3.6. Covalent-organic frameworks

The inherent permanent porosity and channel-like structure of covalent organic frameworks (COFs) make them highly desirable for various applications, including energy storage, chemical sensing, photocatalysis, and gas separation, owing to their high surface areas. Typically, COFs are constructed by linking two multifunctional building blocks using dynamic covalent chemistry, which involves reversible reactions conducted under thermodynamic conditions, allowing for error correction during the reaction process, resulting in crystalline frameworks with long-range order. Moreover, the exchange of building blocks, known as linker exchange, within pre-existing crystalline frameworks offers the opportunity to synthesize COFs with improved crystallinity or access COFs that were previously inaccessible through the condensation of the corresponding building blocks [207–209]. MOFs and COFs both have similar structural characteristics, but COFs differ from MOFs in that they are made of covalently bonded linkers that only contain light elements (H, B, C, and O), which results in a lower mass density and significantly higher gravimetric gas uptakes than MOFs with comparable surface areas [210]. Moreover, according to calculations using the DFT, a key element in determining the hypoCOFs' ability to choose CO<sub>2</sub> is the strength of the hydrogen bonding between CO<sub>2</sub> and the functional group of the linkers (a triazine, and a benzene linker). For instance, from two orthogonal building blocks (spirobifluorene and bicarbazole), a very stiff amine-linked 3D COF was created through a

post-synthetic chemical reduction. Due to the secondary amine connections' provision of CO<sub>2</sub>-chemisorptive sites, it was discovered that the amine-linked 3D COF exhibited substantially greater selectivity than the imine-linked 3D COF [211].

The presence of amine groups in the benzidine linker, specifically 3, 3'-diaminobenzidine ((NH<sub>2</sub>)<sub>2</sub>BD), makes it a compelling option for CO<sub>2</sub>/N<sub>2</sub> separation because of the well-known interaction between amines and CO<sub>2</sub>. This linker has been utilized in the synthesis of various materials, including a benzimidazole-linked covalent organic framework (IISERP-COF3), a semi-crystalline covalent organic polymer, and benzimidazole-based porous organic polymers (POPs) for CO<sub>2</sub> adsorption [207,212]. Mahato et al. [213] reported the highest CO<sub>2</sub>/N<sub>2</sub> IAST selectivity value to date (185.8 at 273 K for 15% CO<sub>2</sub>) for a covalent triazine framework. Yaghi and colleagues [214] explored the doping of aliphatic amine groups into a tetrahydroquinoline-COF. They found significant CO<sub>2</sub> adsorption capacity of 0.304 mmol g<sup>-1</sup> at 0.4 bar and 25 °C, which were relevant conditions for direct air capture. Furthermore, they observed that 50% humidity enhanced the CO<sub>2</sub> uptake to 0.393 mmol g<sup>-1</sup> at 298 K under 1 bar. Solid-state NMR analysis confirmed the formation of carbamates during the adsorption, thereby validating chemisorption interactions. Moreover, the high density of polar groups (amino groups), microporosity, and abundance of imidazolium cations led to increased CO<sub>2</sub> uptake [215]. In prior literature, in addition to the abovementioned factors, when the gas stream is humidified, the CO<sub>2</sub> adsorption capacity rises by around 25% in contrast to

the dry stream at 333 K (RH = 15%) and 343 K (RH = 9.3%) [216].

Dautzenberg et al. [207] successfully synthesized a novel COF denoted as Me<sub>3</sub>TFB-(NH<sub>2</sub>)<sub>2</sub>BD through the implementation of dynamic linker exchange (Fig. 12a) because the direct condensation reaction did not yield access to this specific COF structure. Notably, despite the linker exchange procedure, the COF exhibited substantial retention of porosity, leading to a notable  $S_{\text{BET}}$  of  $1624 \pm 89 \text{ m}^2 \text{ g}^{-1}$  (Fig. 12b). Me<sub>3</sub>TFB-(NH<sub>2</sub>)<sub>2</sub>BD demonstrated commendable CO<sub>2</sub> adsorption capacities, with measured values of  $1.12 \pm 0.26 \text{ mmol g}^{-1}$  at 1 bar and temperatures of 273 K, and  $0.72 \pm 0.07 \text{ mmol g}^{-1}$  at 1 bar and temperatures of 295 K. Furthermore, the COF exhibited a remarkably high CO<sub>2</sub>/N<sub>2</sub> selectivity when subjected to flue gas conditions, with recorded selectivity values of  $83 \pm 11$  at 273 K and  $47 \pm 11$  at 295 K (Fig. 12c) [207].

The integrity of boron-based COFs can be destroyed within hours by even mildly damp air because water can attack the electron-deficient boron sites of these materials nucleophilically. The use of boron-based COFs in practical applications is severely constrained by this instability. Jia et al. [217] addressed a considerable improvement in the hydrostability of boroxine-linked COFs (using COF-1 as an example) through modification with an oligoamine (tetraethylenepentamine, TEPA). Additionally, COF-1's CO<sub>2</sub> sorption capacity and CO<sub>2</sub>/N<sub>2</sub> selectivity have been significantly increased as a result of the oligoamine alteration, particularly in the low-pressure area, where an increase in CO<sub>2</sub> sorption of up to 13 times has been accomplished. This improvement allows the modified COFs to survive in water and maintain stability over time in humid environments.

Hybrid materials made of MOFs and COFs not only combine the benefits of both MOFs and COFs, but they may also perform much better due to a potential synergistic impact at the MOFs-COFs interface. In the work done by Wang et al. [218], some unique core-shell MOFs@COFs hybrids were created by chemically bonding the COFs to the surface of the Zr-based metal-organic frameworks (Zr-MOFs). By coating the COFs on Zr-MOFs through the C=N covalent linkages, the core-shell M@COFs hybrids were successfully made. The Zr-MOFs' stability was improved by the COF coating, which also resulted in the formation of numerous micropores at the interface. The largest  $S_{\text{BET}}$ , V<sub>total</sub>, and plentiful N/S

concentration were thus present in M@COF-SF, which also resulted in the highest CO<sub>2</sub> capture standing for  $170 \text{ mg g}^{-1}$  (273 K and 1 bar). In addition to the mentioned parameters, in core-shell NH<sub>2</sub>-UiO-66@Br-COFs hybrid materials, the hybridization procedure generated a large number of ultramicropores, which improved CO<sub>2</sub> capture up to  $169.5 \text{ mg g}^{-1}$  (273 K, 1.0 bar) [219]. Also, new methods create a covalently connected framework material with an ultrahigh surface area, namely air-liquid interfacial plasma (ALIP) that further enhances the surface area of the pristine COF by 43% while simultaneously increasing CO<sub>2</sub> capture by 67% [220].

In the study done by Zhang, an in situ "bottom-up" growth approach for the facile manufacture of 2D-COF-based mixed-matrix membranes (MMMs) has been described, which involves admixing COF precursors with PEO monomers at the molecular level within a solvent-free environment. A molecular-level homogeneous admixing of COF precursors with PEO monomers was used as opposed to the conventional top-down blending method. By irradiating PEO networks with microwaves, uniformly distributed 2D-COFs were formed. By utilizing the sheltering effects and the interlocking of PEG networks, the method enabled a favorable reduction in COF pore sizes, facilitating the enhancement of COF-polymer interfacial compatibility. With a 185.9% increase in CO<sub>2</sub> permeability and a 177% increase in selectivity compared to plain XLPEO membranes, the resulting MMMs exhibited remarkably improved gas separation performance [221].

Nitrogen doping is another way to raise CO<sub>2</sub> capture by this class of materials. TpPa-NO<sub>2</sub>, a nitro-decorated microporous-COF, has been produced in a one-pot synthesis on a gram scale. Based on ideal adsorption solution theory calculations and transient breakthrough experiments, it can efficiently separate C<sub>2</sub>H<sub>4</sub> from a C<sub>2</sub>H<sub>2</sub>/C<sub>2</sub>H<sub>4</sub>/CO<sub>2</sub> mixture and capture CO<sub>2</sub> from CO<sub>2</sub>/N<sub>2</sub>. At 298 K and 1 bar, respectively, TpPa-NO<sub>2</sub> shows high IAST selectivity of 5.94 and 34.87 for C<sub>2</sub>H<sub>2</sub>/C<sub>2</sub>H<sub>4</sub> (1:99) and CO<sub>2</sub>/N<sub>2</sub> (15:85). The O-H interactions (2.79–3.1 Å) between the H atoms of the imine backbone and CO<sub>2</sub> and the C-O interactions (2.97 Å) between the carbonyl oxygen of TpPa-NO<sub>2</sub> and carbon atoms of CO<sub>2</sub> were responsible for holding CO<sub>2</sub> in position, according to DFT calculations [222].

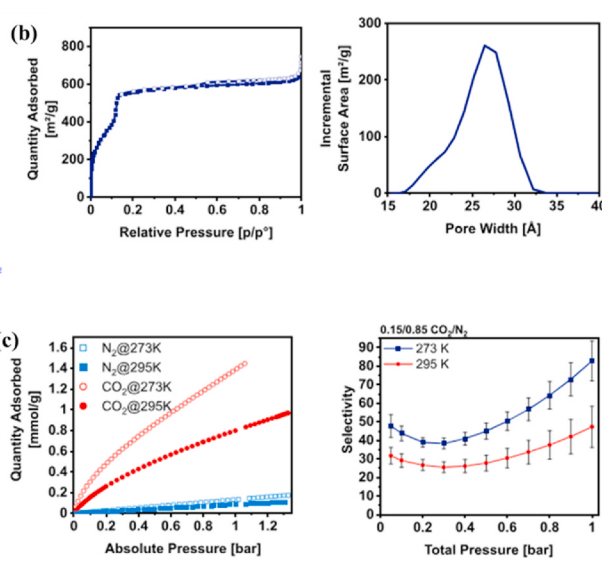
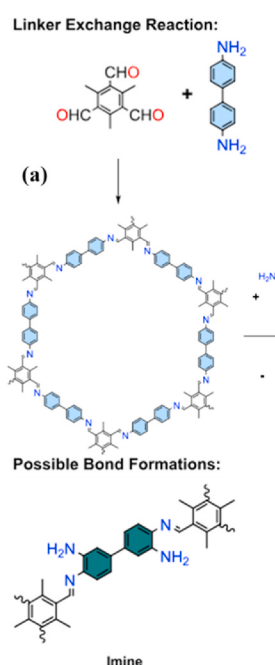


**Fig. 12.** (a) Oversight of the Me<sub>3</sub>TFB-BD COF reaction and the subsequent linker-exchange with (NH<sub>2</sub>)<sub>2</sub>BD to form Me<sub>3</sub>TFB-(NH<sub>2</sub>)<sub>2</sub>B, (b) N<sub>2</sub> adsorption isotherms and pore size distributions of Me<sub>3</sub>TFB-(NH<sub>2</sub>)<sub>2</sub>BD, and (c) CO<sub>2</sub> and N<sub>2</sub> isotherms at 273 and 295 K. IAST selectivity of CO<sub>2</sub>/N<sub>2</sub> (0.15/0.85) mixture. Adapted from Ref. [207]. Copyright CC BY 4.0 (2023) <https://creativecommons.org/licenses/by/4.0/>.

### 3.7. Mesoporous silica

Mesoporous materials (with uniform pore diameter between 2 and 50 nm) possess large  $S_{\text{BET}}$  and pore volume, which makes them capable of adsorbing a variety of substances. Their special pore structure consists of an ordered cylindrical pore system, and highly arrays of nanochannels, which enhances their adsorption capacity [223–225]. Compared with zeolites (that are difficult to adsorb macromolecules), mesoporous materials can adsorb macromolecules practically [226]. Mesoporous silica including periodic mesoporous organosilica, SBA-15, MCM-41, MCM-48, and aerogel mesoporous silica are suitable and popular adsorbents for  $\text{CO}_2$ , which is caused by high surface area, adjustable and ordered porous structure, facile surface functionalization, and high thermal and mechanical stability [227–234]. Lin et al. [235] conducted a study to compare the characteristics and performance of SBA-15 impregnated with PEI and diethylenetriamine (DETA) for  $\text{CO}_2$  sorption. The modified DETA adsorbents exhibited superior pore structure and amine dispersion. However, due to the low molecular weight of DETA, their thermal stability was compromised. On the other hand, PEI-modified adsorbents demonstrated thermal stability up to 200 °C, higher adsorption capacity, and better adsorption kinetics. The results indicated that SBA-15 modified with 50% PEI had better adsorption efficiency and exhibited optimal performance at temperatures above 80 °C.

Due to several advantageous properties including high surface area, large pore volume, abundant hydroxyl structure on the surface, easy-to-adjust pore size of mesoporous silica and its good chemical stability and fast adsorption kinetics, low price and moderate operating temperature and low energy cost of desorption, it has become a common and popular support for amine-functionalized solid adsorbents [236–238]. Kumar

et al. [239] discussed the preparation and testing of various amine-impregnated mesoporous silica (Five types of amines including PEI, TEPA (tetraethylenglyamine), TETA (triethylenetetramine), DETA and EDA (ethylenediamine) to impregnation of three sort of mesoporous silica covering SBA-15, MCM-41 and MCM-48) adsorbents for  $\text{CO}_2$  adsorption. SBA-15 with 50 wt% loading of PEI, TEPA, and TETA showed an enhanced adsorption capacity and PEI and TEPA-impregnated SBA-15 (A little more for PEI) exhibited superior cycling stability compared to the sample with TETA.

Shi et al. [240] prepared novel mesocellular silica foam (MCF) as a mesoporous-supported PEI network (MCF@G-PEI) by impregnating PEI into mesoporous silica modified with epoxy groups. The co-grafting approach was used to anchor PEI (21.3 wt%) onto the pore surface of MCF via epoxy/amine reaction and to stably attach the rest of PEI (14.3 wt%) to the pore surface via interaction with anchored PEI (Fig. 13a-b). The introduction of (3-glycidyloxypropyl) triethoxysilane (GPTES) on the surface of MCF as a bridging medium to utilize the ring-opening reaction of epoxy groups with amine groups, allowed for the covalent bonding of PEI and silica that are much stronger compared to van der Waals forces between amine groups and silica hydroxyl groups, improving the long-term stability and performance of the sorbent. Synthesized MCF@G-35.6% PEI demonstrated high  $\text{CO}_2$  sorption over a span of 30–90 °C, flow rate of 10–40 mL min<sup>-1</sup>, and  $\text{CO}_2$  concentration of 10%–30% vol (Fig. 13c), making it suitable for  $\text{CO}_2$  capture from flue gas streams. The adsorbent showed a maximum adsorption capacity of 2.78 mmol g<sup>-1</sup> for  $\text{CO}_2$  at 50 °C and 50% relative humidity through 50 consecutive adsorption/desorption cycles. The suggested pathways for  $\text{CO}_2$  sorption on immobilized amine sites are depicted in Fig. 13d and Fig. 13e, which demonstrate the adsorption kinetics and intraparticle diffusion kinetics of  $\text{CO}_2$ .

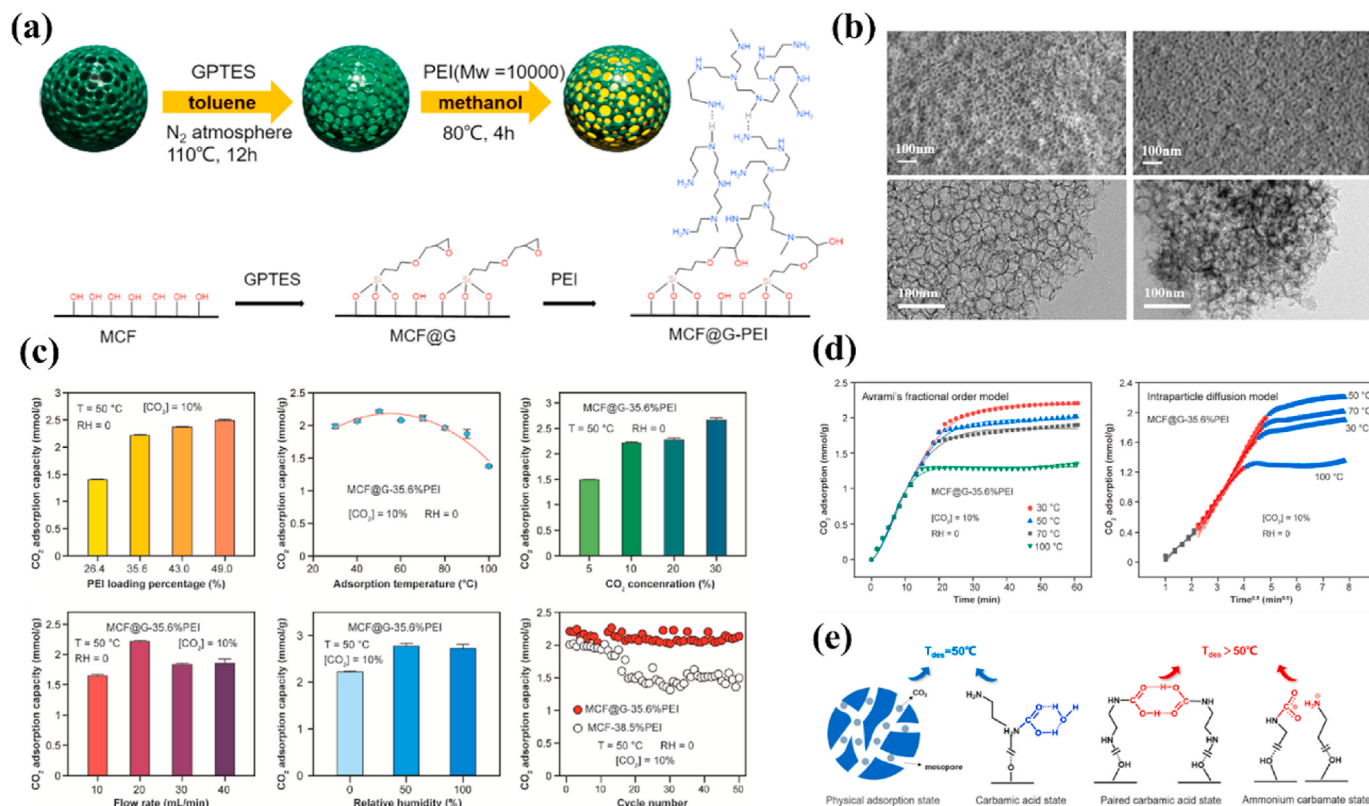


**Fig. 13.** (a) The fabrication procedure of MCF@G-PEI, (b) SEM micrographs of MCF, SEM image of MCF@G-35.6 %PEI, TEM micrographs of MCF and TEM image of MCF@G-35.6 %PEI, (c) Effect of experimental parameters on  $\text{CO}_2$  adsorptive capability of prepared sorbents (in order: PEI loading percentage, sorption temperature,  $\text{CO}_2$  concentration, flow rate, relative humidity, and adsorption/desorption cycle number), (d) Adsorption kinetics and intraparticle diffusion kinetics of  $\text{CO}_2$  on prepared MCF@G-35.6 %PEI, (e) Proposed mechanisms for  $\text{CO}_2$  sorption on immobilized amine sites. Reproduced with permission from Ref. [240]. Copyright (2023) Elsevier.

In the hot and competitive research field of using mesoporous silica for CO<sub>2</sub> sorption with a focus on cost-effective solutions, economic approaches are considered important parameters. Fe/Ti-doped in-situ amine-modified silica aerogel was prepared by Fan et al. [241] from fly ash by grafting with 3-(Aminopropyl) triethoxysilane (APTES). Results indicated that the samples revealed a high CO<sub>2</sub> uptake of 4.95 mmol g<sup>-1</sup> at 70 °C and kept 94.3% of their max capacity after 10 adsorption-desorption cycles. Xu et al. [242] have developed a practical method for utilizing solid waste resources by extracting silica from biomass power plant ash and synthesizing mesoporous silica materials. The process involves mixing biomass ash and sodium hydroxide, followed by roasting through alkali fusion to extract silica. The resulting silica is then used to prepare mesoporous silica through a hydrothermal method using silicon as the raw material. Characterization results indicate a specific surface area of 495.849 m<sup>2</sup> g<sup>-1</sup> and a pore diameter of 3.775 nm, with a hexagonal and two-dimensional structure similar to MCM-41. The synthesized mesoporous silica from biomass ash exhibits a maximum CO<sub>2</sub> adsorption capacity of 0.749 mmol g<sup>-1</sup>. The non-linear Freundlich isotherm model is a better fit than the Langmuir model, indicating that the CO<sub>2</sub> adsorption sites on the mesoporous silica are not uniformly distributed. The adsorption process is classified as physical, given that the equivalent adsorption heat Q<sub>st</sub> measures less than 20 kJ mol<sup>-1</sup>. The mesoporous silica exhibits remarkable cyclic and selective adsorption capabilities, maintaining a CO<sub>2</sub> adsorption capacity of over 90% after five consecutive cycles. Additionally, it demonstrates a CO<sub>2</sub>/N<sub>2</sub> (15/85) adsorption selectivity of 396.6. In further efforts to prepare mesoporous silica from biomaterials, Liou et al. [243] and Gebretatios et al. [244] synthesized mesoporous silica materials from rice husk waste and Aspromont et al. [245] conducted a hydrothermal synthesis of mesoporous silica, incorporating potato and corn starch as

the directing structuring agents. The synthesized mesoporous silica exhibited a remarkably high specific surface area, and its CO<sub>2</sub> capacity was comparable to that of non-functionalized mesoporous silica.

### 3.8. Comparison of different CO<sub>2</sub> adsorbents

The properties of various materials are summarized in Table 1, detailing CO<sub>2</sub> uptake in various temperatures and pressures, surface area, and total pore volume. This data covers different groups of materials, including carbon-based adsorbents, zeolites, magnetite nanoparticles, boron nitrides, COFs, mesoporous silica, and MOFs. This comprehensive overview allows for a comparative analysis of the performance and suitability of these materials for CO<sub>2</sub> capture. According to the results presented in the table, there appears to be no direct correlation between the structural characteristics of the adsorbent and the amount of adsorbed gas. In some cases, despite having relatively low specific surface area and porosity volume, a significant amount of gas adsorption is observed. This suggests that, in addition to textural properties, the morphology and surface chemistry of the adsorbents play a crucial role in influencing adsorption performance.

The commercial viability of adsorbent materials heavily depends on their ability to be regenerated and their low cost. The majority of absorption processes employed in CCS procedures involve chemical interactions that result in the formation of CO<sub>2</sub>-based molecular structures. Subsequently, captured CO<sub>2</sub> is regenerated through a temperature increase achieved by heating. Regeneration, constituting the bulk of the power requirement in CCS, underscores the necessity to develop efficient materials and processes for CO<sub>2</sub> capture. This endeavor aims to significantly reduce operation costs by lowering the expenses associated with regeneration [269]. Lian et al. conducted a review on

**Table 1**  
Common nanomaterials as CO<sub>2</sub> adsorbents.

Material	Specific surface area (m <sup>2</sup> ·g <sup>-1</sup> )	Total pore volume (cm <sup>3</sup> ·g <sup>-1</sup> )	Temperature (K)	Pressure (bar)	CO <sub>2</sub> adsorption capacity (mmol·g <sup>-1</sup> )	Ref.
Zeolite 13X	488	0.27	298	1	1.66	[246]
Hierarchical zeolite A	8.11	0.038	273	1	1.3	[160]
Zeolite A (Z7)	3.4	0.005	308	1	2.18	[247]
MIL-100(Fe)/Indonesian-activated natural zeolite	432.610 (Langmuir)	0.2864	Room temperature	1	7.01	[155]
Functionalized MWCNTs with 1,6-diaminohexane	83.09	0.46	303	17	253.99 mg g <sup>-1</sup>	[248]
Graphene	N.A.	0.46 (V <sub>micro</sub> + V <sub>meso</sub> )	Room temperature	1	4.6	[249]
GO/MWCNT(1:1) <sub>50</sub> - LDH *	103.51 ± 0.36	0.41	573	0.2	0.49	[250]
2D boron-carbon-nitride (BCN)	3310.4	1.75	273, 298	1	3.96, 2.39	[251]
MOF/GO*	635	0.304	273	1	6.8	[252]
Hierarchical porous metal organic framework aerogel	636.62	N.A.	273	1	7.29	[253]
N-doped porous carbons	2363	1.00	273, 298	1	6.24, 4.13	[254]
Self-heteroatom-doped porous carbon	1506	0.58	273, 298	1	6.91, 4.4	[255]
Carbon-doped boron nitride	767	0.32	273, 298, 308	1	3.43, 1.97, 1.74	[256]
Activated porous carbons	1470–2740	0.59–0.71	273, 298, 323	1	7.4, 5.0, 2.7	[257]
Hierarchical porous carbon from discarded shells of crustaceans	1734.64	1.48	298	1	4.32	[258]
Ti <sub>2</sub> C-MXene/activated carbon	871	0.96	273	1	67.83 cm <sup>3</sup> g <sup>-1</sup>	[259]
Green Self-activated porous carbon	1126	0.7	298	9.5	9.57	[45]
MOF-74(Ni)-24-140	1129	0.58	273, 298	100 kPa	8.29, 6.61	[260]
Aromatic Amine-Functionalized COF	1624 ± 89	0.90 ± 0.05	273, 295	1	1.12 ± 0.26, 0.72 ± 0.07	[261]
Core-shell NH <sub>2</sub> -UiO-66@Br-COFs	966	0.655	273	1	169.5 mg g <sup>-1</sup>	[219]
TPE-COF-II	2168	2.14	273	1	118.8 cm <sup>3</sup> g <sup>-1</sup>	[262]
Amine-Modified Hierarchical Silica	17	0.35	303	N.A.	5.20	[263]
Cellulose-derived biochar/layered double oxides composite	N.A.	N.A.	298	N.A.	1.24	[264]
Ordered mesoporous silica	495.849	0.679	298	1	0.749	[242]
Mesoporous magnesium silicate	373.00	0.248	298	1	1.02	[265]
N, O co-doped carbon nanotubes and activated carbon composites	1003–1443	0.420–0.619	298	1	3.77	[266]
ZIF-8*	1092	0.65	303	30	7.72	[267]
NaY-ZIF@polyacrylate	202.2	0.196	298	1	1.61	[268]

N.A., Not applicable; GO/MWCNT, Graphene oxide/Multiwall carbon nanotube-layered double hydroxides; MOF, Metal organic frameworks; ZIF, Zeolitic imidazolate framework.

ionic liquids (ILs) absorbents, demonstrating that the primary advantage of an ILs-based process over a monoethanolamine (MEA)-based process lies in its economic efficiency. Their findings revealed that an ILs-based process can save between 24.8% and 30.01% in energy consumption and 29.99% in primary costs, attributed to the less energy-intensive nature of its absorption and desorption processes. In the absorption process, an ILs-based system operates at a lower pressure (30 bar) compared to an MEA system, which necessitates a pressure exceeding 30 bar and thus requires a multistage compressor. Additionally, the heat required for desorption in an MEA process is significantly higher, at 393.75 kW, whereas an IL desorption process requires only 172.26 kW. Moreover, an initial report on steam consumption for CO<sub>2</sub> capture processes indicated that ammonia-based systems use less than one-third of the steam required by amine-based systems for equivalent CO<sub>2</sub> recovery. Furthermore, it is notable that the total energy consumption for ammonia-based CO<sub>2</sub> capture can be reduced to approximately 27% of that of MEA-based systems, but the hazards associated with ammonia cannot be overlooked. Furthermore, due to NH<sub>3</sub>'s relatively high vapor pressure, there is a risk of considerable solvent loss. This problem can be addressed by implementing cleanup procedures, which would likely increase capital costs, or by using various organic additives [270,271]. Adsorption is a cost-effective method for CO<sub>2</sub> capture, primarily due to its low energy requirements for regeneration, achieved through thermal or pressure modulation, and the absence of water use. It is particularly effective for dilute gas mixtures and offers a high CO<sub>2</sub> carrying capacity. The process is versatile, operating efficiently across a wide range of temperatures and pressures, and is characterized by fast reaction rates and minimal pressure drop. Additionally, adsorption systems are attractive because they require low maintenance, demonstrate long-term stability, have a low heat capacity for adsorbents, and do not necessitate moisture removal from flue gas [272]. Moreover, solid adsorbents present several advantages over liquid adsorbents. They can operate effectively across a broader temperature range, from ambient temperatures up to 700 °C, generate less waste during cycles, and can be disposed of with minimal environmental precautions [273]. Atom economy is critical in sorbent production due to the significant scale involved, emphasizing the need to minimize waste generated per unit mass of sorbent. The use of additional reagents, such as solvents, bases, and catalysts, is undesirable. To accurately assess the cost, one should consider the total expense of all chemicals used in the reaction stoichiometry to determine the per-mass cost of the sorbents. This approach provides a meaningful evaluation and establishes a ceiling price for the sorbent, as industrial production will typically be more cost-effective [274]. Parasitic energy provides a practical measure of the efficiency of solid sorbents in large-scale separations. It refers to the energy consumed by auxiliary systems essential for a process's operation but not directly contributing to its primary function or output. Notably, Mg-MOF-74 exhibits a significantly lower parasitic energy requirement of 727 kJ per kg of CO<sub>2</sub> compared to over 1000 kJ per kg of CO<sub>2</sub> for state-of-the-art aqueous amine technologies [275]. However, the synthesis of many MOFs often requires expensive ligands or the use of costly, non-reusable solvents. A straightforward method to calculate the production cost of MOF MIL-160(Al) material has been established based on a simulated process, utilizing data from large-scale laboratory pilot tests. This MOF cost evaluation method considers all process parameters for the first time, including scale, raw material costs, recirculation, and washing. The investment needed for a production plant serves as the basis for estimating the overall cost. The projected cost ranges from approximately \$55 per kg for an annual production of 100 tons, decreasing to \$29.5 per kg for an annual production of 1 kiloton. From a longer-term perspective, the cost is expected to drop below \$10 per kg when bio-derived ligands are used for large-scale bioplastic production [276]. Moreover, a general evaluation metric (GEM) has been developed based on pressure swing adsorption modeling of 190 materials to rank the performance of adsorbent materials by their cost-effectiveness for post-combustion CO<sub>2</sub> capture. This metric, which

only requires isotherm data and the N<sub>2</sub> internal energy of adsorption, prioritizes the N<sub>2</sub> working capacity as its most crucial component, followed by the CO<sub>2</sub> working capacity, the CO<sub>2</sub>/N<sub>2</sub> selectivity at desorption conditions, and the N<sub>2</sub> internal energy of adsorption. According to the results, for the most promising MOFs, the cost to capture a ton of CO<sub>2</sub> is estimated to be \$30–\$40, excluding the cost of compressing the CO<sub>2</sub> product [277]. However, it appears that these predicted values differ significantly from market prices. For instance, a market sample of MOF costs approximately \$50 per gram (MOFs ZIF-8 Powder, Jiangsu Xfnano Materials Tech Co., Ltd.), with some variations reaching up to \$120 per gram (MOF-74 Metal ligand, Luoyang Tongrun Info Technology Co., Ltd.), which effectively limits their practical use for adsorption applications. Similarly, the price of a COF in the market is around \$15 per milligram (DAAQ-TFP-COF), making it difficult for these materials to compete with commercial alternatives like activated carbon and zeolite. The affordability of activated carbon (\$2 per kilogram, Zhengzhou Kelin Water Purification Material Co., Ltd.) in the market is due to the availability of inexpensive precursors like biomass, various synthesis methods suitable for commercialization, and environmentally friendly activators that do not require ligands. These factors contribute to its prominence over other carbon materials such as graphene (\$3 per gram) and multi-walled carbon nanotubes (\$170 per kilogram). While mesoporous silica is priced at approximately \$10 per kilogram in the market, its widespread application in other fields may overshadow its potential as an adsorbent. Additionally, materials like magnetic nanomaterials (\$150.00 per kilogram, iron oxide Fe<sub>3</sub>O<sub>4</sub> nanopowder, Shanghai Epoch Material Co., Ltd.) and boron nitride, though prominent in laboratory settings, are still in the early stages of commercialization for this specific application. To provide a general comparison of sorbents, Table 2 summarizes their synthesis costs, advantages, and disadvantages.

#### 4. Machine learning

Newly, advances in artificial intelligence-aided material design (AIMD) are spreading premier impact on fields of study that enumerate physics, chemistry, and materials science [278,279]. Multiple machine learning (ML) techniques were conducted to accelerate the frontiers of soft computing learning from extensive datasets using statistics and algorithms for reducing greenhouse gas emissions [280–282]. ML directions may help to disclose the hidden relations in datasets by conventional, optimized, and nature-derived algorithms along with model construction to correlate descriptors with the performance of various targets of gas adsorption [283,284]. The inherent potential of algorithms as a significant emerging means for carbon capture on various physical adsorption fields as well [285,286]. In particular, ML techniques prominently collaborated as assistants for descending climate change specifically CO<sub>2</sub> capture. ML advantages are particularly implemented at various scales such as synthesis configuration, material properties, optimization of tuning parameters, and AI-adsorbent generation [287–289]. Fig. 14 illustrates the summary of ML procedures and options for porous carbon and advanced adsorbents.

Although the goals of ML-assistant are almost the same for both adsorbent types, there are slight differences that depend on the type of adsorbents (porous carbon, MOFs, Zeolite, polymer, etc.) and algorithms. Many ML-based training and optimization algorithms such as boosting techniques, nature- and biological-derived have been invented, developed, and presented that mostly have been applied to CO<sub>2</sub> subjects. The dataset sizes and the complexity of input features are the major differences between simple and advanced adsorbents in the subjects of CO<sub>2</sub> sorption. MOFs include well-known databases such as Cambridge Crystallographic Data (CSD) Center [290], Computation-Ready Experimental (CoRE) [291], and Materials Cloud [292] containing several thousand data points while porous carbon adsorbents faced with several hundreds of datasets. ML can be assisted in validating the experimental results of simple solid adsorbent materials such as porous carbon, biochar, and activated carbon for CO<sub>2</sub> adsorption. Moreover, well-known

**Table 2**

Comparison of different adsorbents in terms of cost of synthesis, commercial price, pros and cons.

Material	Cost of synthesis	Commercial price	Advantages	Disadvantages
MOF	High	50–200 \$/g Jiangsu Xfnano Materials Tech Co., Ltd.	<ul style="list-style-type: none"> <li>• High surface area</li> <li>• Selective adsorption</li> <li>• Tunable pore size</li> <li>• Reversible adsorption/desorption</li> <li>• Regenerability</li> <li>• Low energy requirement</li> <li>• High capacity</li> <li>• Customizable functionality</li> </ul>	<ul style="list-style-type: none"> <li>• Scalability issues</li> <li>• Moisture sensitivity</li> <li>• Stability concerns</li> <li>• Complex synthesis process</li> <li>• Limited industrial application data</li> <li>• Environmental impact of synthesis</li> <li>• Potential for degradation</li> <li>• Solvent use and disposal</li> <li>• Expensive ligands are required</li> <li>• The possibility of structure collapse during synthesis</li> </ul>
COF	Very high	1000 \$/g, Jiangsu Xfnano Materials Tech Co., Ltd.	<ul style="list-style-type: none"> <li>• High surface area</li> <li>• Porosity tunability</li> <li>• Chemical stability</li> <li>• Lightweight structure</li> <li>• Thermal stability</li> <li>• Recyclability</li> <li>• Low density</li> <li>• High CO<sub>2</sub> uptake capacity</li> <li>• Selective adsorption</li> </ul>	<ul style="list-style-type: none"> <li>• Complex synthesis process</li> <li>• Scalability issues</li> <li>• Structural fragility</li> <li>• Limited industrial application data</li> <li>• Moisture sensitivity</li> <li>• Energy-intensive regeneration</li> <li>• Limited chemical stability in harsh conditions</li> <li>• Functionalization challenges</li> <li>• Potential for low yield</li> </ul>
BN	Moderate	0.1–4 \$/g, Alfa Aesar, MaTecK GmbH	<ul style="list-style-type: none"> <li>• Thermal stability</li> <li>• Chemical stability</li> <li>• Structural tunability</li> <li>• Environmental friendliness</li> </ul>	<ul style="list-style-type: none"> <li>• Lower CO<sub>2</sub> capacity</li> <li>• High cost</li> <li>• Scalability challenges</li> <li>• Porosity issues</li> <li>• Lower strength</li> <li>• Temperature sensitivity</li> <li>• Specialized shapes cost</li> <li>• Hysteresis losses</li> <li>• Eddy's current losses</li> <li>• Surface Modification Requirements</li> </ul>
Magnetic Nanoparticles	Low	0.02–0.15 \$/g	<ul style="list-style-type: none"> <li>• High stability</li> <li>• Cost-effective</li> <li>• High permeability</li> <li>• Corrosion resistance</li> </ul>	<ul style="list-style-type: none"> <li>• Low selectivity</li> <li>• Potential for Pore Blockage</li> <li>• Lower Capacity at Ambient Conditions</li> </ul>
Porous carbon	Low	5 \$/kg	<ul style="list-style-type: none"> <li>• Chemical stability</li> <li>• Low density</li> <li>• High mechanical strength</li> <li>• Large specific surface area</li> <li>• Thermal stability</li> <li>• Low-cost precursors</li> <li>• Various synthesis methods</li> <li>• Industrial scale</li> <li>• Ease of Functionalization</li> <li>• Eco friendly</li> <li>• Tunable porosity</li> <li>• High surface area</li> <li>• Exceptional conductivity</li> <li>• Mechanical strength</li> <li>• Chemical stability</li> <li>• Flexibility</li> <li>• High permeability</li> <li>• High strength</li> <li>• Low weight</li> <li>• Large surface area</li> </ul>	<ul style="list-style-type: none"> <li>• Scalability issues</li> <li>• Environmental concerns</li> <li>• Oxidative susceptibility</li> <li>• Agglomeration Tendency</li> <li>• Limited Surface Functionalization</li> </ul>
Graphene	Moderate	0.5–250 \$/g, Merck GmbH		
SWCNT/MWCNT	Moderate	0.04–3.8 \$/g, Nanochemzone		<ul style="list-style-type: none"> <li>• High cost of manufacturing</li> <li>• Limited commercial applications</li> <li>• Complex synthesis process</li> <li>• Low selectivity</li> <li>• Moderated adsorption capacity</li> <li>• Aggregation Tendency</li> <li>• Pore Accessibility</li> </ul>
Mesoporous silica	Moderate to high	0.05–60 \$/g, Sigma-Aldrich	<ul style="list-style-type: none"> <li>• Well-defined pore structure</li> <li>• Can be synthesized from low-cost precursors</li> </ul>	<ul style="list-style-type: none"> <li>• Potential challenges in scalability</li> <li>• High synthesis cost due to expensive inorganic precursors</li> <li>• Lack of microporosity in the structure</li> <li>• Mechanical Fragility</li> <li>• Unstable in the presence of moisture and acidic or basic environments</li> <li>• Limited to specific minerals</li> <li>• Challenges in controlling framework types during synthesis</li> <li>• Low selectivity</li> <li>• Sensitivity to Moisture</li> <li>• Limited CO<sub>2</sub> Adsorption Capacity</li> </ul>
Zeolite	Moderate	0.02–1.97 \$/g, Nanochemzone, Nanoshell, India Mart	<ul style="list-style-type: none"> <li>• Ordered crystalline structure</li> <li>• Susceptible to various modifications</li> <li>• Greater stability in reaction environments</li> <li>• Scalable</li> </ul>	

molecular dynamic (MD) simulation and DFT calculation can synergistically strengthen the ML role by comparing or combining [280,293]. The study of advanced material for CO<sub>2</sub> permeability mostly started with High-throughput computational screening (HTCS), MD, and Grand Canonical Monte Carlo (GCMC) simulations. The targets of single or mixed

routes (ML or combined ML/MD, etc.) are generally divided into (i) CO<sub>2</sub> uptake, (ii) optimizing fabrication procedures, independent variables, and gas adsorption amounts, (iii) disclosing the effectiveness level of features and (iv) screening and discovery of superior adsorbents. As shown in Fig. 15, the solid adsorbents have been synthesized by multiple

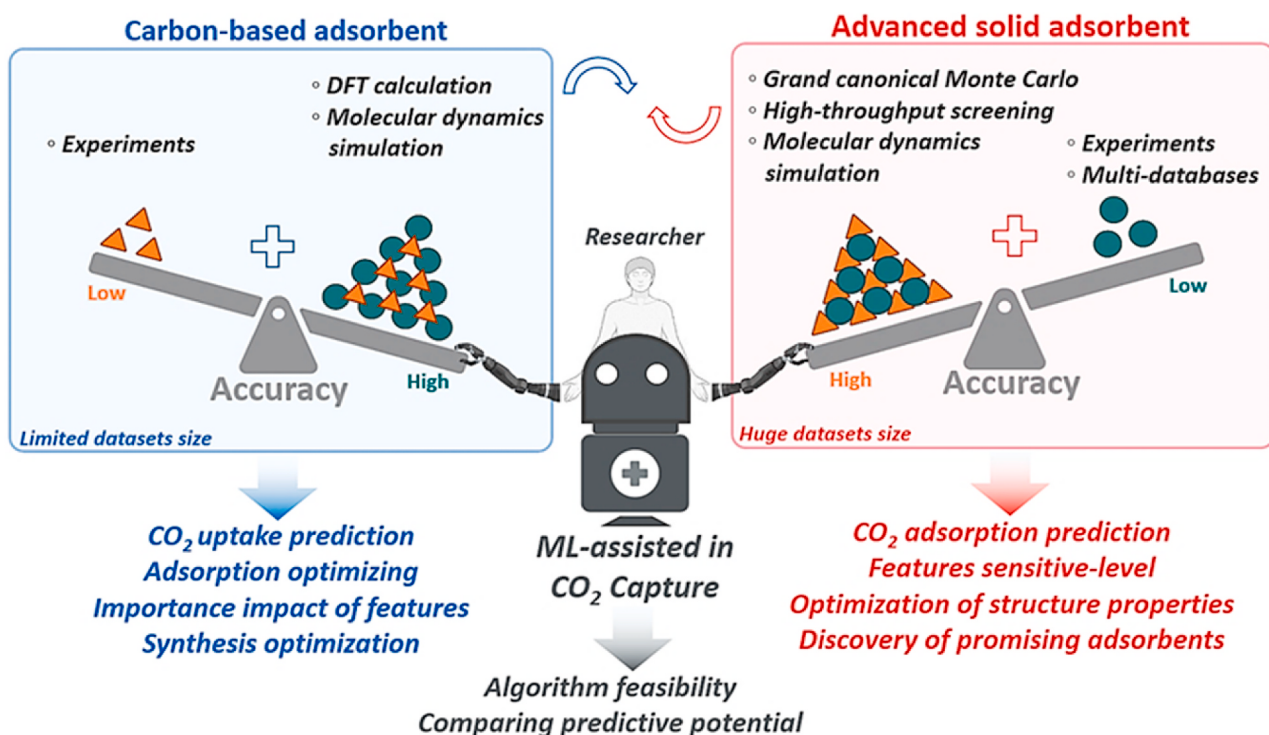


Fig. 14. The survey of ML application in CO<sub>2</sub> adsorption challenges in various solid adsorbent materials.

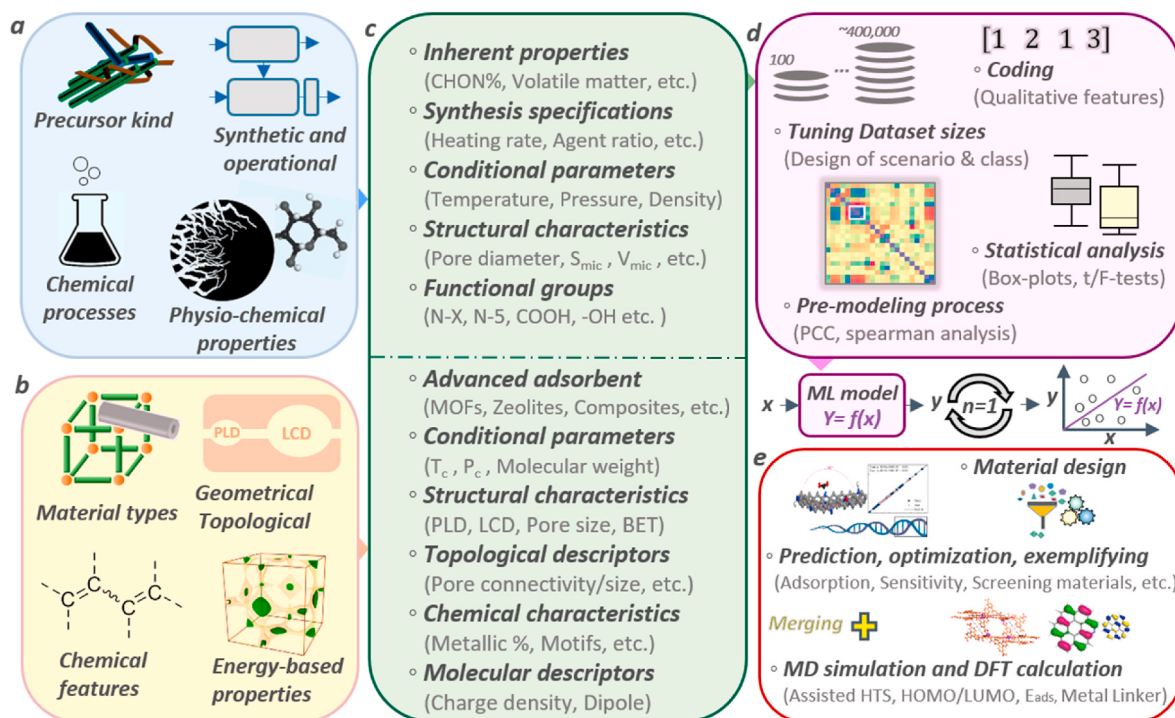


Fig. 15. The steps of pre-modelling, modelling, and post-modelling processes by ML techniques by evaluating (a) the porous carbons' and (b) advanced materials' modeling maps by specifying the various scenarios as input categories. (c) Selection and preparing the multi-hypothetical parameters and datasets (d) Pre-modelling and modelling processes for standardization and modifying the datasets, independent variables, and statistical criteria. (e) The achieved targets of ML modeling and merging with MD simulation and DFT calculation approaches. Adapted with permission from Refs. [278,280,301–303]. Copyright (2023) American Chemical Society; Copyright (2021) Elsevier; Copyright (2022) Elsevier.

precursors (bio, artificial, semi-artificial raw materials), various thermochemical conversions (chemical, physical, physicochemical), and chemical agents (alkali, metallic, acidic, polymeric, etc.). These donate

the ideal geometrical, heteroatoms functionalities and energy-based properties to adsorbents' structures. The procedures include wide tunable parameters and chemical materials that affect the

physiochemical characteristics of porous adsorbent. As shown in Fig. 15a-b, the main step of modeling is accurately assuming the principal categories of descriptors or inputs from material fabrication and attributed characteristics. The datasets consist of the proposed independent variables that could be extracted from the details of the experimental or database resources. As illustrated in Fig. 15c, porous carbon adsorbents' independent variables can be classified in inherent properties, synthesis specifications, conditional/structural characteristics [294], and particular heteroatom functionalities. Porous carbons are mostly fabricated by bio-precursors through multiple thermochemical conversion synthesis routes. The novel ML approach can be used to construct a CO<sub>2</sub> uptake prediction model based on the synthetic (purifying, carbonization, chemical activating/doping, and impurity removing), micro-structural characteristics such as (specific surface area (SSA), micropore volume (MPV) and conditional tuning parameters (cryogenic/room temperatures and high/low pressures) of bio-derived activated carbons (ACs) or bio-porous carbon. For this purpose, multiple works train and test datasets of porous carbon materials and various types of ML models. Namdeo et al. [295] comparatively employed several supervised algorithms such as gradient boosting decision tree (GBDT), light gradient boosting machine (LGBM), extreme gradient boost (XGB), random forest (RF), categorical boosting (Catboost) and adaptive boosting (Adaboost) for predication of CO<sub>2</sub> permeability. The variables include SSA ( $\text{m}^2 \cdot \text{g}^{-1}$ ), MPV ( $\text{cm}^3 \cdot \text{g}^{-1}$ ), total pore volume (TPV) and C%, H%, N %, O%, S% at various temperatures and pressures (T = 0–25 °C, P = 0.15–1 bar). This scenario and inputs attracted a high reputation for evaluating porous carbon for CO<sub>2</sub> uptake. As another alternative, Ma et al. synergistically merged self-experiments, ML modeling, and GCMC simulation to calculate the CO<sub>2</sub> adsorption isotherms with different pore sizes and O/N functional groups [296]. Post-modeling processes finalizing with complementary analyses such as feature importance level, Shapley additive explanations (SHAP), and contour map [297,298]. Zhu et al. [294] obtained the relative importance of integrated influential factors with various pressures 0–0.2, 0.2–0.6, and 0.6–1 bar at room and cryogenic temperatures. Microstructural and chemical features exhibited ~55% and ~25% of importance levels at pressures between 0.6 and 1 bar. The pre-modeling processes mostly run by Pearson correlation coefficient (PCC) analysis were mostly used for observing significant level p-value (in three levels of 0.01, 0.05, and 0.1.), linear correlation (0–1), and collinearity value [286,289]. PCC analysis can statistically evaluate the quantitative independent variables. Thence, out of these features, the type of precursors, carbonization, and chemical agent type can be considered non-quantitative inputs in ML models which can be specified with codes. Mashhadimoslem et al. constructed two practical RBF-NN and MLP-NN for CO<sub>2</sub> capture prediction by merging ANN models with MLP and RBF algorithms. Four hundred datasets were gathered from the kinds of literature on biomass-based activated carbon for CO<sub>2</sub> adsorption. Bio-precursors (shell, leaves, stone, etc.), pyrolysis temperature, and activating agents (KOH, ZnCl<sub>2</sub>, and NaNH<sub>2</sub>) with conditional parameters utilized for BET surface area, and CO<sub>2</sub> adsorption predictions. Bio-precursors and activating agent types transferred to quantitative input by considering some codes and labels [299]. The main aim of ML is to improve or optimize the adsorption process by predicting the thermodynamic properties of adsorbents. Moreover, ML models can be employed for the equilibrium prediction of CO<sub>2</sub> in a pervasive range of adsorbents. Wang et al. presented an empirical function based on fitting the experimental data of CO<sub>2</sub> adsorptions by considering the micro-textural properties. The equal is obtained  $E_{\text{ads}}^{\text{CO}_2} = 0.095 + 2.10 \times V_{\text{mic}} + 3.51 \times V_{\text{mic}} \times V_{\text{mes}}$  that  $V_{\text{mic}}/V_{\text{mic}}$  are micro/mesopore volumes of porous carbons [300]. During the ML pre-processing phases, dataset sizes and scenarios are specified by considering the targets by applying statistical tests such as PCC and Spearman correlations analyses, etc. as shown in Fig. 15d-e. Coding of some inputs in algorithms' structure such as precursors, motifs, linker type, etc. Can develop the ML model to be

the constructive version for CO<sub>2</sub> capture predictions. The targets can be classified into single or combined approaches after one or multiple ML model runs. The well-known targets are the prediction of CO<sub>2</sub> permeability, sensitivity analysis on descriptors, optimization of materials' characteristics, adsorbent discovery, etc. ML can be synergistically combined with MD simulations or DFT calculation for an in-depth evaluation of the adsorbent potential for CO<sub>2</sub> uptake. The details of recent significant approaches are presented in Table 3.

Besides, advanced materials contain wide descriptors such as the structural formula of a linker [312], metal node [21], topology [312], motifs [282], and molecular descriptors. As shown in Fig. 16, ML techniques model MOF screening include features of non-zero accessible gravimetric and volumetric surface areas, pore limiting diameter (PLD), global cavity diameter (GCD), largest cavity diameter (LCD), void fraction ( $\phi$ ), density ( $\rho$ ), accessible volume (AV) and free volume (V<sub>free</sub>) [24, 309,312]. ML is used to promote accurate quantitative structure/property relationship (QSPR) approaches to predict the CO<sub>2</sub> adsorption capacity. 350,000 MOFs had been constructed from types of building units in hundreds of net topologies that were utilized to train and test the models. Fig. 16a presents the PCC analysis between chemical and structural descriptors for initial datasets. Fig. 16b comparatively shows the excellent 1000 MOFs predicted by the ML model and GCMC simulation (top of the dashed line and the right of the solid line, respectively). Thus, the intersection of lines (red area) displays MOFs rediscovered by the ML model [282]. The performance of CO<sub>2</sub> adsorption of advanced materials was evaluated between MOFs and IL/MOFs composites as shown in Fig. 16c. From the hidden structure-performance relationships perspective, 20 different features (LCD, PLD, IL (wt %), CHON%, metalloids%, metal%, etc. were used as inputs for ML-guided discovery of the MOF-based composites. Statistical criteria of R-squared (R<sup>2</sup>), root-mean-square deviation (RMSE), and mean absolute error (MAE) were evaluated and 0.97, 0.55, and 0.11 were achieved, respectively. The aforementioned algorithms tend to accurately and confidently depict system complexity as well as the inherent relationship between characteristics and adsorption. Newly, ML has proceeded beyond its primary capabilities by combining with approaches such as molecular simulation, DFT calculation, and Raman spectroscopy [280,305].

As shown in Fig. 17a-b, the types of gases as targets are classified by considering the kind of bonds and unit constructions. The heat map of micropore to mesopore volumes (2–50 nm) merged with the ML technique to disclose the ideal values of 0.4–0.9 cm<sup>3</sup>g<sup>-1</sup> for higher CO<sub>2</sub> adsorption [297,312]. Rahimi et al. applied the ML technique with DFT calculation that has been combined with two computational techniques as shown in Fig. 17c-d. ML/DFT calculation utilized the N/O-enriched activated carbon datasets from the various biomass resources for CO<sub>2</sub> capture. Four nitrogen functional groups such as pyridinic nitrogen (N-6), pyrolytic nitrogen (N-5), oxidized nitrogen (N-X), graphitic nitrogen (N-Q), and oxygen content with microstructural features modeled by RBF-NN for CO<sub>2</sub> permeability predictions [280]. Then, the electronic and structural specifications of N-doped ACs during their interaction with CO<sub>2</sub> have been optimized using the B3LYP level of theory.

The adsorption energy (E<sub>ads</sub>) values and the energy gap between the highest-/lowest unoccupied molecular orbital (HOMO/LUMO) of ACs with CO<sub>2</sub> molecule are achieved. The tiny band gap (E<sub>g</sub>) indicates the high reactivity with values of ACs due to CO<sub>2</sub> adsorption had been predicted 0.7, ~2.8, 2.65, and 2.3 eV for N-Graphitic, N-Pyridinic, N-Pyrolytic, N-Oxidized, respectively [280]. Guan et al. used the RF model to predict CO<sub>2</sub>/CH<sub>4</sub> separation based on the literature data which revealed the ideal MOF structure with a pore size of less than 1 nm and a surface area of 800 m<sup>2</sup> g<sup>-1</sup>. On the other side, optimum MOFs were blended into the polymer of intrinsic microporosity-1 to synthesize MMMs. As shown in Fig. 18a-c, the Cu-CAT-1 composite is achieved by MD simulation and the scatterplots show the distributions of predicted CO<sub>2</sub> permeability by using literature materials, experimental, and

**Table 3**The multi-approaches of ML techniques with advanced perspectives in CO<sub>2</sub> capture.

Subject	Area	Process	Achievements	Ref
Bio-derived porous carbon/Porous carbon/Coal	CO <sub>2</sub> uptake capacity predicted on N/O rich functional porous ACs by GA-ML model merging with DFT calculation at various temperatures (room and cryogenic) and pressures (0.15–1 bar).	RBF-DFT optimized E <sub>ads</sub> of HOMO-LUMO and geometry of N-doped ACs. MD simulation was run in Material Studio software. 217 data points used in various ANN training algorithms Bayesian regulation, quasi-Newton, additive momentum, and self-adaptive learning rate. The predictive performance of multi-ML models compared. Then, the feature importance level was observed for all variables.	E <sub>ads</sub> were obtained in a range of −15.93 to −17.38 kJ mol <sup>−1</sup> . Nitrogen groups such as N-X and N-Q indicated the main impacts on CO <sub>2</sub> uptake. The accuracies achieved MAPE of ~3.5% and R <sup>2</sup> range of 0.97–0.99.	[280]
	Hundreds of data points containing physicochemical and operational features are applied in RF, GBDTs, LGBs, and XGB models to disclose the features' impacts and gas capture value prediction.		The k-fold method and hyper-parameter tuning effectively improved the predictions by achieving R <sup>2</sup> of 0.84–0.98.	[304]
	Various biomass-derived porous carbon main properties such as precursor type, activators, and carbonization parameters employed in MLP and RBF algorithms. CNN model used hypothetical porous carbon for constructing a model at 77 K for CO <sub>2</sub> uptakes under ambient pressure.	Non-quantitative inputs were coded in two ML models for the SSA (by BET) and CO <sub>2</sub> permeability predictions.	Number of neurons in the models optimized for BET and CO <sub>2</sub> adsorption capacity predictions with the greatest MSE validation results of R <sup>2</sup> > 0.99.	[281]
	ML model consumed datasets of CO <sub>2</sub> adsorption from various bio-preursors synthesized to porous carbon through thermal conversion methods (carbonization, oxidation)	Million hypothetical porous carbons used in CNN model in varying adsorption isotherms CO <sub>2</sub> /N <sub>2</sub> uptake performance. Chemical compositions and pore-/surface characteristics are assumed as inputs. Sensitivity analysis exhibited N% content as an effective feature on CO <sub>2</sub> capture.	Proposing an empirical function for predicting CO <sub>2</sub> uptake named as (M <sub>ads</sub> <sup>CO<sub>2</sub></sup> ): 0.095 + 2.10 × V <sub>mic</sub> + 3.51 × V <sub>mic</sub> × V <sub>mes</sub> . RF algorithm predicted the CO <sub>2</sub> storage by R <sup>2</sup> and RMSE (0.93–0.95 and 0.1 to 0.3, respectively) in pressures of 0.1–1 bar.	[300] [294]
	CH <sub>4</sub> /CO <sub>2</sub> selectivity modeled by MLP, and 2794 datasets extracted from publications that include multi-synthesizing procedures.	To predict the adsorption capacities of gases, SSA, V <sub>mic</sub> , and V <sub>mes</sub> were utilized as input variables with one layer, and three hidden layers with 64, 32, and 16 neurons. Nitrogen content of porous carbon and ultra-micro pores have the greatest impact on CO <sub>2</sub> capture at 0–0.15 and 0.15–1 bar, respectively.	The contour maps of CO <sub>2</sub> uptake were evaluated based on the function of meso-/micro textural properties at room temperature under 1, 5, 10, and 20 bar.	[297]
	Textural-chemical descriptors used for predicting the CO <sub>2</sub> adsorption by RF scheme based on 1594 datasets. The raw precursors included biomass, organic salt, MOF, polymer, etc.	Algorithms proceeded to classify the bio-carbon samples based on the temperature and precursor material.	Eight particular adsorption conditions were modeled by combining 0–25 °C and 0–1 bar with high R <sup>2</sup> (~0.99) and RMSE 0.05 to 1.5.	[296]
	Simple and N-rich biowastes were chemically activated by metal chloride and carbonized in various temperatures. Then, DL-based algorithms were applied to the results for the classification of CO <sub>2</sub> adsorbents.		By increasing the activation temperature, the CO <sub>2</sub> removal efficiency varied from 2.11 to 5.48 mmol g <sup>−1</sup> at 25 °C under 3 bar pressure with 100% accuracy of classification by DL algorithms.	[305]
	311 experimental datasets of CO <sub>2</sub> adsorption used for training by Levenberg-Marquardt, Bayesian Regularization, and Scaled Conjugate algorithms.	Time, temperature, and pressure were considered as inputs for CO <sub>2</sub> prediction. The effects of neuron layer size for MLP and RBF were observed.	MLP, RBF, and RSM models were adequate for modeling the CO <sub>2</sub> adsorption with correlation coefficients of 0.99784, 0.9497, and 0.8958.	[306]
	Six supervised ML models GBDT, XGB, LBGM, RF, Catboost, and Adaboost were comparatively used for predicting the CO <sub>2</sub> capture.	PCC analysis was applied to physico-chemical features such as elemental (N%, O%, etc.), MPV, and operational parameters before ML modeling.	The accuracies were MAPE (14–20%), RMSE (0.075–0.8), R <sup>2</sup> (0.72–0.99) and MSE (0–0.64). SHAP and instance force plots showed SSA and MPV as high-impact features.	[295]
	Eight input features including pressure, elemental, and microstructural features of porous carbon selected in four ML models.	RF, SVM, LR, and MLP models were evaluated and SHAP analysis was conducted between various elements (O%, N%, and H%).	The accuracies achieved are based on R <sup>2</sup> and RMSE (0.83–0.91 and 0.31 to 0.41, respectively).	[298]
	Biomass was experimentally synthesized in the green procedure (steam) and the results were comparatively compared with the ML model.	Then MLP and RSM models were applied to the experiments for CO <sub>2</sub> adsorption. The model used 22 epochs in the validation phase.	Prediction criteria resulted in MSE and R <sup>2</sup> 0.001 and 0.99.	[307]
	Seven supervised ML techniques (DT, RF, GBR, KNN, ANN, FNs, and ANFIS) for modeling CO <sub>2</sub> capture on coal's physical and chemical properties.	A thousand datasets including properties such as moisture, ash, volatile matter, fixed carbon, vitrinite reflectance, and particle size were used to predict CO <sub>2</sub> adsorption.	Sensitivity analysis was conducted out on input parameters and R <sup>2</sup> of prediction achieved from 0.88 to 1.	[308]
	Hundreds of characterized MOFs focusing on the VSA method are considered as a Low-energy CO <sub>2</sub> capture route.	Thousands of datasets were extracted from the CoRE database. Next, 32 well-known MOFs, 16 zeolites, and porous polymers were used in GCMC. The validated material used in the GA algorithm.	95 to 90 % CO <sub>2</sub> purity and recovery targets were achieved, respectively. 97 MOFs disclosed to have PE < 250 kWhe (lower than solvent-based capture route).	[279]
MOF@zeolite/polymer IL composites MOF	Filler datasets including eight thousand MOF@IL composites with chemical descriptors GCD, LCD, ϕ, ρ, AV, and V <sub>free</sub> with many structural descriptors correlated then used in the RF model.	Geometrical properties of IL@MOF composites such as PLD, etc. were computed by performing Zeo++ code. RF model prediction accuracy obtained 0.72 of R <sup>2</sup> .	The importance of the top 4 descriptors achieved AV > ρ > V <sub>free</sub> > PLD. The structure-performance optimized AV (0.176–0.444 cm <sup>3</sup> g <sup>−1</sup> ), ρ (1.295–2.046 g cm <sup>−3</sup> ), V <sub>free</sub> (1724–4785 Å <sup>3</sup> ) and PLD (3.921–10.952 Å).	[309]
	RF-based transfer learning modeling carried out based on variables of: i. Intrinsic properties of MOFs,	RF-aided KNN models performed for MMMs (polymer type, CO <sub>2</sub> permeability, etc.) based on two MOFs' hexagonal pores (type, particle size, SSA, etc.) by the coordination between Cu <sup>2+</sup> and THQ or HHTP.	Examplig optimum MOF structure of a pore size >1 nm and surface area 800 m <sup>2</sup> g <sup>−1</sup> .	[310]
	ii. Properties of polymeric matrix,		ML showed 0.2 to 1.45 of RMSE and 0.7–0.91 R <sup>2</sup> in the train and test phases.	

(continued on next page)

**Table 3 (continued)**

Subject	Area	Process	Achievements	Ref
MOF	iii. Characteristics of loaded MOF and membrane thickness. iv. Testing conditions The features of MOFs + polymers and operational parameters were cage size, filler type, loading amount, BET, aperture size, filler size; and pressure and temperature. MOF composites were observed for CO <sub>2</sub> uptake. The 20 experimental structural, chemical, and energy-based features are used to develop ML models to predict the CO <sub>2</sub> /N <sub>2</sub> uptakes.	These features are considered input variables for MLP-/RBF-/ELM-BAT models that are comparatively compared based on R, RMSE, and MAE criteria.	By comparing the hybrid model ELM-BAT could estimate permeability with the lowest RMSE (0.38) and MAE (0.3).	[311]
	HTCS, MD simulation, ML applied to study 6013 computation-ready MOF. PLD, LCD, $\phi$ , $\rho$ , AV and	Experimental, GCMC, and ML approaches are comparatively applied for evaluating the selectivity potentials of ML-prediction and GCMC-simulated MOFs.	The accuracies of R <sup>2</sup> , RMSE, and MAE obtained 0.77 to 0.89, 0.033 to 0.59, and 0.021 to 0.36, respectively.	[301]
	Adsorptive performance of MOFs evaluated by RNN for CO <sub>2</sub> in the humid atmosphere by using inputs of 27 various merged metal nodes and topology characteristics based on the ZINC database. 342,489 h-MOFs generated from 23 to 175 in-/organic SBUs of units arranged in over a thousand net topologies and functionalized with groups used in the AP-RDF novel model.	CoRE and CCDC databases were utilized for experimental MOFs and crystal structures.	ML methods have accuracies of 0.90–0.99 of R <sup>2</sup> in BPNN, RF, DT, and SVM. 14 MOFs with the best properties were screened out for low-concentration CO <sub>2</sub> capturing.	[24]
	MOFs are screened by ML algorithms as classifiers to achieve the ideal MOF structure with optimal catalytic performance.	Structure-property evaluation recognized the best diameter of the sphere within 14.18 Å and SSA of 1750 m <sup>2</sup> g <sup>-1</sup> values are desirable for high-performing MOFs for CO <sub>2</sub> capture. a supercell as the minimum (3 × 3 × 3) for each	Ideal promising MOF designed by RNN with optimum accessible surface area with R of 6–8.	[21]
	28 adsorption properties of thousands of screened h-MOFs and seven high-performance MOFs for CO <sub>2</sub> adsorption were aimed in the DeppFM model.	MOF was constructed for the GCMC simulations with a run rate of 40,000 cycles. The training phase of the ML model continued to explore 1311 h-MOFs, and several structures displayed a strong catalytic ability. Surface area, PLD, LCD, metal linker, porosity, functional groups, and topology are input features. 80 % of 229,768 datasets were shuffled as the train set on the SVD model and the DeepFM models and 20 % of data were tested.	AP-RDF usefully predicted CO <sub>2</sub> uptake based on various combinations of geometric Geo, BOA, and CMD with an R <sup>2</sup> of 0.95.	[282]
	ALIGNN method modeled h-MOF databases with 137,953 MOFs merging with GCMC. Gravimetric/volumetric surface areas, void fraction, largest cavity/pore limiting diameters. 320,000 DDEC atomic charges computed on a bunch of CoRE-MOF databases for coupled ML-GCMC processes.	The training phase of the ML model continued to explore 1311 h-MOFs, and several structures displayed a strong catalytic ability. Surface area, PLD, LCD, metal linker, porosity, functional groups, and topology are input features. 80 % of 229,768 datasets were shuffled as the train set on the SVD model and the DeepFM models and 20 % of data were tested.	Six metals and several ligands can be combined into 24 MOFs, which have strong potential catalysts for carbon dioxide fixation.	[302]
	MLP-NN model (GA-BPNN function) evaluated the MOF potential for CO <sub>2</sub> capture.	QMOF, hMOF, and CoreMOF (2019) databases were used with comparative actual GCMC and ALIGNN predictions of CO <sub>2</sub> capture in various pressures.	DeppFM model predicted the CO <sub>2</sub> capture MAE of 0.017 and R <sup>2</sup> of 0.97.	[312]
	Several classification ML algorithms have been applied to the parameters of MOF modeled through the MD approach. The h-MOFs used from the database with atomic coordinates of 137,953 structures. Descriptors for modeling arranged with structural + building blocks or + atom types CoRE MOF databases are used by merging with GCMC and DFT.	In a supervised ML strategy, a model is trained using different algorithms of LR, NNs, GBDTs, and RF. SSA, pore volume, pressure, and temperature were used as inputs and the optimal values were determined through TOPSIS. CO <sub>2</sub> molecule's force field parameters were achieved from the TraPPE force field.	The model achieved the best accuracies of multi-criteria such as R <sup>2</sup> , RMSE, MAE, and MAD.	[303]
	Hundred building blocks with functional groups geometrically assembled using a construction algorithm Tinkertoy that generated 138,000 MOFs. DT-based techniques such as CatBoost, LightGBM, XGBoost, and RF used for thousand MOF structures	Geometric descriptors such as density, void fraction, SSA, dominant/and maximum pore diameters are applied in ML modeling.	The prediction accuracies are achieved 0.02–0.1, 0.04–0.085, and 0.91–0.99 for MAE, RMSE and R <sup>2</sup> .	[313]
	Structural parameters of the XANES spectrum system, several ML models, extra trees, Ridge Regression, and Neural Networks used for Ni-MOFs. Four features (Filler dosage, temperature, pressure, and polymer type) are used in the CCN model for CO <sub>2</sub> uptake prediction. Experimental and ML results compared various MOFs used for CO <sub>2</sub> capture	ML modeling process achieved in 0.1–10 bar at 250 and 350 K with probe parameters such as V <sub>probes</sub> , Q <sub>probes</sub> , and D <sub>probes</sub> . MLP and LSTM ML models observed CO <sub>2</sub> uptake in 0.5–2.5 bar	ANN model reported R values within 0.99.	[314]
Zeolite	Some simple textural and conditional parameters were used in CART models.	Univariate analysis was used for structures–performance relationship and XGBoost was performed accuracy of 0.81–0.89. RF predicted CO <sub>2</sub> adsorption in various pressures and temperatures with 0.574–0.95 of R <sup>2</sup>	[315]	
	Parameters such as distance from Ni to the molecule, angles of the molecule as rigid body relative to Ni–O1 direction, etc.	The best accuracy achieves ~0.90 of R <sup>2</sup> .	[317]	
	CCN usefully adjusted with a 4-11-1 topology with the highest accuracy.	prediction accuracies ascended in 1 and 2.5 bar with R <sup>2</sup> of >0.94	[318]	
	Matern, exponential, squared exponential, and rational quadratic functions are applied in GPR.	The CO <sub>2</sub> uptake was predicted between 0.94 and 0.99 and RMSE of 0.25–2.00.	[319]	
	The ranking of descriptors' importance was evaluated with DT, RF, LR, and GBR. Also,	Experimental difference spectrum compared with the spectra for the MOF structures predicted by ML models.	[320]	
Zeolite	CCN showed accuracies of multi-criteria; AARD = 2.92%, MSE = 1.55, R = 0.9964	CCN showed accuracies of multi-criteria; AARD = 2.92%, MSE = 1.55, R = 0.9964	[321]	
	Among the 218 zeolites, the model predicted one type that has the best CO <sub>2</sub> adsorption with a relevancy factor of 0.68 and R <sup>2</sup> achieved 0.99.	The pressure showed a high relevancy factor of 0.68 and R <sup>2</sup> achieved 0.99.	[322]	

(continued on next page)

**Table 3 (continued)**

Subject	Area	Process	Achievements	Ref
	material studio. RF model merged with MD simulation. Five hundred experimental datasets of CO <sub>2</sub> adsorption in five zeolites were used for ML-based modeling.	the training size varied from 40 to 90% with R <sup>2</sup> of 0.62–0.93. ML models such as ANFIS, PSO-ANFIS, and LSSVM are used for the prediction of the CO <sub>2</sub> capture on various zeolites. Data was split into 70/30% of all data in train and test.	percentage weight of 69.88% at 298 K and 1 bar which is close to 63.65%. The ML predictive performance for five types of zeolites was compared by using MSE, R <sup>2</sup> , and AARD % criteria.	[323]
Graphene oxide	Seven ML models applied on GO properties and conditional for CO <sub>2</sub> adsorption.	Temperature, Pressure, and SSA are used as inputs. Hyper-parameters of ML models evaluated for improving the accuracy.	Multi-criteria R <sup>2</sup> , RMSE, MAE, and MSE were evaluated. ANN-MLP proposed the ideal values for high CO <sub>2</sub> capture.	[324]

GO: Graphene oxide, CARTs: Classification and regression trees, LightGBM: Light gradient boosting machine LSTM: Long short-term memory, TRappe: Transferable potentials for phase equilibria, FN: Function networks, LSSVM: Least-squares support vector machine, PSO: Particle swarm optimization, ANFIS: Adaptive network-based fuzzy inference system, GBR: Gradient boosting regression, LR: logistic regression, RSM: Response surface methodology, MBE: Mean bias error, TOPSIS: Technique for order of preference by similarity to the ideal solution, GA-BPNN: Genetic algorithm back-propagation neural network, DDEC: Density-derived electrostatic and chemical, DL: Deep learning, LBGM: Light boost gradient machine, CM5: Charge model 5, MSE: Mean squared error, BPNN: Back propagation neural network, PLS: Partial least-square, CNNs: Convolutional neural networks, CCN: Cascade neural networks, GCD: Global cavity diameter, MAD: Mean absolute deviation, AP-RDF: Atomic property-weighted radial distribution function, ALIGNN: Atomistic Line Graph Neural Network, BPNN: back propagation neural network, AV: Accessible volume, VSA: Vacuum swing adsorption, PE: Parasitic energy, GPR: Gaussian process regression, THQL: Tetrahydroxy-1,4-quinone, HHTP: 2,3,6,7,10,11-hexahydroxytriphenylene, CMD: Chemical motifs, BOA: Bag-of-atoms, Geo: Geometric, GA: Genetic algorithm, RNN: Recurrent neural network, SBUs: Structural building units.

\* This section includes the nomenclature of the terms related to machine learning, computational techniques, and properties in the table.

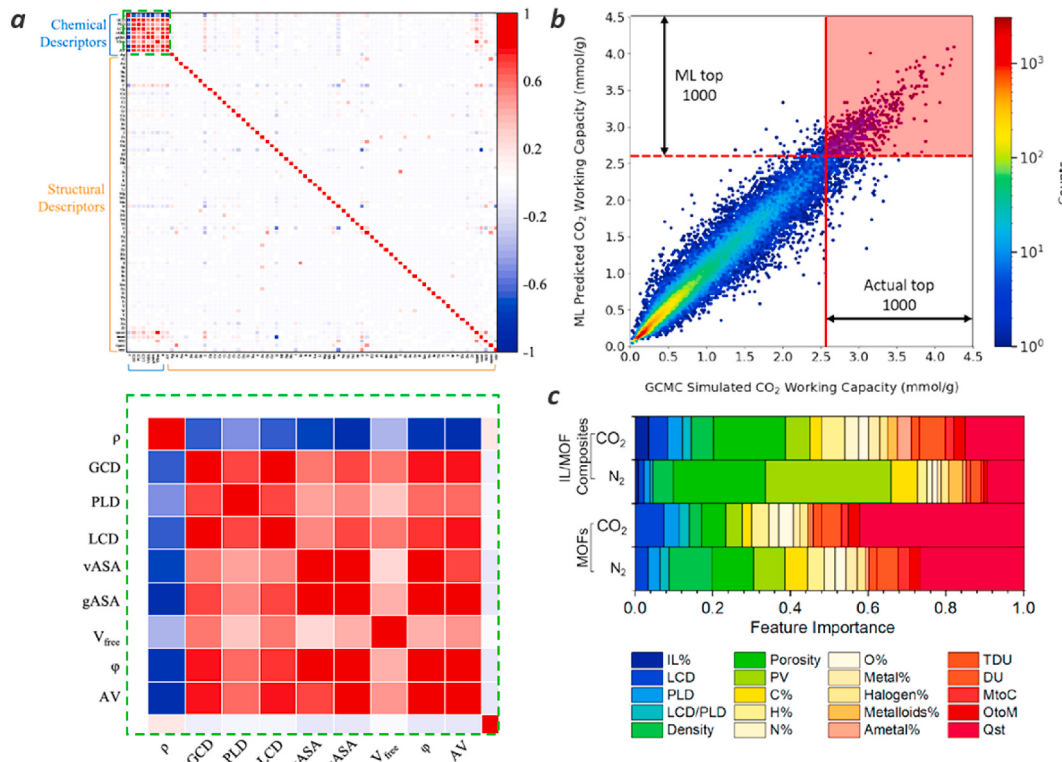


**Fig. 16.** (a) PCC matrix of the chemical and structural descriptors. Adapted from Ref. [325]. Under a Creative Commons Attribution 3.0 Unported Licence (CC BY 3.0). (b) Heat map of the ML-based CO<sub>2</sub> uptake prediction as a function of the GCMC simulated CO<sub>2</sub> working capacity. Reprinted with permission from Ref. [282]. Copyright (2020) American Chemical Society. (c) Feature importance analysis for the gas adsorption properties of IL/MOF composites and pristine MOFs. Adapted from Ref. [301]. Copyright CC BY 4.0 (2023) <https://creativecommons.org/licenses/by/4.0/>.

original/revised models. The effect of Cu-CAT-1 loading values on CO<sub>2</sub> sorption amounts was surveyed which ML model demonstrated high predictive accuracies compared with experimental results. As illustrated in Fig. 18 d, qualitative descriptors such as polymer and MOF types were used in the ML model that showed important values on CO<sub>2</sub> permeability. The RF model applied the sensitivity analysis based on the permutation importance method. The most effective properties of polymers comprise the polymer type with ~0.14 score, control permeability/selectivity, and intrinsic gas transport rates which play

important roles in the gas separation efficiency of MMMs. As can be noted, the specifications of polymers directly influence the contributions of MOFs to membrane performances. MOFs' relatively rigid framework structure is mainly related to the polymer type. Meanwhile, specifications such as BET surface area, and pore-/particle size are features and particle loading 0.4, 0.9, and 0.9 scores, respectively; that are prominent factors, while aperture size is less significant. Also, sensitivity analysis comparatively disclosed other variables, membrane thickness, and testing conditions play low roles with sensitivity level <0.4 [310].

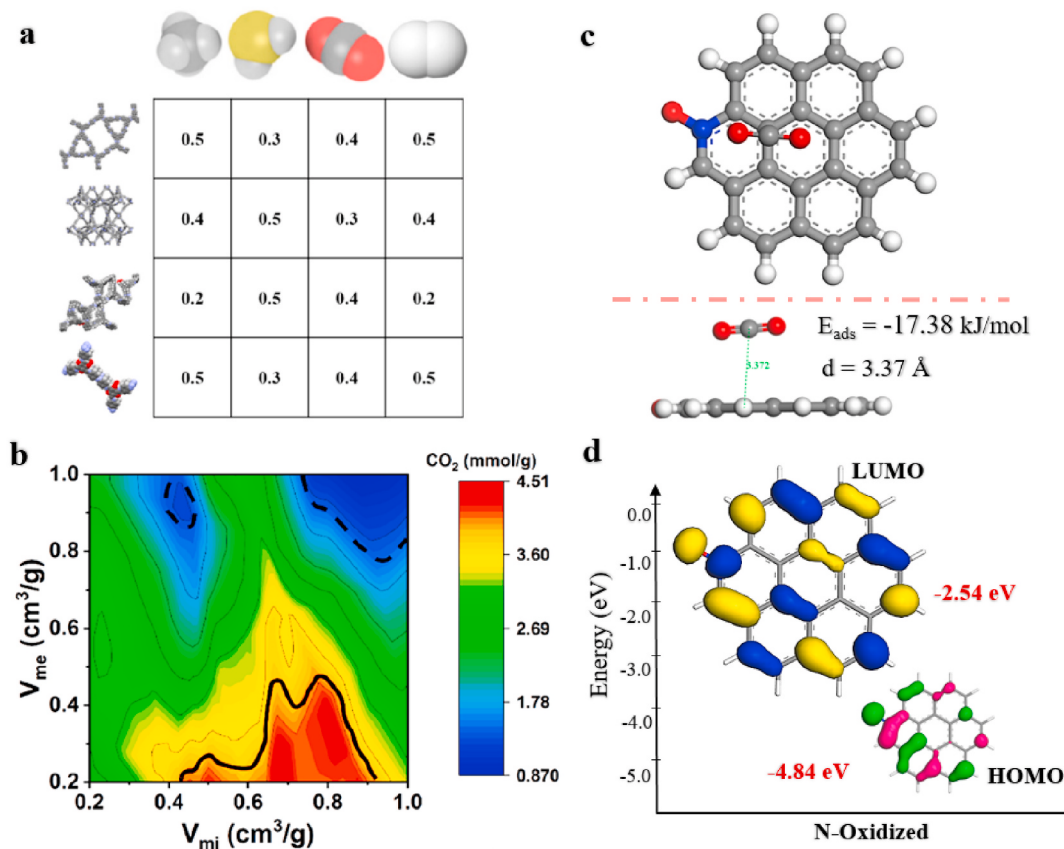


**Fig. 17.** (a) Data classifications of various gases capture based on structure units. Reproduced with permission from Ref. [312]. Copyright (2022) Elsevier., (b) CO<sub>2</sub> uptake based on the functions of micro and mesopores volumes at 25 °C and under 0.5 bar. Reproduced with permission from Ref. [297]. Copyright (2021) Elsevier., (c) and (d) Optimized geometry of nitrogen-doped activated carbon by GA-RBF model for CO<sub>2</sub> physisorption by HOMO/LUMO orbitals. Reproduced with permission from Ref. [280]. Copyright (2022) American Chemical Society.

Discovering the process of appropriate MOF-based composites is effectively considered a great challenge. ML technique needs a huge filler database of composites by inserting molecules into computation-ready and experimental metal-organic frameworks. There are thousands of combined hypothetical MOFs (h-MOF) that by mixed with hundreds of metals and organic ligands as the components of MOF [303]. Zhang et al. used the configurationally-bias Monte Carlo (CBMC) method, GCMC simulations, and ML technique on ion liquid (IL) structure ([NH<sub>2</sub>-Pmim][Tf<sub>2</sub>N]) into each MOF in computation-ready, experimental metal-organic frameworks into MOFs. The [NH<sub>2</sub>-Pmim][Tf<sub>2</sub>N] was selected based on features such as imidazolium function with -NH<sub>2</sub> and -CF<sub>3</sub> functional groups that are promising for CO<sub>2</sub> capture [309]. The evaluation of hyperparameters of ML models can be regarded as a post-modeling achievement. As shown in Fig. 19, the feasibility of ML models can be comparatively compared with tunable parameters and statistical routes (CPU hardware type, Taylor diagram, etc.). As shown in Fig. 19a-b, the neural networks (NNs) model had been significantly optimized by Bayesian regulation backpropagation (BP), quasi-Newton (QD), and resilient backpropagation [280]. The mean absolute percent error (MAPE) criteria are achieved less than 5%. Moreover, the spread parameter was evaluated in the range of 0.1–1 for CO<sub>2</sub> adsorption in the room and cryogenic temperatures (0 and 25 °C) can be seen in Fig. 19c-d [280]. The generalizability of algorithms has been compared from computation times, complexity, and mathematical routes point of view in Fig. 19e-f. The evaluation classifying performance of algorithms is evaluated with precision, recall, and the F1-score for decision tree (DT), k-nearest neighbors (KNN), and support vector machine (SVM). The accuracy scores were obtained between ~0.65 and 0.95 [302]. The MOF Groups 1 to 3 (see Fig. 19e-f), represent various HTS scenarios including

MOFs of tiny (<200 atoms), normal (200–500 atoms), and huge (500–1000) unit cell sizes. Further superior computational speed ascended by 35, 40, and 27% for groups as the cluster size increased from 32 to 80 CPUs [313]. In another study, Alizamir et al. comparatively utilized the Taylor diagram (Fig. 19g) to reveal the extreme learning machines (ELM) as a significant model. The MOF's cage size and the kind of polymer matrix were shown to be the most important variables in predicting the permeability of MOF-based MMMs. In contrast, the amount of loading and pressure were found to be crucial selectivity factors [311].

## 5. Conclusion and outlook

The primary challenge facing modern society is the growing issue of climate change driven by increased CO<sub>2</sub> emissions. Processes for capturing CO<sub>2</sub> pose numerous technological, financial, and environmental challenges. Ionic liquid absorption, for instance, has been proposed and used in industry as a new technique for eliminating CO<sub>2</sub> from flue gases. However, this approach often suffers from high operational costs, solvent toxicity, significant solvent losses, and solvent degradation.

In this review, the latest developments in solid adsorbents are reviewed. Based on statistics derived from literature studies, it is reasonable to infer that research in solid adsorbents for CO<sub>2</sub> adsorption will continue expanding over time. The main driver of this expansion will be the quest for new, environmentally friendly methods of developing advanced adsorbents with specific characteristics such as large surface area, configurable porosity (size, volume, and morphology), and customizable surface chemistry. The most suitable sorbent would ideally

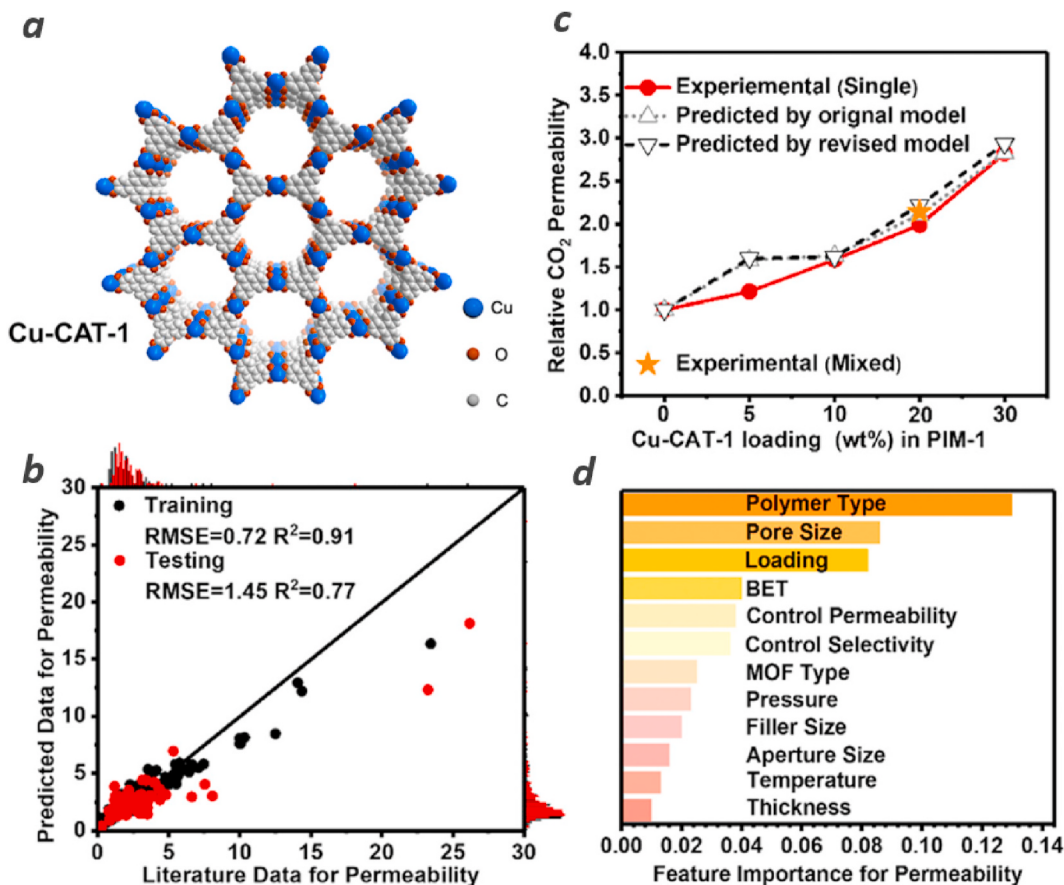


**Fig. 18.** (a) Schematic of Cu-CAT-1 with (b) the scatterplot exhibits the distribution of predicted and literature values of CO<sub>2</sub> permeability and (c) various mass loading through experimental and predictive approaches. (d) Sensitivity analysis for ranking relative feature importance CO<sub>2</sub> uptake. Reproduced with permission from Ref. [310]. Copyright (2022) Elsevier.

possess high CO<sub>2</sub> adsorptive capacity/selectivity, affordable pricing, thermal and chemical stability, moderate heat adsorption, and quick kinetics. Therefore, selecting the optimal adsorbent is the most crucial step in the sorption process. New developments in the creation of different high-tech solid adsorbents including zeolites, carbon-based materials, MOFs, COFs, boron nitride, magnetic nanoparticles, and mesoporous silica, with a particular emphasis on their CO<sub>2</sub> adsorption capacity, have been highlighted in this review. The mechanism of adsorption by solid adsorbents, focusing on establishing a link between structural characteristics and adsorption efficiency, has been thoroughly reviewed. Additionally, the merits and demerits of the mentioned adsorbents for CO<sub>2</sub> capture have been evaluated.

In brief, the key components of this review are as follows.

- While solid adsorbents offer numerous benefits, they also have several drawbacks that prevent them from being ideal adsorbents. These drawbacks include poor diffusion, pore blockage, inclusion of contaminants, moisture sensitivity, difficult functionalization, and high reagent costs. Finding solutions to these issues, such as modifying the synthesis procedure or functionalizing the structure, is vital.
- The primary advantage of the materials under investigation is their versatility; they are not only effective as adsorbents but can also function as fillers in membranes, supports or substrates, or components of composites to enhance adsorption kinetics.
- There does not seem to be a straightforward correlation between the structural characteristics of an adsorbent—such as total pore volume, pore size distribution, and BET surface area—and the quantity of gas adsorbed. In certain cases, substantial gas adsorption occurs despite

the adsorbent having a relatively low specific surface area and pore volume. This observation implies that factors beyond textural properties, specifically the morphology and surface chemistry of the adsorbents, play a complementary role in determining adsorption performance.

- Some adsorbents, like MOFs and COFs, are categorized as laboratory adsorbents and are not competitive with commercial adsorbents such as activated carbon and zeolite for industrial applications due to their high costs. Additionally, reliable methods for their large-scale synthesis are lacking, as their production relies on laboratory trial and error.
- Machine learning algorithms can prove useful in CO<sub>2</sub> capture alongside advancements in the synthesis technology of solid adsorbents. Therefore, various models including RBF, MLP, ANFIS, and hybrid variations of them, have been reviewed to predict physical features, expedite the selection of the best adsorbents, optimize sorbent synthesis conditions, and comprehend helpful parameters for effective sorption. However, for machine learning to be effective, algorithms need ample time to evolve and learn, ensuring they achieve their objectives with high precision and relevance. This process demands considerable computational resources, often requiring enhanced processing power. Interpreting the output generated by these algorithms poses another major challenge. Furthermore, choosing the right algorithms to meet ML requirements is prone to potential errors.

Despite the severe difficulties associated with practical CO<sub>2</sub> sorption using solid adsorbents, the potential for tremendous environmental advantages of sustainable CO<sub>2</sub> uptake and storage cannot be overlooked.

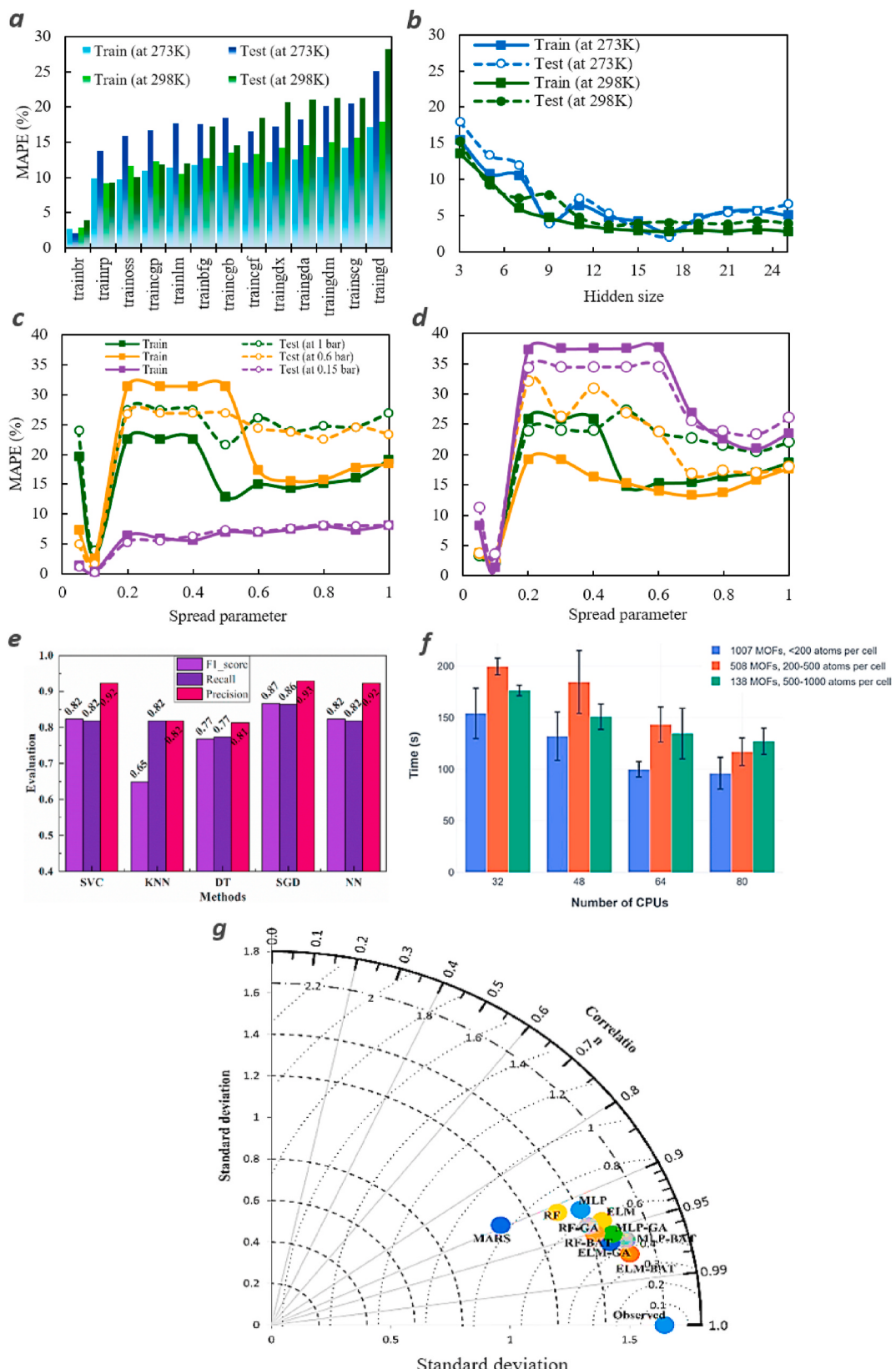


**Fig. 19.** The evaluation of the generalizability of the ANN model by (a) training algorithms and (b) hidden size in the middle layer. Also, the spread parameters of RBF-NN tuned at (c) 273 and (d) 298 K for CO<sub>2</sub> capture prediction. Reproduced with permission from Ref. [280]. Copyright (2022) American Chemical Society. The evaluation of various predictive performances of models based on (e) accuracy. Reproduced with permission from Ref. [302]. Copyright (2021) Elsevier., (f) CPU values. Reproduced with permission from Ref. [313]. Copyright (2021) American Chemical Society., and (g) Taylor diagram. Reproduced with permission from Ref. [311]. Copyright (2023) Elsevier.

The conversion of extracted CO<sub>2</sub> also addresses the issue of climate change since solid adsorbents have the potential to remove the captured CO<sub>2</sub> and use it for product conversion (such as methanol, formate, methane, ethylene, and valuable fuels). More exploratory research should be conducted in the future to integrate their CO<sub>2</sub> conversion capabilities with ML algorithms.

In summary, the use of solid adsorbents for CO<sub>2</sub> capture is still in its nascent stages, indicating substantial opportunities for advancements in both the materials used and the associated process technologies. Future research should concentrate on creating new, highly efficient CO<sub>2</sub> capture agents and refining current adsorbents to achieve superior CO<sub>2</sub> adsorption capabilities.

#### CRediT authorship contribution statement

**Mobin Safarzadeh Khosrowshahi:** Writing – review & editing, Writing – original draft, Visualization, Validation, Supervision, Software, Resources, Project administration, Methodology, Investigation, Funding acquisition, Formal analysis, Data curation, Conceptualization. **Amirhossein Afshari Aghajari:** Writing – review & editing, Writing – original draft, Visualization, Validation, Supervision, Software, Resources, Funding acquisition, Formal analysis, Data curation, Conceptualization. **Mohammad Rahimi:** Writing – review & editing, Writing – original draft, Visualization, Validation, Supervision, Software, Resources, Project administration, Methodology, Investigation, Funding acquisition, Formal analysis, Data curation, Conceptualization. **Farid Maleki:** Writing – review & editing, Writing – original draft, Visualization, Validation, Supervision, Software, Resources, Funding acquisition, Formal analysis, Data curation, Conceptualization. **Elahe Ghiyabi:** Writing – review & editing, Writing – original draft, Visualization, Validation, Supervision, Software, Resources, Funding acquisition, Formal analysis, Data curation, Conceptualization. **Armin Rezanezhad:** Writing – review & editing, Writing – original draft, Visualization, Validation, Supervision, Software, Resources, Funding acquisition, Formal analysis, Data curation, Conceptualization. **Ali Bakhshi:** Writing – review & editing, Writing – original draft, Visualization, Validation, Supervision, Software, Resources, Funding acquisition, Formal analysis, Data curation, Conceptualization. **Ehsan Salari:** Writing – review & editing, Writing – original draft, Visualization, Validation, Supervision, Software, Resources, Funding acquisition, Formal analysis, Data curation, Conceptualization. **Hadi Shayesteh:** Writing – review & editing, Writing – original draft, Visualization, Validation, Supervision, Software, Resources, Funding acquisition, Formal analysis, Data curation, Conceptualization. **Hadi Mohammadi:** Writing – review & editing, Visualization, Validation, Supervision, Software, Resources, Funding acquisition, Formal analysis, Data curation, Conceptualization.

#### Declaration of competing interest

The authors declare that they have no known competing financial interests or personal relationships that could have appeared to influence the work reported in this paper.

#### Data availability

No data was used for the research described in the article.

#### Acknowledgment

This research work was conducted under the kind support of the Iran University of Science and Technology.

#### References

- [1] T.M. Gür, Carbon dioxide emissions, capture, storage and utilization: Review of materials, processes and technologies, *Prog. Energy Combust. Sci.* 89 (2022) 100965.
- [2] J. Rogelj, et al., A new scenario logic for the Paris Agreement long-term temperature goal, *Nature* 573 (7774) (2019) 357–363.
- [3] E. Benhelal, et al., Global strategies and potentials to curb CO<sub>2</sub> emissions in cement industry, *J. Clean. Prod.* 51 (2013) 142–161.
- [4] V.J. Aimikhe, M.S. Anyebe, M. Ibezim-Ezeani, Development of composite activated carbon from mango and almond seed shells for CO<sub>2</sub> capture, *Biomass Conversion and Biorefinery* (2022) 1–15.
- [5] L. Li, et al., Separation of CO<sub>2</sub>/CH<sub>4</sub> and CH<sub>4</sub>/N<sub>2</sub> mixtures by M/DOBDC: a detailed dynamic comparison with MIL-100 (Cr) and activated carbon, *Microporous Mesoporous Mater.* 198 (2014) 236–246.
- [6] N.A. Qasem, et al., Synthesis, characterization, and CO<sub>2</sub> breakthrough adsorption of a novel MWCNT/MIL-101 (Cr) composite, *J. CO<sub>2</sub> Util.* 22 (2017) 238–249.
- [7] S. Yousef, et al., CO<sub>2</sub>/CH<sub>4</sub>, CO<sub>2</sub>/N<sub>2</sub> and CO<sub>2</sub>/H<sub>2</sub> selectivity performance of PES membranes under high pressure and temperature for biogas upgrading systems, *Environ. Technol. Innov.* 21 (2021) 101339.
- [8] H.J. Yoon, K.B. Lee, Introduction of chemically bonded zirconium oxide in CaO-based high-temperature CO<sub>2</sub> sorbents for enhanced cyclic sorption, *Chem. Eng. J.* 355 (2019) 850–857.
- [9] M. Aghaie, N. Rezaei, S. Zendehboudi, A systematic review on CO<sub>2</sub> capture with ionic liquids: Current status and future prospects, *Renew. Sustain. Energy Rev.* 96 (2018) 502–525.
- [10] X. Ma, et al., Heteroatom-doped porous carbons exhibit superior CO<sub>2</sub> capture and CO<sub>2</sub>/N<sub>2</sub> selectivity: understanding the contribution of functional groups and pore structure, *Sep. Purif. Technol.* 259 (2021) 118065.
- [11] M. Plaza, et al., Green coffee based CO<sub>2</sub> adsorbent with high performance in postcombustion conditions, *Fuel* 140 (2015) 633–648.
- [12] N. Mittal, et al., Postcombustion CO<sub>2</sub> capture using N-(3-trimethoxysilylpropyl) diethylenetriamine-grafted solid adsorbent, *Energy Sci. Eng.* 3 (3) (2015) 207–220.
- [13] L. Grima, et al., High CO<sub>2</sub> permeability in supported molten-salt membranes with highly dense and aligned pores produced by directional solidification, *J. Membr. Sci.* 630 (2021) 119057.
- [14] P. Zhang, et al., A new choice of polymer precursor for solvent-free method: Preparation of N-enriched porous carbons for highly selective CO<sub>2</sub> capture, *Chem. Eng. J.* 355 (2019) 963–973.
- [15] T. Lu, et al., Self-activating Approach for Synthesis of 2, 6-naphthalene disulfonic acid di sodium salt-derived porous Carbon and CO<sub>2</sub> capture performance, *Energy Fuels* 37 (5) (2023) 3886–3893.
- [16] G. Singh, et al., A combined strategy of acid-assisted polymerization and solid state activation to synthesize functionalized nanoporous activated biocarbons from biomass for CO<sub>2</sub> capture, *Microporous Mesoporous Mater.* 271 (2018) 23–32.
- [17] G. Chakraborty, P. Das, S.K. Mandal, Efficient and highly selective CO<sub>2</sub> capture, separation, and chemical Conversion under ambient Conditions by a polar-group-appended copper (II) metal-organic framework, *Inorg. Chem.* 60 (7) (2021) 5071–5080.
- [18] R. Poloni, B. Smit, J.B. Neaton, Ligand-assisted enhancement of CO<sub>2</sub> capture in metal-organic frameworks, *J. Am. Chem. Soc.* 134 (15) (2012) 6714–6719.
- [19] B. Petrovic, M. Gorbounov, S.M. Soltani, Influence of surface modification on selective CO<sub>2</sub> adsorption: a technical review on mechanisms and methods, *Microporous Mesoporous Mater.* 312 (2021) 110751.
- [20] M. Fernandez, et al., Rapid and accurate machine learning recognition of high performing metal organic frameworks for CO<sub>2</sub> capture, *J. Phys. Chem. Lett.* 5 (17) (2014) 3056–3060.
- [21] X. Zhang, et al., Machine learning-driven discovery of metal-organic frameworks for efficient CO<sub>2</sub> capture in humid condition, *ACS Sustain. Chem. Eng.* 9 (7) (2021) 2872–2879.
- [22] M.S. Khosrowshahi, H. Mashhadimoslem, Molecular dynamics of polymeric adsorbents, in: *Polymeric Adsorbents*, Elsevier, 2024, pp. 433–460.
- [23] H. Mashhadimoslem, F. Maleki, M.S. Khosrowshahi, Modeling of polymeric adsorbent behavior, in: *Polymeric Adsorbents*, Elsevier, 2024, pp. 393–432.
- [24] X. Deng, et al., Large-scale screening and machine learning to predict the computation-ready, experimental metal-organic frameworks for CO<sub>2</sub> capture from air, *Appl. Sci.* 10 (2) (2020) 569.
- [25] R. Anderson, et al., Role of pore chemistry and topology in the CO<sub>2</sub> capture capabilities of MOFs: from molecular simulation to machine learning, *Chem. Mater.* 30 (18) (2018) 6325–6337.
- [26] M. Mikkelsen, M. Jørgensen, F.C. Krebs, The teraton challenge. A review of fixation and transformation of carbon dioxide, *Energy Environ. Sci.* 3 (1) (2010) 43–81.
- [27] H. Seo, M. Rahimi, T.A. Hatton, Electrochemical carbon dioxide capture and release with a redox-active amine, *J. Am. Chem. Soc.* 144 (5) (2022) 2164–2170.
- [28] I. Sullivan, et al., Coupling electrochemical CO<sub>2</sub> conversion with CO<sub>2</sub> capture, *Nat. Catal.* 4 (11) (2021) 952–958.
- [29] J. He, et al., Liquefiable biomass-derived porous carbons and their applications in CO<sub>2</sub> capture and conversion, *Green Chem.* 24 (9) (2022) 3376–3415.
- [30] R.M. Moghazy, S.M. Abdo, R.H. Mahmoud, Algal biomass as a promising tool for CO<sub>2</sub> sequestration and wastewater bioremediation: an integration of green technology for different aspects, in: *Handbook of Algal Biofuels*, Elsevier, 2022, pp. 149–166.

- [31] C. Goel, H. Bhunia, P.K. Bajpai, Novel nitrogen enriched porous carbon adsorbents for CO<sub>2</sub> capture: Breakthrough adsorption study, *J. Environ. Chem. Eng.* 4 (1) (2016) 346–356.
- [32] A. Samanta, et al., Post-combustion CO<sub>2</sub> capture using solid sorbents: a review, *Ind. Eng. Chem. Res.* 51 (4) (2012) 1438–1463.
- [33] Z. Zhang, et al., Rational design of tailored porous carbon-based materials for CO<sub>2</sub> capture, *J. Mater. Chem. A* 7 (37) (2019) 20985–21003.
- [34] P. Madejski, et al., Methods and techniques for CO<sub>2</sub> capture: Review of potential solutions and applications in modern energy technologies, *Energies* 15 (3) (2022) 887.
- [35] M. Feng, et al., Cooperative chemisorption-induced Physisorption of CO<sub>2</sub> Molecules by metal-organic chains, *ACS Nano* 9 (12) (2015) 12124–12136.
- [36] A.H. Berger, A.S. Bhowm, Comparing physisorption and chemisorption solid sorbents for use separating CO<sub>2</sub> from flue gas using temperature swing adsorption, *Energy Proc.* 4 (2011) 562–567.
- [37] M. Atif, et al., Physisorption and chemisorption trends in surface modification of carbon black, *Surface. Interfac.* 31 (2022) 102080.
- [38] A. Salehabadi, et al., Carbon-based nanocomposites in solid-state hydrogen storage technology: an overview, *Int. J. Energy Res.* 44 (14) (2020) 11044–11058.
- [39] H. Dong, et al., B40 fullerene: an efficient material for CO<sub>2</sub> capture, storage and separation, *Curr. Appl. Phys.* 15 (9) (2015) 1084–1089.
- [40] N. Abuelnoor, et al., Activated carbons from biomass-based sources for CO<sub>2</sub> capture applications, *Chemosphere* 282 (2021) 131111.
- [41] J.J. Manyá, et al., Ultra-microporous adsorbents prepared from vine shoots-derived biochar with high CO<sub>2</sub> uptake and CO<sub>2</sub>/N<sub>2</sub> selectivity, *Chem. Eng. J.* 345 (2018) 631–639.
- [42] L. Rao, et al., Nitrogen enriched porous carbons from d-glucose with excellent CO<sub>2</sub> capture performance, *Chem. Eng. J.* 362 (2019) 794–801.
- [43] G. Srinivas, et al., Exceptional CO<sub>2</sub> capture in a hierarchically porous carbon with simultaneous high surface area and pore volume, *Energy Environ. Sci.* 7 (1) (2014) 335–342.
- [44] S.K. Nabil, et al., Bifunctional gas diffusion electrode enables in situ Separation and Conversion of CO<sub>2</sub> to Ethylene from dilute stream, *Adv. Mater.* (2023) 2300389.
- [45] M.S. Khosrowshahi, et al., Green self-activating synthesis system for porous carbons: Celery biomass wastes as a typical case for CO<sub>2</sub> uptake with kinetic, equilibrium and thermodynamic studies, *Diam. Relat. Mater.* 127 (2022) 109204.
- [46] H. Mashhadimoslem, et al., Adsorption equilibrium, thermodynamic, and kinetic study of O<sub>2</sub>/N<sub>2</sub>/CO<sub>2</sub> on functionalized granular activated carbon, *ACS Omega* 7 (22) (2022) 18409–18426.
- [47] X. Liu, et al., Orderly porous covalent organic frameworks-based materials: superior adsorbents for pollutants removal from aqueous solutions, *Innovation* (1) (2021) 2.
- [48] W. Gao, T. Zhou, Q. Wang, Controlled synthesis of MgO with diverse basic sites and its CO<sub>2</sub> capture mechanism under different adsorption conditions, *Chem. Eng. J.* 336 (2018) 710–720.
- [49] Y. Liu, et al., Theoretical studies of CO<sub>2</sub> adsorption mechanism on linkers of metal-organic frameworks, *Fuel* 95 (2012) 521–527.
- [50] X. Song, et al., Exploring a new method to study the effects of surface functional groups on adsorption of CO<sub>2</sub> and CH<sub>4</sub> on activated carbons, *Langmuir* 36 (14) (2020) 3862–3870.
- [51] M. Kwiatkowski, et al., Evaluation of CO<sub>2</sub> interactions with S-doped nanoporous carbon and its composites with a reduced GO: Effect of surface features on an apparent physical adsorption mechanism, *Carbon* 98 (2016) 250–258.
- [52] W. Xing, et al., Superior CO<sub>2</sub> uptake of N-doped activated carbon through hydrogen-bonding interaction, *Energy Environ. Sci.* 5 (6) (2012) 7323–7327.
- [53] P. Psarras, J. He, J. Wilcox, Effect of water on the CO<sub>2</sub> adsorption capacity of amine-functionalized carbon sorbents, *Ind. Eng. Chem. Res.* 56 (21) (2017) 6317–6325.
- [54] C. Xu, E. Dinka, N. Hedin, Hydrophobic porous polyketimines for the capture of CO<sub>2</sub>, *ChemPlusChem* 81 (1) (2016) 58–63.
- [55] W. Zhang, Y. Bao, A. Bao, Preparation of nitrogen-doped hierarchical porous carbon materials by a template-free method and application to CO<sub>2</sub> capture, *J. Environ. Chem. Eng.* 8 (3) (2020) 103732.
- [56] V. Indira, K. Abhitha, A review on recent developments in Zeolite A synthesis for improved carbon dioxide capture: Implications for the water-energy nexus, *Energy Nexus* 7 (2022) 100095.
- [57] Z. Zhang, et al., Enhancement of CO<sub>2</sub> adsorption and CO<sub>2</sub>/N<sub>2</sub> selectivity on ZIF-8 via postsynthetic modification, *AIChE J.* 59 (6) (2013) 2195–2206.
- [58] X. Lv, et al., High CO<sub>2</sub>/N<sub>2</sub> and CO<sub>2</sub>/CH<sub>4</sub> selectivity in a chiral metal-organic framework with contracted pores and multiple functionalities, *Chem. Commun.* 50 (52) (2014) 6886–6889.
- [59] M.S. Khosrowshahi, et al., Natural products derived porous Carbons for CO<sub>2</sub> capture, *Adv. Sci.* 10 (36) (2023) 2304289.
- [60] C. Quan, et al., Biomass-based carbon materials for CO<sub>2</sub> capture: a review, *J. CO<sub>2</sub> Util.* 68 (2023) 102373.
- [61] J.J. Delgado-Marín, et al., New generation of MOF-monoliths based on metal foams, *Molecules* 27 (6) (2022) 1968.
- [62] Z. Yao, et al., Direct evidence of CO<sub>2</sub> capture under low partial pressure on a pillared metal-organic framework with improved stabilization through intramolecular hydrogen bonding, *ChemPlusChem* 81 (8) (2016) 850–856.
- [63] S. Builes, et al., Microporous carbon adsorbents with high CO<sub>2</sub> capacities for industrial applications, *Phys. Chem. Chem. Phys.* 13 (35) (2011) 16063–16070.
- [64] O.H. Gunawardene, et al., Carbon Dioxide capture through physical and chemical adsorption using porous carbon materials: a review, *Atmosphere* 13 (3) (2022) 397.
- [65] C. Zhang, et al., Molecular simulation on carbon dioxide capture performance for carbons doped with various elements, *Energy Storage and Saving* 2 (2) (2023) 435–441.
- [66] M. Cox, R. Mokaya, Ultra-high surface area mesoporous carbons for colossal pre combustion CO<sub>2</sub> capture and storage as materials for hydrogen purification, *Sustain. Energy Fuels* 1 (6) (2017) 1414–1424.
- [67] X. Yu, C.T. Williams, Recent advances in the applications of mesoporous silica in heterogeneous catalysis, *Catal. Sci. Technol.* 12 (19) (2022) 5765–5794.
- [68] E. Salari, et al., The relationship between cellular microstructure and the mechanical properties of styrene/methyl methacrylate copolymer-silica nanocomposite foams prepared by a supercritical CO<sub>2</sub> blowing agent, *Polym. Eng. Sci.* (2024).
- [69] D.-W. Lee, et al., Alcohol and water free synthesis of mesoporous silica using deep eutectic solvent as a template and solvent and its application as a catalyst support for formic acid dehydrogenation, *ACS Sustainable Chemistry & Engineering* 6 (9) (2018) 12241–12250.
- [70] C. Qian, et al., Imine and imine-derived linkages in two-dimensional covalent organic frameworks, *Nat. Rev. Chem.* 6 (12) (2022) 881–898.
- [71] D. Huisingsh, et al., Recent advances in carbon emissions reduction: policies, technologies, monitoring, assessment and modeling, *J. Clean. Prod.* 103 (2015) 1–12.
- [72] A.R. Bagheri, et al., Covalent organic frameworks as robust materials for mitigation of environmental pollutants, *Chemosphere* 270 (2021) 129523.
- [73] W. Zhao, et al., Using sound to synthesize covalent organic frameworks in water, *Nature Synthesis* 1 (1) (2022) 87–95.
- [74] E. Rezaie, et al., Magnetoreological studies of polymer nanocomposites, in: *Rheology of Polymer Blends and Nanocomposites*, Elsevier, 2020, pp. 263–294.
- [75] P. Nezhad-Mokhtari, et al., Magnetic nanoparticles: an emergent Platform for future cancer theranostics, *Nanobiotechnology in Diagnosis, Drug Delivery, and Treatment* (2020) 171–195.
- [76] I. Adánez-Rubio, et al., Coal and biomass combustion with CO<sub>2</sub> capture by CLOU process using a magnetic Fe-Mn-supported CuO oxygen carrier, *Fuel* 314 (2022) 122742.
- [77] W. Li, et al., Surface tunable magnetic nano-sorbents for carbon dioxide sorption and separation, *Chem. Eng. J.* 313 (2017) 1160–1167.
- [78] A. Rezanezhad, et al., Outstanding supercapacitor performance of Nd–Mn co-doped perovskite LaFeO<sub>3</sub>@nitrogen-doped graphene oxide nanocomposites, *Electrochim. Acta* 335 (2020) 135699.
- [79] A. Rezanezhad, et al., Superparamagnetic magnetite nanoparticles for cancer cells treatment via magnetic hyperthermia: effect of natural capping agent, particle size and concentration, *J. Mater. Sci. Mater. Electron.* 32 (19) (2021) 24026–24040.
- [80] S. Rodríguez-García, et al., Role of the structure of graphene oxide sheets on the CO<sub>2</sub> adsorption properties of nanocomposites based on graphene oxide and polyaniiline or Fe3O4-nanoparticles, *ACS Sustain. Chem. Eng.* 7 (14) (2019) 12464–12473.
- [81] M. Helmi, et al., Synthesis, characterization and performance evaluation of NaOH@ Chitosan-Fe3O4 as an adsorbent for CO<sub>2</sub> capture, *Fuel* 338 (2023) 127300.
- [82] Y. Wang, et al., Hybrid carbon molecular sieve membranes having ordered Fe3O4@ZIF-8-derived microporous structure for gas separation, *J. Membr. Sci.* 666 (2023) 121127.
- [83] Z. Otgonbayar, C.-M. Yoon, W.-C. Oh, Photoelectrocatalytic CO<sub>2</sub> reduction with ternary nanocomposite of MXene (Ti3C2)-Cu2O-Fe3O4: Comprehensive utilization of electrolyte and light-wavelength, *Chem. Eng. J.* 464 (2023) 142716.
- [84] S. Roy, et al., Selective CO<sub>2</sub> reduction to methane catalyzed by mesoporous Ru-Fe3O4/CeOx-SiO2 in a fixed bed flow reactor, *Mol. Catal.* 528 (2022) 112486.
- [85] A.K. Mishra, S. Ramaprabhu, Nano magnetite decorated multiwalled carbon nanotubes: a robust nanomaterial for enhanced carbon dioxide adsorption, *Energy Environ. Sci.* 4 (3) (2011) 889–895.
- [86] A. Hakim, et al., Studies on CO<sub>2</sub> adsorption and desorption properties from various types of iron oxides (FeO, Fe2O3, and Fe3O4), *Ind. Eng. Chem. Res.* 55 (29) (2016) 7888–7897.
- [87] E. Oddo, et al., Amino-functionalized magnetic nanoparticles for CO<sub>2</sub> capture, *Int. J. Soc. Netw. Min.* 12 (4) (2021) 472–490.
- [88] N. Guha, et al., Environmentally benign melamine functionalized silica-coated iron oxide for selective CO<sub>2</sub> capture and fixation into cyclic carbonate, *J. CO<sub>2</sub> Util.* 49 (2021) 101575.
- [89] N. Ali, et al., Hollow, porous, and flexible Co3O4-doped carbon Nanofibers for efficient CO<sub>2</sub> capture, *Adv. Eng. Mater.* 25 (6) (2023) 2201335.
- [90] L. Li, et al., MgAl2O4 spinel-stabilized calcium oxide absorbents with improved durability for high-temperature CO<sub>2</sub> capture, *Energy Fuels* 24 (6) (2010) 3698–3703.
- [91] A.H. Lahuri, et al., Kinetics and thermodynamic modeling for CO<sub>2</sub> capture using NiO supported activated carbon by temperature swing adsorption, *Biointerface Research in Applied Chemistry* 12 (3) (2022) 4200–4219.
- [92] N. Gómez-Garduño, et al., Unveiling the different physicochemical properties of M-doped β-NaFeO<sub>2</sub> (where M= Ni or Cu) materials evaluated as CO<sub>2</sub> sorbents: a combined experimental and theoretical analysis, *J. Mater. Chem. A* 11 (20) (2023) 10938–10954.
- [93] J.F. Gómez-García, H. Pfeiffer, Effect of chemical composition and crystal phase of (Li, Na) FeO<sub>2</sub> ferrites on CO<sub>2</sub> capture properties at high temperatures, *J. Phys. Chem. C* 122 (37) (2018) 21162–21171.

- [94] Z. Sun, et al., Ca2Fe2O5: a promising oxygen carrier for CO/CH4 conversion and almost-pure H2 production with inherent CO2 capture over a two-step chemical looping hydrogen generation process, *Appl. Energy* 211 (2018) 431–442.
- [95] I. Yanase, et al., CO2 capture from ambient air by  $\beta$ -NaFeO2 in the presence of water vapor at 25–100°C, *Powder Technol.* 348 (2019) 43–50.
- [96] M. Zhu, et al., Preparation of pineapple waste-derived porous carbons with enhanced CO2 capture performance by hydrothermal carbonation-alkali metal oxalates assisted thermal activation process, *Chem. Eng. Res. Des.* 146 (2019) 130–140.
- [97] V. Singh, et al., Graphene based materials: past, present and future, *Prog. Mater. Sci.* 56 (8) (2011) 1178–1271.
- [98] J. Li, et al., Enhanced CO2 capture on graphene via N, S dual-doping, *Appl. Surf. Sci.* 399 (2017) 420–425.
- [99] F. Zhou, et al., Ultrathin graphene oxide-based hollow fiber membranes with brush-like CO2-phobic agent for highly efficient CO2 capture, *Nat. Commun.* 8 (1) (2017) 2107.
- [100] Y. Wang, et al., Nitrogen, hydrogen, carbon dioxide, and water vapor sorption properties of three-dimensional graphene, *J. Chem. Eng. Data* 56 (3) (2011) 642–645.
- [101] X. Huang, et al., Graphene-based materials: synthesis, characterization, properties, and applications, *Small* 7 (14) (2011) 1876–1902.
- [102] J. Wu, X. Qiu, S. Chen, Preparation and characterization of an amine-modified graphene aerogel for enhanced carbon dioxide adsorption, *J. Mater. Sci.* 57 (3) (2022) 1727–1737.
- [103] E. Vilarrasa-García, et al., CO2 adsorption on APTES functionalized mesocellular foams obtained from mesoporous silicas, *Microporous Mesoporous Mater.* 187 (2014) 125–134.
- [104] S. Shang, et al., Facile synthesis of CuBTC and its graphene oxide composites as efficient adsorbents for CO2 capture, *Chem. Eng. J.* 393 (2020) 124666.
- [105] S. Chowdhury, G.K. Parshetti, R. Balasubramanian, Post-combustion CO2 capture using mesoporous TiO2/graphene oxide nanocomposites, *Chem. Eng. J.* 263 (2015) 374–384.
- [106] X. Li, et al., Efficient CO2 capture by functionalized graphene oxide nanosheets as fillers to fabricate multi-permselective mixed matrix membranes, *ACS Appl. Mater. Interfaces* 7 (9) (2015) 5528–5537.
- [107] B. Luan, et al., Crown nanoparticles in graphene for CO2 capture and filtration, *ACS Nano* 16 (4) (2022) 6274–6281.
- [108] B. Gao, et al., Doping of calcium in C60 fullerene for enhancing CO2 capture and N2O transformation: a theoretical study, *J. Phys. Chem. A* 115 (35) (2011) 9969–9976.
- [109] L. Cheng, et al., g-C3N4 nanosheets with tunable affinity and sieving effect endowing polymeric membranes with enhanced CO2 capture property, *Sep. Purif. Technol.* 250 (2020) 117200.
- [110] R. Bahadur, et al., BCN nanostructures conjugated nanoporous carbon with oxygenated surface and high specific surface area for enhanced CO2 capture and supercapacitance, *Chem. Eng. J.* 460 (2023) 141793.
- [111] K.-Y. Tao, et al., A template co-pyrolysis strategy towards the increase of amino/imino content within g-C3N4 for efficient CO2 photoreduction, *Chem. Eng. J.* 455 (2023) 140630.
- [112] Y. Dai, et al., 1D-2D intercalated network CMC@g-C3N4/IL membrane with high permeability and selectivity for the CO2 capture, *J. Membr. Sci.* 686 (2023) 122019.
- [113] B. Zhu, et al., Adsorption investigation of CO2 on g-C3N4 surface by DFT calculation, *J. CO2 Util.* 21 (2017) 327–335.
- [114] Y. Liu, et al., Hydrogenated Si-doped g-C3N4: Promising electrocatalyst for CO2 capture and conversion, *Appl. Surf. Sci.* 614 (2023) 156195.
- [115] C. Sathish, et al., Ordered mesoporous boron carbon nitrides with tunable mesopore nanoarchitectonics for energy storage and CO2 adsorption properties, *Adv. Sci.* 9 (16) (2022) 2105603.
- [116] S. Zohdi, M. Anbia, S. Salehi, Improved CO2 adsorption capacity and CO2/CH4 and CO2/N2 selectivity in novel hollow silica particles by modification with multi-walled carbon nanotubes containing amine groups, *Polyhedron* 166 (2019) 175–185.
- [117] M.-S. Lee, S.-J. Park, Silica-coated multi-walled carbon nanotubes impregnated with polyethyleneimine for carbon dioxide capture under the flue gas condition, *J. Solid State Chem.* 226 (2015) 17–23.
- [118] A. Sayari, Y. Belmabkhout, Stabilization of amine-containing CO2 adsorbents: dramatic effect of water vapor, *J. Am. Chem. Soc.* 132 (18) (2010) 6312–6314.
- [119] M.-S. Lee, S.-Y. Lee, S.-J. Park, Preparation and characterization of multi-walled carbon nanotubes impregnated with polyethyleneimine for carbon dioxide capture, *Int. J. Hydrogen Energy* 40 (8) (2015) 3415–3421.
- [120] S.-C. Hsu, et al., Thermodynamics and regeneration studies of CO2 adsorption on multiwalled carbon nanotubes, *Chem. Eng. Sci.* 65 (4) (2010) 1354–1361.
- [121] Y. Zhang, et al., Multi-walled carbon nanotubes/carbon foam nanocomposites derived from biomass for CO2 capture and supercapacitor applications, *Fuel* 305 (2021) 121622.
- [122] N.A. Zubbri, et al., Enhancement of CO2 adsorption on biochar sorbent modified by metal incorporation, *Environ. Sci. Pollut. Control Ser.* 27 (2020) 11809–11829.
- [123] H. Cui, et al., Facile fabrication of nitrogen doped carbon from filter paper for CO2 adsorption, *Energy* 187 (2019) 115936.
- [124] R.-L. Liu, et al., Fabrication of nitrogen-doped hierarchically porous carbons through a hybrid dual-template route for CO2 capture and haemoperfusion, *Carbon* 76 (2014) 84–95.
- [125] L. Xie, et al., Porous carbons synthesized by templating approach from fluid precursors and their applications in environment and energy storage: a review, *Carbon* 170 (2020) 100–118.
- [126] L.-P. Guo, et al., Interfacial assembled preparation of porous carbon composites for selective CO2 capture at elevated temperatures, *J. Mater. Chem. A* 7 (10) (2019) 5402–5408.
- [127] Y. Li, X. Wang, M. Cao, Three-dimensional porous carbon frameworks derived from mangosteen peel waste as promising materials for CO2 capture and supercapacitors, *J. CO2 Util.* 27 (2018) 204–216.
- [128] Q. Yu, et al., One-pot synthesis of melamine formaldehyde resin-derived N-doped porous carbon for CO2 capture application, *Molecules* 28 (4) (2023) 1772.
- [129] I. Ozdemir, et al., Preparation and characterization of activated carbon from grape stalks by zinc chloride activation, *Fuel Process. Technol.* 125 (2014) 200–206.
- [130] X. Zhang, et al., Biobased hierarchically porous carbon featuring micron-sized honeycomb architecture for CO2 capture and water remediation, *J. Environ. Chem. Eng.* 10 (3) (2022) 107460.
- [131] Y. Wang, et al., N-doped porous carbon Derived from solvent-free Synthesis of cross-linked triazine Polymers for simultaneously achieving CO2 Capture and supercapacitors, *Chem.-Eur. J.* 27 (29) (2021) 7908–7914.
- [132] X. Gao, et al., Carbonaceous materials as adsorbents for CO2 capture: synthesis and modification, *Carbon Capture Science & Technology* 3 (2022) 100039.
- [133] A. Heidari, et al., Evaluation of CO2 adsorption with eucalyptus wood based activated carbon modified by ammonia solution through heat treatment, *Chem. Eng. J.* 254 (2014) 503–513.
- [134] L. Yue, et al., Efficient CO2 adsorption on nitrogen-doped porous carbons derived from d-glucose, *Energy Fuels* 32 (6) (2018) 6955–6963.
- [135] M.S. Khosrowshahi, et al., The role of surface chemistry on CO2 adsorption in biomass-derived porous carbons by experimental results and molecular dynamics simulations, *Sci. Rep.* 12 (1) (2022) 8917.
- [136] M. Vafaeinia, et al., Oxygen and nitrogen enriched pectin-derived micro-meso porous carbon for CO2 uptake, *RSC Adv.* 12 (1) (2022) 546–560.
- [137] C. Ma, et al., Nitrogen-doped porous carbons from polyacrylonitrile fiber as effective CO2 adsorbents, *J. Environ. Sci.* 125 (2023) 533–543.
- [138] G. Ma, G. Ning, Q. Wei, S-doped carbon materials: synthesis, properties and applications, *Carbon* 195 (2022) 328–340.
- [139] J. Bai, et al., One-pot synthesis of self S-doped porous carbon for efficient CO2 adsorption, *Fuel Process. Technol.* 244 (2023) 107700.
- [140] X. Ren, et al., N-doped porous carbons with exceptionally high CO2 selectivity for CO2 capture, *Carbon* 114 (2017) 473–481.
- [141] Y. Wang, et al., Nitrogen and oxygen codoped porous carbon with superior CO2 adsorption performance: a combined experimental and DFT calculation study, *Ind. Eng. Chem. Res.* 58 (29) (2019) 13390–13400.
- [142] A.H. Bhatti, et al., Metal impregnated activated carbon as cost-effective and scalable catalysts for amine-based CO2 capture, *J. Environ. Chem. Eng.* 11 (1) (2023) 109231.
- [143] K. Malini, D. Selvakumar, N. Kumar, Activated carbon from biomass: preparation, factors improving basicity and surface properties for enhanced CO2 capture capacity—A review, *J. CO2 Util.* 67 (2023) 102318.
- [144] B. Zhu, et al., Naturally derived porous carbon with selective metal-and/or nitrogen-doping for efficient CO2 capture and oxygen reduction, *J. Mater. Chem. A* 3 (9) (2015) 5212–5222.
- [145] R. Dubadi, M. Jaroniec, One-pot mechanochemical Synthesis of Carbons with high Microporosity and ordered Mesopores for CO2 Uptake at ambient conditions, *Nanomaterials* 13 (15) (2023) 2262.
- [146] J.H. Lee, et al., Combined CO2-philicity and ordered mesoporosity for highly selective CO2 capture at high temperatures, *J. Am. Chem. Soc.* 137 (22) (2015) 7210–7216.
- [147] A. Iqbal, et al., Synthesis and characterization of pure phase zeolite 4A from coal fly ash, *J. Clean. Prod.* 219 (2019) 258–267.
- [148] A. Gandhi, M.M. Faruque Hasan, A graph theoretic representation and analysis of zeolite frameworks, *Comput. Chem. Eng.* 155 (2021) 107548.
- [149] F. Bahmanzadegan, M.A. Pordsari, A. Ghaemi, Improving the efficiency of 4A-zeolite synthesized from kaolin by amine functionalization for CO2 capture, *Sci. Rep.* 13 (1) (2023) 12533.
- [150] D.G. Boer, et al., Binderless zeolite LTA beads with hierarchical porosity for selective CO2 adsorption in biogas upgrading, *Microporous Mesoporous Mater.* 344 (2022) 112208.
- [151] A. Gutierrez-Ortega, et al., A fast methodology to rank adsorbents for CO2 capture with temperature swing adsorption, *Chem. Eng. J.* 435 (2022) 134703.
- [152] A. Gęsickiewicz-Puchalska, et al., Changes in porous Parameters of the ion exchanged X Zeolite and their Effect on CO2 adsorption, *Molecules* (2021) 26, <https://doi.org/10.3390/molecules26247520>.
- [153] H. Wang, et al., Multi-factor study of the effects of a trace amount of water vapor on low concentration CO2 capture by 5A zeolite particles, *RSC Adv.* 10 (11) (2020) 6503–6511.
- [154] G. Papanikolaou, et al., Zeolite templated carbon from Beta replica as metal-free electrocatalyst for CO2 reduction, *Appl. Mater. Today* 26 (2022) 101383.
- [155] W.W. Lestari, et al., Fabrication of composite materials MIL-100(Fe)/Indonesian activated natural zeolite as enhanced CO2 capture material, *Chem. Pap.* 75 (7) (2021) 3253–3263.
- [156] W. Liang, et al., Amine-immobilized HY zeolite for CO2 capture from hot flue gas, *Chin. J. Chem. Eng.* 43 (2022) 335–342.
- [157] S.K. Wahono, et al., Amine-functionalized natural zeolites prepared through plasma polymerization for enhanced carbon dioxide adsorption, *Plasma Process. Polym.* 18 (8) (2021) 2100028.

- [158] J. Wang, Y. Zhou, X. Hu, Adsorption of CO<sub>2</sub> by a novel zeolite doped amine modified ternary aerogels, *Environ. Res.* 214 (2022) 113855.
- [159] Z. Razavi, N. Mirghaffari, M. Soleimani, Reduction of CO<sub>2</sub> emission through a photocatalytic process using powder and coated zeolite-supported TiO<sub>2</sub> under concentrated sunlight irradiation, *Environ. Sci. Pollut. Control Ser.* 30 (12) (2023) 32524–32538.
- [160] V. Indira, K. Abhitha, Mesoporogen-free synthesis of hierarchical zeolite A for CO<sub>2</sub> capture: Effect of freeze drying on surface structure, porosity and particle size, *Results in Engineering* 17 (2023) 100886.
- [161] M. Rafiq, et al., Recent advances in structural engineering of 2D hexagonal boron nitride electrocatalysts, *Nano Energy* 91 (2022) 106661.
- [162] R. Shankar, et al., Porous boron nitride for combined CO<sub>2</sub> capture and photoreduction, *J. Mater. Chem. A* 7 (41) (2019) 23931–23940.
- [163] H. Jiang, et al., Three-dimensional porous boron nitride foam for effective CO<sub>2</sub> adsorption, *Solid State Commun.* 294 (2019) 1–5.
- [164] S. Chen, et al., Carbon doping of hexagonal boron nitride porous materials toward CO<sub>2</sub> capture, *J. Mater. Chem. A* 6 (4) (2018) 1832–1839.
- [165] Y. Li, et al., Synergy of developed micropores and electronic structure defects in carbon-doped boron nitride for CO<sub>2</sub> capture, *Sci. Total Environ.* 811 (2022) 151384.
- [166] J. Gou, et al., Densification and pelletization of porous boron nitride fibers for effective CO<sub>2</sub> adsorption, *Ceram. Int.* 48 (8) (2022) 11636–11643.
- [167] H. Nan, et al., Strong photoluminescence enhancement of MoS<sub>2</sub> through defect engineering and oxygen bonding, *ACS Nano* 8 (6) (2014) 5738–5745.
- [168] W. Lei, et al., Porous boron nitride nanosheets for effective water cleaning, *Nat. Commun.* 4 (1) (2013) 1777.
- [169] J. Ding, et al., Effects of La–doping and preparation conditions on magnesia-based adsorption materials prepared by salicylic acid complex-combustion method for CO<sub>2</sub> capture, *J. Environ. Chem. Eng.* 11 (2) (2013) 109391.
- [170] H. Li, M. Qu, Y. Hu, Preparation of spherical Li<sub>4</sub>SiO<sub>4</sub> pellets by novel agar method for high-temperature CO<sub>2</sub> capture, *Chem. Eng. J.* 380 (2020) 122538.
- [171] Q. Sun, et al., Charge-controlled switchable CO<sub>2</sub> capture on boron nitride nanomaterials, *J. Am. Chem. Soc.* 135 (22) (2013) 8246–8253.
- [172] K. Huang, et al., Aminopolymer functionalization of boron nitride nanosheets for highly efficient capture of carbon dioxide, *J. Mater. Chem. A* 5 (31) (2017) 16241–16248.
- [173] H. Choi, et al., Ambient carbon dioxide capture by boron-rich boron nitride nanotube, *J. Am. Chem. Soc.* 133 (7) (2011) 2084–2087.
- [174] R. Mighri, et al., Nanostructured carbon-doped BN for CO<sub>2</sub> capture applications, *Nanomaterials* 13 (17) (2023) 2389.
- [175] X. Zeng, et al., “Intermediate template” assisted assembly growth of transition metal doped 2D porous boron nitride sheet as an efficient adsorbent for CO<sub>2</sub> capture, *Surface. Interfac.* 35 (2022) 102459.
- [176] R. Aniruddha, I. Sreedhar, B.M. Reddy, *MOFs in carbon capture-past, present and future*. Journal of CO<sub>2</sub> Utilization 42 (2020) 101297.
- [177] N. Kundu, S. Sarkar, Porous organic frameworks for carbon dioxide capture and storage, *J. Environ. Chem. Eng.* 9 (2) (2021) 105090.
- [178] H. Lyu, et al., Carbon dioxide capture chemistry of amino acid functionalized metal–organic frameworks in humid flue gas, *J. Am. Chem. Soc.* 144 (5) (2022) 2387–2396.
- [179] H. Tang, et al., Rapid screening of metal–organic frameworks for propane/propylene separation by synergizing molecular simulation and machine learning, *ACS Appl. Mater. Interfaces* 13 (45) (2021) 53454–53467.
- [180] H. Furukawa, et al., Isoreticular expansion of metal–organic frameworks with triangular and square building units and the lowest calculated density for porous crystals, *Inorg. Chem.* 50 (18) (2011) 9147–9152.
- [181] H. Furukawa, et al., Ultrahigh porosity in metal–organic frameworks, *Science* 329 (5990) (2010) 424–428.
- [182] R. Grünker, et al., A new metal–organic framework with ultra-high surface area, *Chem. Commun.* 50 (26) (2014) 3450–3452.
- [183] S. Mahajan, M. Lahtinen, Recent progress in metal–organic frameworks (MOFs) for CO<sub>2</sub> capture at different pressures, *J. Environ. Chem. Eng.* (2022) 108930.
- [184] J.-J. You, et al., A cage-based metal–organic framework with a unique tetrahedral node for size-selective CO<sub>2</sub> capture, *J. Solid State Chem.* 311 (2022) 123140.
- [185] W. Gong, et al., Chiral metal–organic frameworks, *Chem. Rev.* 122 (9) (2022) 9078–9144.
- [186] W. Liang, et al., Metal–organic framework-based enzyme biocomposites, *Chem. Rev.* 121 (3) (2021) 1077–1129.
- [187] V.F. Yusuf, N.I. Malek, S.K. Kailasa, Review on metal–organic framework classification, synthetic approaches, and influencing factors: Applications in energy, drug delivery, and wastewater treatment, *ACS Omega* 7 (49) (2022) 44507–44531.
- [188] I. Senkovska, et al., Understanding MOF flexibility: an analysis Focused on pillared layer MOFs as a model system, *Angew. Chem. Int. Ed.* (2023) e202218076.
- [189] W. Zhang, et al., Regulation of Porosity in MOFs: a Review on tunable Scaffolds and related Effects and Advances in different applications, *J. Environ. Chem. Eng.* (2022) 108836.
- [190] S. Bhattacharyya, T.K. Maji, Multi-dimensional metal–organic frameworks based on mixed linkers: Interplay between structural flexibility and functionality, *Coord. Chem. Rev.* 469 (2022) 214645.
- [191] T. Ghanbari, F. Abnisa, W.M.A.W. Daud, A review on production of metal organic frameworks (MOF) for CO<sub>2</sub> adsorption, *Sci. Total Environ.* 707 (2020) 135090.
- [192] R.W. Al-Saeed, A review on modified MOFs as CO<sub>2</sub> adsorbents using mixed metals and functionalized linkers, *Samarra Journal of Pure and Applied Science* 5 (1) (2023) 1–18.
- [193] L. Ding, et al., In situ Growth of Cs<sub>3</sub>Bi<sub>2</sub>Br<sub>9</sub> quantum Dots on Bi-MOF Nanosheets via coresharing bismuth Atoms for CO<sub>2</sub> Capture and photocatalytic reduction, *Inorg. Chem.* 62 (5) (2023) 2289–2303.
- [194] R. Gaikwad, S. Gaikwad, S. Han, Bimetallic UTSA-16 (Zn, X= Mg, Mn, Cu) metal organic framework developed by a microwave method with improved CO<sub>2</sub> capture performances, *J. Ind. Eng. Chem.* 111 (2022) 346–355.
- [195] H.A. Evans, et al., Aluminum formate, Al (HCOO) 3: An earth-abundant, scalable, and highly selective material for CO<sub>2</sub> capture, *Sci. Adv.* 8 (44) (2022) eade1473.
- [196] Z.-H. Guo, et al., Highly efficient I<sub>2</sub> sorption, CO<sub>2</sub> capture, and catalytic Conversion by introducing nitrogen donor Sites in a microporous Co (II)-Based metal–organic framework, *Inorg. Chem.* 61 (18) (2022) 7005–7016.
- [197] S. Shang, et al., CO<sub>2</sub> capture from wet flue gas using transition metal inserted porphyrin-based metal–organic frameworks as efficient adsorbents, *Sep. Purif. Technol.* 301 (2022) 122058.
- [198] L. Lei, et al., Taming structure and modulating carbon dioxide (CO<sub>2</sub>) adsorption isosteric heat of nickel-based metal organic framework (MOF-74 (Ni)) for remarkable CO<sub>2</sub> capture, *J. Colloid Interface Sci.* 612 (2022) 132–145.
- [199] Y. Wu, et al., Tuning secondary building unit of Cu-BTC to simultaneously enhance its CO<sub>2</sub> selective adsorption and stability under moisture, *Chem. Eng. J.* 355 (2019) 815–821.
- [200] J.M. Park, et al., Amine and fluorine co-functionalized MIL-101 (Cr) synthesized via a mixed-ligand strategy for CO<sub>2</sub> capture under humid conditions, *Chem. Eng. J.* 444 (2022) 136476.
- [201] Y. He, et al., Implementation of a core–shell design Approach for constructing MOFs for CO<sub>2</sub> capture, *ACS Appl. Mater. Interfaces* 15 (19) (2023) 23337–23342.
- [202] V.A. Dubskikh, et al., Enhanced adsorption selectivity of carbon dioxide and ethane on porous metal–organic framework functionalized by a sulfur-rich heterocycle, *Nanomaterials* 12 (23) (2022) 4281.
- [203] S.-Q. Yang, et al., Immobilization of the polar Group into an ultramicroporous metal–organic framework enabling benchmark inverse selective CO<sub>2</sub>/C<sub>2</sub>H<sub>2</sub> Separation with record C<sub>2</sub>H<sub>2</sub> production, *J. Am. Chem. Soc.* (2023).
- [204] Z. Cai, et al., Insights into CO<sub>2</sub> Adsorption in M–OH functionalized MOFs, *Chem. Mater.* 32 (10) (2020) 4257–4264.
- [205] M. Abbas, et al., Transformation of a copper-based metal–organic polyhedron into a mixed linker MOF for CO<sub>2</sub> capture, *Dalton Trans.* 52 (14) (2023) 4415–4422.
- [206] F. Liu, et al., Modified metal–organic framework by a novel coordinatively unsaturated amine grafting mechanism for direct air capture of CO<sub>2</sub>, *Chem. Eng. J.* 454 (2023) 140431.
- [207] E. Dautzenberg, G. Li, L.C. De Smet, Aromatic amine-functionalized covalent organic frameworks (COFs) for CO<sub>2</sub>/N<sub>2</sub> separation, *ACS Appl. Mater. Interfaces* 15 (4) (2023) 5118–5127.
- [208] H. Fan, et al., High-flux vertically aligned 2D covalent organic framework membrane with enhanced hydrogen separation, *J. Am. Chem. Soc.* 142 (15) (2020) 6872–6877.
- [209] N. Singh, et al., Band gap engineering in solvochromic 2D covalent organic framework photocatalysts for visible light-driven enhanced solar fuel production from carbon dioxide, *ACS Appl. Mater. Interfaces* 13 (12) (2021) 14122–14131.
- [210] G.O. Aksu, et al., Accelerating discovery of COFs for CO<sub>2</sub> capture and H<sub>2</sub> purification using structurally guided computational screening, *Chem. Eng. J.* 427 (2022) 131574.
- [211] L. Zhang, et al., Construction of rigid amine-linked three-dimensional covalent organic frameworks for selectively capturing carbon dioxide, *Chem. Commun.* 59 (33) (2023) 4911–4914.
- [212] S. Altarawneh, et al., Effect of acid-catalyzed formation rates of benzimidazole-linked polymers on porosity and selective CO<sub>2</sub> capture from gas mixtures, *Environ. Sci. Technol.* 49 (7) (2015) 4715–4723.
- [213] M. Mahato, et al., Electronically conjugated multifunctional covalent triazine Framework for unprecedented CO<sub>2</sub> Selectivity and high-power flexible supercapacitor, *Adv. Funct. Mater.* 32 (5) (2022) 2107442.
- [214] H. Lyu, et al., Covalent organic frameworks for carbon dioxide capture from air, *J. Am. Chem. Soc.* 144 (28) (2022) 12989–12995.
- [215] M. Yin, L. Wang, S. Tang, Amino-functionalized ionic-liquid-grafted covalent organic Frameworks for high-efficiency CO<sub>2</sub> Capture and conversion, *ACS Appl. Mater. Interfaces* 14 (50) (2022) 55674–55685.
- [216] H. Veldhuizen, et al., Competitive and cooperative CO<sub>2</sub>–H<sub>2</sub>O Adsorption through humidity Control in a polyimide covalent organic framework, *ACS Appl. Mater. Interfaces* (2023).
- [217] C. Jia, et al., Boosting Hydrostability and carbon dioxide Capture of boroxine-linked covalent organic Frameworks by one-pot oligoamine modification, *Chem.–Eur. J.* 29 (29) (2023) e202300186.
- [218] J. Wang, et al., Bifunctional core–shell Zr-MOFs@ COFs hybrids for CO<sub>2</sub> capture and photocatalytic oxidative amine coupling, *Chem. Eng. Sci.* 281 (2023) 119171.
- [219] J. Wang, et al., Covalently connected core–shell NH<sub>2</sub>-UiO-66@ Br-COFs hybrid materials for CO<sub>2</sub> capture and I<sub>2</sub> vapor adsorption, *Chem. Eng. J.* 438 (2022) 135555.
- [220] H. Jyoti Bora, et al., Enabling ultrahigh surface Area of covalently-linked organic Framework for boosted CO<sub>2</sub> capture: an air liquid interfacial Plasma as post-furnishing protocol, *Chem.–Eur. J.* 29 (38) (2023) e202300756.
- [221] Y. Zhang, et al., Facile manufacture of COF-based mixed matrix membranes for efficient CO<sub>2</sub> separation, *Chem. Eng. J.* 430 (2022) 133001.
- [222] X.-H. Xiong, et al., Nitro-decorated microporous covalent organic framework (TpPa-NO<sub>2</sub>) for selective separation of C<sub>2</sub>H<sub>4</sub> from a C<sub>2</sub>H<sub>2</sub>/C<sub>2</sub>H<sub>4</sub>/CO<sub>2</sub> mixture and CO<sub>2</sub> capture, *ACS Appl. Mater. Interfaces* 14 (28) (2022) 32105–32111.

- [223] S. Mukherjee, A.N. Samanta, Amine-impregnated MCM-41 in post-combustion CO<sub>2</sub> capture: synthesis, characterization, isotherm modelling, *Adv. Powder Technol.* 30 (12) (2019) 3231–3240.
- [224] Y. Wei, et al., Periodic mesoporous organosilica nanocubes with ultrahigh surface areas for efficient CO<sub>2</sub> adsorption, *Sci. Rep.* 6 (1) (2016) 20769.
- [225] L. Fu, et al., Research progress on CO<sub>2</sub> capture and utilization technology, *J. CO<sub>2</sub> Util.* 66 (2022) 102260.
- [226] A. Velty, A. Corma, Advanced zeolite and ordered mesoporous silica-based catalysts for the conversion of CO<sub>2</sub> to chemicals and fuels, *Chem. Soc. Rev.* 52 (5) (2023) 1773–1946.
- [227] Y. Fan, X. Jia, Progress in amine-functionalized silica for CO<sub>2</sub> capture: Important roles of support and amine structure, *Energy Fuels* 36 (3) (2022) 1252–1270.
- [228] W. Henao, et al., Insights into the CO<sub>2</sub> capture over amine-functionalized mesoporous silica adsorbents derived from rice husk ash, *J. Environ. Chem. Eng.* 8 (5) (2020) 104362.
- [229] M. Liu, et al., New insight into multiple hydrogen-bond networks of functional organosilicas system for collaborative transformation of CO<sub>2</sub> under mild conditions, *Sep. Purif. Technol.* 317 (2023) 123937.
- [230] P. Huang, et al., Facile fabrication of silica aerogel supported amine adsorbent pellets for Low-concentration CO<sub>2</sub> removal from confined spaces, *Chem. Eng. J.* 468 (2023) 143629.
- [231] D.K. Pandey, et al., Ordered mesoporous silica matrices supported ionic liquids for efficient CO<sub>2</sub> separation from CO<sub>2</sub>/CH<sub>4</sub> gas mixture: experimental and theoretical investigation, *J. Mol. Liq.* 368 (2022) 120569.
- [232] O. Ajumobi, et al., Design of nanostraws in amine-functionalized MCM-41 for improved adsorption capacity in carbon capture, *Energy Fuels* 37 (16) (2023) 12079–12088.
- [233] A.A. Al-Absi, et al., CO<sub>2</sub> capture using in-situ polymerized amines into pore-expanded-SBA-15: Performance evaluation, kinetics, and adsorption isotherms, *Fuel* 333 (2023) 126401.
- [234] X. Cheng, et al., Fabrication of robust and bifunctional cyclotriphosphazene-based periodic mesoporous organosilicas for efficient CO<sub>2</sub> adsorption and catalytic conversion, *Chem. Eng. J.* 418 (2021) 129360.
- [235] L. Lin, et al., Comparison of characteristics and performance between PEI and DETA impregnated on SBA-15 for CO<sub>2</sub> capture, *Sep. Purif. Technol.* (2023) 124346.
- [236] L. Lin, et al., Characteristics, application and modeling of solid amine adsorbents for CO<sub>2</sub> capture: a review, *J. Environ. Manag.* 325 (2023) 116438.
- [237] X. Li, et al., Amine-impregnated porous carbon-silica sheets derived from vermiculite with superior adsorption capability and cyclic stability for CO<sub>2</sub> capture, *Chem. Eng. J.* 464 (2023) 142662.
- [238] H. Yan, et al., High CO<sub>2</sub> adsorption on amine-functionalized improved macro-/mesoporous multimodal pore silica, *Fuel* 315 (2022) 123195.
- [239] R. Kumar, et al., Amine-impregnated nanoarchitectonics of mesoporous silica for capturing dry and humid 400 ppm carbon dioxide: a comparative study, *Microporous Mesoporous Mater.* 338 (2022) 111956.
- [240] H. Shi, et al., Co-grafting of polyethylenimine on mesocellular silica foam for highly efficient CO<sub>2</sub> capture, *Sep. Purif. Technol.* 325 (2023) 124608.
- [241] L. Fan, et al., In-situ Fe/Ti doped amine-grafted silica aerogel from fly ash for efficient CO<sub>2</sub> capture: Facile synthesis and super adsorption performance, *Chem. Eng. J.* 452 (2023) 138945.
- [242] S. Xu, et al., Synthesis of ordered mesoporous silica from biomass ash and its application in CO<sub>2</sub> adsorption, *Environ. Res.* 231 (2023) 116070.
- [243] T.-H. Liou, et al., Sustainable utilization of rice husk waste for preparation of ordered nanostructured mesoporous silica and mesoporous carbon: Characterization and adsorption performance, *Colloids Surf. A Physicochem. Eng. Asp.* 636 (2022) 128150.
- [244] A.G. Gebretatos, et al., Rice husk waste into various template-engineered mesoporous silica materials for different applications: a comprehensive review on recent developments, *Chemosphere* 310 (2023) 136843.
- [245] S. Aspromonte, et al., Mesoporous bio-materials synthesized with corn and potato starches applied in CO<sub>2</sub> capture, *J. Environ. Chem. Eng.* 11 (4) (2023) 109542.
- [246] J. McEwen, J.-D. Hayman, A. Ozgur Yazaydin, A comparative study of CO<sub>2</sub>, CH<sub>4</sub> and N<sub>2</sub> adsorption in ZIF-8, Zeolite-13X and BPL activated carbon, *Chem. Phys. 412* (2013) 72–76.
- [247] M.R. Oliveira, et al., Microwave-assisted Synthesis of zeolite A from Metakaolinite for CO<sub>2</sub> adsorption, *Int. J. Mol. Sci.* (2023) 24, <https://doi.org/10.3390/ijms241814040>.
- [248] N.S. Ardali, et al., Experimental investigation of carbon dioxide adsorption using functionalized MWCNTs with 1, 6-diaminohexane, *Fuel* 338 (2023) 127213.
- [249] G. Zelenková, et al., Graphene as a promising additive to hierarchically porous carbon monoliths for enhanced H<sub>2</sub> and CO<sub>2</sub> sorption, *J. CO<sub>2</sub> Util.* 68 (2023) 102371.
- [250] M. De Marco, et al., Hybrid effects in graphene oxide/carbon nanotube-supported layered double hydroxides: enhancing the CO<sub>2</sub> sorption properties, *Carbon* 123 (2017) 616–627.
- [251] P. Panda, R. Samanta, S. Barman, Facile Synthesis of two-dimensional (2D) boron Carbonitride and 2D porous boron Carbonitride for excellent energy Storage and gas adsorption applications, *Energy Fuels* 37 (7) (2023) 5540–5555.
- [252] L. Asgharnejad, A. Abbasí, A. Shakeri, Ni-based metal-organic framework/GO nanocomposites as selective adsorbent for CO<sub>2</sub> over N<sub>2</sub>, *Microporous Mesoporous Mater.* 262 (2018) 227–234.
- [253] G. Zhao, et al., Hierarchical porous metal organic framework aerogel for highly efficient CO<sub>2</sub> adsorption, *Sep. Purif. Technol.* 315 (2023) 123754.
- [254] J. Yang, et al., CO<sub>2</sub> Adsorption of nitrogen-doped carbons Prepared from nitric acid preoxidized petroleum coke, *Energy Fuels* 31 (10) (2017) 11060–11068.
- [255] J. Shao, et al., Unlocking the potential of N-doped porous Carbon: Facile synthesis and superior CO<sub>2</sub> adsorption performance, *Sep. Purif. Technol.* 333 (2024) 125891.
- [256] R. Mighri, et al., Nanostructured carbon-doped BN for CO<sub>2</sub> capture applications, *Nanomaterials* (2023) 13, <https://doi.org/10.3390/nano13172389>.
- [257] O.F. Cruz, et al., Activated carbons with high micropore volume obtained from polyurethane foams for enhanced CO<sub>2</sub> adsorption, *Chem. Eng. Sci.* 273 (2023) 118671.
- [258] S. Shao, et al., Sustainable preparation of hierarchical porous carbon from discarded shells of crustaceans for efficient CO<sub>2</sub> capture, *Fuel* 355 (2024) 129287.
- [259] M. Aliyu, et al., TiC-MXene/activated carbon nanocomposite for efficient CO<sub>2</sub> capture: Insights into thermodynamics properties, *Sep. Purif. Technol.* 340 (2024) 126737.
- [260] L. Lei, et al., Taming structure and modulating carbon dioxide (CO<sub>2</sub>) adsorption isosteric heat of nickel-based metal organic framework (MOF-74(Ni)) for remarkable CO<sub>2</sub> capture, *J. Colloid Interface Sci.* 612 (2022) 132–145.
- [261] E. Dautzenberg, G. Li, L.C.P.M. de Smet, Aromatic amine-functionalized covalent organic frameworks (COFs) for CO<sub>2</sub>/N<sub>2</sub> separation, *ACS Appl. Mater. Interfaces* 15 (4) (2023) 5118–5127.
- [262] Q. Gao, et al., Covalent organic framework with frustrated bonding network for enhanced carbon dioxide storage, *Chem. Mater.* 30 (5) (2018) 1762–1768.
- [263] V. Kulkarni, D. Panda, S.K. Singh, Direct air Capture of CO<sub>2</sub> over amine-modified hierarchical silica, *Ind. Eng. Chem. Res.* 62 (8) (2023) 3800–3811.
- [264] T. Taher, et al., Facile synthesis of biochar/layered double oxides composite by one-step calcination for enhanced carbon dioxide (CO<sub>2</sub>) adsorption, *Mater. Lett.* 338 (2023) 134068.
- [265] J. Ai, et al., Synthesis of mesoporous magnesium silicate from coal gangue for efficient CO<sub>2</sub> adsorption at room temperature, *Fuel* 341 (2023) 127692.
- [266] J. Yuan, et al., Preparation of N, O co-doped carbon nanotubes and activated carbon composites with hierarchical porous structure for CO<sub>2</sub> adsorption by coal pyrolysis, *Fuel* 333 (2023) 126465.
- [267] A. Mohammadi, A. Nakhaei Pour, Triethylenetetramine-impregnated ZIF-8 nanoparticles for CO<sub>2</sub> adsorption, *J. CO<sub>2</sub> Util.* 69 (2023) 102424.
- [268] S. Chi, et al., Porous molecular sieve polymer composite with high CO<sub>2</sub> adsorption efficiency and hydrophobicity, *Sep. Purif. Technol.* 307 (2023) 122738.
- [269] R. Ben-Mansour, et al., Carbon capture by physical adsorption: materials, experimental investigations and numerical modeling and simulations—a review, *Appl. Energy* 161 (2016) 225–255.
- [270] S.Y.W. Chai, L.H. Ngu, B.S. How, Review of carbon capture absorbents for CO<sub>2</sub> utilization, *Greenhouse Gases: Sci. Technol.* 12 (3) (2022) 394–427.
- [271] C.C. Chatzistergiou, E.S. Kikkiniades, M.C. Georgiadis, Recent advances on the modeling and optimization of CO<sub>2</sub> capture processes, *Comput. Chem. Eng.* 165 (2022) 107938.
- [272] J.Y. Lai, L.H. Ngu, S.S. Hashim, A review of CO<sub>2</sub> adsorbents performance for different carbon capture technology processes conditions, *Greenhouse Gases: Sci. Technol.* 11 (5) (2021) 1076–1117.
- [273] Q. Wang, et al., CO<sub>2</sub> capture by solid adsorbents and their applications: current status and new trends, *Energy Environ. Sci.* 4 (1) (2011) 42–55.
- [274] H.A. Patel, J. Byun, C.T. Yavuz, Carbon dioxide capture adsorbents: chemistry and methods, *ChemSusChem* 10 (7) (2017) 1303–1317.
- [275] Z. Hu, et al., CO<sub>2</sub> capture in metal-organic framework adsorbents: an engineering perspective, *Advanced Sustainable Systems* 3 (1) (2019) 1800080.
- [276] M.I. Severino, et al., MOFs industrialization: a complete assessment of production costs, *Faraday Discuss.* 231 (2021) 326–341.
- [277] K.T. Leperi, et al., Development of a general evaluation metric for rapid screening of adsorbent materials for postcombustion CO<sub>2</sub> capture, *ACS Sustain. Chem. Eng.* 7 (13) (2019) 11529–11539.
- [278] A.R. Vakili, et al., Toward Modeling the in vitro gas production Process by using propolis extract oil treatment: machine Learning and kinetic models, *Ind. Eng. Chem. Res.* (2022).
- [279] T.D. Burns, et al., Prediction of MOF performance in vacuum swing adsorption systems for postcombustion CO<sub>2</sub> capture based on integrated molecular simulations, process optimizations, and machine learning models, *Environ. Sci. Technol.* 54 (7) (2020) 4536–4544.
- [280] M. Rahimi, et al., Modeling and optimizing N/O-enriched bio-derived adsorbents for CO<sub>2</sub> capture: machine learning and DFT calculation approaches, *Ind. Eng. Chem. Res.* 61 (30) (2022) 10670–10688.
- [281] H. Mashhadimoslem, et al., Development of predictive models for activated carbon synthesis from different biomass for CO<sub>2</sub> adsorption using artificial neural networks, *Ind. Eng. Chem. Res.* 60 (38) (2021) 13950–13966.
- [282] J. Burner, et al., High-performing deep learning regression models for predicting low-pressure CO<sub>2</sub> adsorption properties of metal-organic frameworks, *J. Phys. Chem. C* 124 (51) (2020) 27996–28005.
- [283] M. Rahimi, M.-R. Pourramezan, A. Rohani, Modeling and classifying the in-operando effects of wear and metal contaminations of lubricating oil on diesel engine: a machine learning approach, *Expert Syst. Appl.* 203 (2022) 117494.
- [284] H.V. Thanh, et al., Hydrogen storage on porous carbon adsorbents: rediscovery by nature-derived algorithms in random forest machine learning model, *Energies* 16 (5) (2023) 2348.
- [285] H.V. Thanh, et al., Predicting the wettability rocks/minerals-brine-hydrogen system for hydrogen storage: Re-evaluation approach by multi-machine learning scheme, *Fuel* 345 (2023) 128183.
- [286] M. Rahimi, M.H. Abbaspour-Fard, A. Rohani, Machine learning approaches to rediscovery and optimization of hydrogen storage on porous bio-derived carbon, *J. Clean. Prod.* 329 (2021) 129714.

- [287] H. Zhang, et al., Improving predictions of shale wettability using advanced machine learning techniques and nature-inspired methods: Implications for carbon capture utilization and storage, *Sci. Total Environ.* 877 (2023) 162944.
- [288] M. Rahimi, et al., A multi-criteria decision-making (MCDM) approach to determine the synthesizing routes of biomass-based carbon electrode material in supercapacitors, *J. Clean. Prod.* 397 (2023) 136606.
- [289] M. Safaei-Farouji, et al., Exploring the power of machine learning to predict carbon dioxide trapping efficiency in saline aquifers for carbon geological storage project, *J. Clean. Prod.* 372 (2022) 133778.
- [290] C.R. Groom, et al., The Cambridge structural database, *Acta Crystallogr. B: Structural Science, Crystal Engineering and Materials* 72 (2) (2016) 171–179.
- [291] P.Z. Moghadam, et al., Development of a Cambridge Structural Database subset: a collection of metal–organic frameworks for past, present, and future, *Chem. Mater.* 29 (7) (2017) 2618–2625.
- [292] L. Talirz, et al., Materials Cloud, a platform for open computational science, *Sci. Data* 7 (1) (2020) 299.
- [293] F.O. Okello, et al., Towards estimation and mechanism of CO<sub>2</sub> adsorption on zeolite adsorbents using molecular simulations and machine learning, *Mater. Today Commun.* 36 (2023) 106594.
- [294] X. Zhu, et al., Machine learning exploration of the critical factors for CO<sub>2</sub> adsorption capacity on porous carbon materials at different pressures, *J. Clean. Prod.* 273 (2020) 122915.
- [295] S. Namdeo, V.C. Srivastava, P. Mohanty, Machine learning implemented exploration of the adsorption mechanism of carbon dioxide onto porous carbons, *J. Colloid Interface Sci.* 647 (2023) 174–187.
- [296] X. Ma, et al., Insights into CO<sub>2</sub> capture in porous carbons from machine learning, experiments and molecular simulation, *Sep. Purif. Technol.* 306 (2023) 122521.
- [297] C. Zhang, et al., Machine learning assisted rediscovery of methane storage and separation in porous carbon from material literature, *Fuel* 290 (2021) 120080.
- [298] C. Xie, et al., Explainable machine learning for carbon dioxide adsorption on porous carbon, *J. Environ. Chem. Eng.* 11 (1) (2023) 109053.
- [299] M. Rahimi, et al., Yield prediction and optimization of biomass-based products by multi-machine learning schemes: neural, regression and function-based techniques, *Energy* 283 (2023) 128546.
- [300] S. Wang, et al., Prediction by convolutional neural networks of CO<sub>2</sub>/N<sub>2</sub> selectivity in porous carbons from N<sub>2</sub> adsorption isotherm at 77 K, *Angew. Chem. Int. Ed.* 59 (44) (2020) 19645–19648.
- [301] H. Daglar, et al., Integrating molecular Simulations with machine learning Guides in the Design and Synthesis of [BMIM][BF<sub>4</sub>]/MOF Composites for CO<sub>2</sub>/N<sub>2</sub> separation, *ACS Appl. Mater. Interfaces* 15 (13) (2023) 17421–17431.
- [302] S. Li, et al., Predicting metal–organic frameworks as catalysts to fix carbon dioxide to cyclic carbonate by machine learning, *Journal of Materomics* 7 (5) (2021) 1029–1038.
- [303] K. Choudhary, et al., Graph neural network predictions of metal organic framework CO<sub>2</sub> adsorption properties, *Comput. Mater. Sci.* 210 (2022) 111388.
- [304] X. Yuan, et al., Applied machine learning for prediction of CO<sub>2</sub> adsorption on biomass waste-derived porous carbons, *Environ. Sci. Technol.* 55 (17) (2021) 11925–11936.
- [305] D. Kumbhar, et al., Rapid discrimination of porous bio-carbon derived from nitrogen rich biomass using Raman spectroscopy and artificial intelligence methods, *Carbon* 178 (2021) 792–802.
- [306] A. Ghaemi, M.K. Dehnavi, Z. Khoshraftar, Exploring artificial neural network approach and RSM modeling in the prediction of CO<sub>2</sub> capture using carbon molecular sieves, *Case Studies in Chemical and Environmental Engineering* 7 (2023) 100310.
- [307] Z. Khoshraftar, A. Ghaemi, Evaluation of pistachio shells as solid wastes to produce activated carbon for CO<sub>2</sub> capture: isotherm, response surface methodology (RSM) and artificial neural network (ANN) modeling, *Current Research in Green and Sustainable Chemistry* 5 (2022) 100342.
- [308] A. Alanazi, et al., Machine learning framework for estimating CO<sub>2</sub> adsorption on coalbed for carbon capture, utilization, and storage applications, *Int. J. Coal Geol.* (2023) 104297.
- [309] Z. Zhang, et al., Machine learning aided high-throughput prediction of ionic liquid@ MOF composites for membrane-based CO<sub>2</sub> capture, *J. Membr. Sci.* 650 (2022) 120399.
- [310] J. Guan, et al., Design and prediction of metal organic framework-based mixed matrix membranes for CO<sub>2</sub> capture via machine learning, *Cell Reports Physical Science* 3 (5) (2022).
- [311] M. Alizamir, et al., Accurately predicting the performance of MOF-based mixed matrix membranes for CO<sub>2</sub> removal using a novel optimized extreme learning machine by BAT algorithm, *Sep. Purif. Technol.* 325 (2023) 124689.
- [312] M. Feng, et al., Finding the optimal CO<sub>2</sub> adsorption material: Prediction of multi-properties of metal-organic frameworks (MOFs) based on DeepFM, *Sep. Purif. Technol.* 302 (2022) 122111.
- [313] S. Kancharlapalli, et al., Fast and accurate machine learning strategy for calculating partial atomic charges in metal–organic frameworks, *J. Chem. Theor. Comput.* 17 (5) (2021) 3052–3064.
- [314] F. Yulia, I. Chairina, A. Zulyas, Multi-objective genetic algorithm optimization with an artificial neural network for CO<sub>2</sub>/CH<sub>4</sub> adsorption prediction in metal–organic framework, *Therm. Sci. Eng. Prog.* 25 (2021) 100967.
- [315] Y. Situ, et al., Large-scale Screening and machine Learning for metal–organic framework Membranes to capture CO<sub>2</sub> from flue gas, *Membranes* 12 (7) (2022) 700.
- [316] G.S. Fanourgakis, et al., A universal machine learning algorithm for large-scale screening of materials, *J. Am. Chem. Soc.* 142 (8) (2020) 3814–3822.
- [317] G.S. Fanourgakis, et al., A generic machine learning algorithm for the prediction of gas adsorption in nanoporous materials, *J. Phys. Chem. C* 124 (13) (2020) 7117–7126.
- [318] W. Guo, et al., Deep learning models for predicting gas adsorption capacity of nanomaterials, *Nanomaterials* 12 (19) (2022) 3376.
- [319] J. Abdi, et al., Modeling of CO<sub>2</sub> adsorption capacity by porous metal organic frameworks using advanced decision tree-based models, *Sci. Rep.* 11 (1) (2021) 24468.
- [320] A. Guda, et al., Machine learning approaches to XANES spectra for quantitative 3D structural determination: The case of CO<sub>2</sub> adsorption on CPO-27-Ni MOF, *Radiat. Phys. Chem.* 175 (2020) 108430.
- [321] S.A. Abdollahi, et al., Simulating and comparing CO<sub>2</sub>/CH<sub>4</sub> separation Performance of membrane–zeolite Contactors by cascade neural networks, *Membranes* 13 (5) (2023) 526.
- [322] M. Gheytanzadeh, et al., Towards estimation of CO<sub>2</sub> adsorption on highly porous MOF-based adsorbents using Gaussian process regression approach, *Sci. Rep.* 11 (1) (2021) 15710.
- [323] M. Raji, et al., Novel prosperous computational estimations for greenhouse gas adsorptive control by zeolites using machine learning methods, *J. Environ. Manag.* 307 (2022) 114478.
- [324] F. Fathalian, et al., Intelligent prediction models based on machine learning for CO<sub>2</sub> capture performance by graphene oxide-based adsorbents, *Sci. Rep.* 12 (1) (2022) 21507.
- [325] H. Park, et al., Inverse Design of Metal-Organic Frameworks for Direct Air Capture of CO<sub>2</sub> via Deep Reinforcement Learning, 2023.